5

Magnetic field gradients and spin translation

When the very first NMR experiments were performed on liquids, the role of the laboratory magnet in determining the linewidth of the spectrum was evident. Inhomogeneity of the magnetic field led to a range of Larmor frequencies and hence the natural relaxation-limited linewidth was buried under the much larger inhomogeneous broadening. Only when the spin echo was used to refocus the effects of phase-spreading under the inhomogeneous field was it possible to see the slowly decaying exponential of the echo envelope. This was the decay arising from relaxation, a time-domain attenuation representing the Fourier conjugate of the homogeneous spectral linewidth.

And so magnetic field inhomogeneities were seen from the beginning as a mixed blessing. From a frequency-domain perspective they were a nuisance, a resolution-limiting imperfection, to be minimised by the use of correction coils and strategically placed magnetic metal foils known as shims. Shimming, which is, in its modern version, the independent adjustment of currents in multiple coils representing various orders of magnetic field harmonics, is a familiar ritual in setting up high resolution NMR spectrometers. But from a time-domain perspective the field inhomogeneity was a help rather than a hindrance. Its very existence made possible the echo phenomenon, and the shape of the echo was determined by the field distribution. But, more importantly, it was realised by Erwin Hahn [1] that translational motion of spin-bearing molecules over the duration of the echo formation led to imperfect refocusing and hence to an echo attenuation. Thus the echo became a window on molecular motion itself, and the sensitivity to that motion was governed by the local gradient in the magnetic field. In other words, inhomogeneous fields were useful.

Of course, a spatially varying magnetic field is the fundamental tool of magnetic resonance imaging. It may seem surprising that so much time elapsed since the discovery of NMR in 1945 to the suggestion of MRI in 1973 [2, 3], before the practitioners of magnetic resonance realised that using magnetic field gradients to measure molecular motion naturally had a counterpart in using magnetic field gradients to determine molecular position. Such are the strange twists and turns of scientific discovery. In the opinion of this author, the key precursor to MRI was the integration of the computer with the NMR spectrometer. As so often is the case, new technology generates new science, the two being irrevocably intertwined.

Translational Dynamics and Magnetic Resonance, First Edition, Paul T. Callaghan, © Paul T. Callaghan 2011.
Published in 2011 by Oxford University Press.

5.1 Gradient fields and Maxwell's equations

The physical principle underlying the usefulness of the inhomogeneous magnetic field is the Larmor equation, $\omega_0 = \gamma B_0$. In other words, a field $B_0(\mathbf{r})$ leads to a spatially varying frequency $\omega_0(\mathbf{r})$, and frequency, along with its associated phase shifts, is what we measure in magnetic resonance.

Generally, for an optimally shimmed magnetic resonance system, we find it convenient to separate the main field, $B_0\hat{\mathbf{k}}$,[1] which is taken to be uniform and oriented along z, from any spatially varying part $\mathbf{B}(\mathbf{r})$. This latter is usually deliberately applied as an additional field by a special set of coils whose currents are independently controlled. Consider what Maxwell's equations tell us about this spatially dependent magnetic field, in the absence of any local currents, the usual case for the magnetic resonance sample where all conductors are external to the sample space. For local current density $\mathbf{J} = 0$ and for static or slowly varying fields where the displacement current $\partial\mathbf{D}/\partial t$ may be neglected,

$$\begin{aligned} \nabla \cdot \mathbf{B} &= 0 \\ \nabla \times \mathbf{B} &= 0. \end{aligned} \tag{5.1}$$

Expressing the divergenceless nature of the field in Cartesian coordinates we have

$$\frac{\partial B_x}{\partial x} + \frac{\partial B_y}{\partial y} + \frac{\partial B_z}{\partial z} = 0 \tag{5.2}$$

The curl equation leads to equalities of the form $\partial B_x/\partial y = \partial B_y/\partial x$. A little algebra leads then to $\nabla^2\mathbf{B} = 0$, showing that the magnetic field obeys the Laplace equation. This useful result facilitates the use of the various Laplace eigenmode solutions in designing magnetic field gradients in the presence of known boundary conditions.

Equation 5.2 tells us that a gradient in the field, such as a term $\partial B_z/\partial z$, cannot exist in isolation but requires the existence of terms $\partial B_y/\partial y$, and $\partial B_x/\partial x$. These latter are known as concomitant fields, and the effect is illustrated in Fig. 5.1. We will show that, in the presence of a much larger magnetic field, B_0, oriented along z, only the parallel field term $\partial B_z/\partial z$ makes a significant contribution. However, in low fields these concomitant field effects may be very important.

Suppose we attempt to create a spatial variation in the Larmor frequency by adding to $B_0\hat{\mathbf{k}}$ a gradient field $\mathbf{B}(\mathbf{r})$, which, in the vicinity of the sample centre, is zero, with local gradient $\nabla\mathbf{B}(\mathbf{r})$. Off-centre, the total field is

$$\mathbf{B}_{tot}(x, y, z) = (\mathbf{r} \cdot \nabla B_x)\hat{\mathbf{i}} + (\mathbf{r} \cdot \nabla B_y)\hat{\mathbf{j}} + (B_0 + \mathbf{r} \cdot \nabla B_z)\hat{\mathbf{k}}. \tag{5.3}$$

Of course the spins care not a jot about the orientation of $\mathbf{B}_{tot}(x, y, z)$, taking its local direction to be their quantisation axis and precessing about that axis accordingly. In other words, the spins are sensitive to $|\mathbf{B}_{tot}|$ so that the proper form of the Larmor equation should be

$$\omega_0 = \gamma|\mathbf{B}_{tot}|. \tag{5.4}$$

[1] We use unit vectors $\hat{\mathbf{i}}$, $\hat{\mathbf{j}}$, and $\hat{\mathbf{k}}$ for the respective x-, y-, and z-axes.

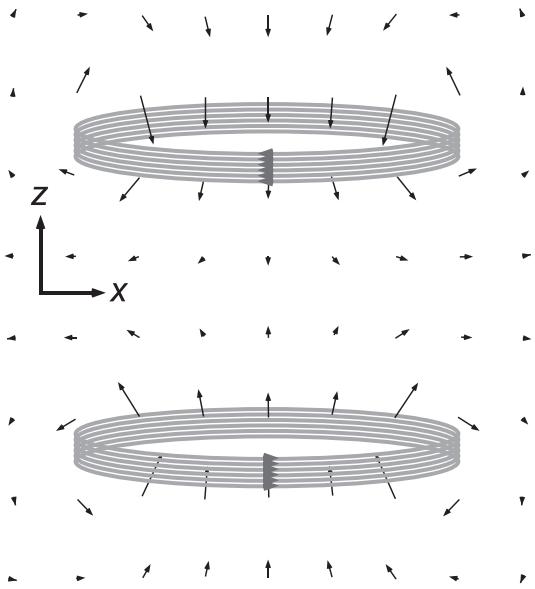

Fig. 5.1 Magnetic field vectors in the plane $y = 0$ and in the vicinity of Maxwell pair gradient coil set, designed to produce a linear magnetic field gradient, $B_z/\partial z$. The effect of the concomitant gradient, $\partial B_x/\partial x$ is apparent.

Let us evaluate $|\mathbf{B}_{tot}|$ when B_0 is much larger than the gradient fields, $x\partial B_x/\partial x$, and so on. Then

$$\begin{aligned} |\mathbf{B}_{tot}| &= [(\mathbf{r}\cdot\nabla B_x)^2 + (\mathbf{r}\cdot\nabla B_y)^2 + (B_0 + \mathbf{r}\cdot\nabla B_z)^2]^{1/2} \\ &\approx B_0 + \mathbf{r}\cdot\nabla B_z + \frac{1}{2}B_0^{-1}[(\mathbf{r}\cdot\nabla B_x)^2 + (\mathbf{r}\cdot\nabla B_y)^2 + (\mathbf{r}\cdot\nabla B_z)^2] \\ &\approx B_0 + \mathbf{r}\cdot\nabla B_z \end{aligned} \tag{5.5}$$

The reason the concomitant fields have disappeared is that they are orthogonal in direction to the main field and so slightly tilt its direction, but influence its magnitude only to second order.

So, the case of a dominant uniform field is easy to deal with. We may ignore concomitant fields and apply gradients in B_z at will, for example using coils that produce, in effect, pure $\partial B_z/\partial x$, $\partial B_z/\partial y$ and $\partial B_z/\partial z$. Indeed, we may write

$$\mathbf{G} = \nabla B_z \tag{5.6}$$

and

$$\omega_0(\mathbf{r}) = \gamma B_0 + \mathbf{r}\cdot\mathbf{G}. \tag{5.7}$$

What then for low B_0 fields, where $B_0 \sim B(\mathbf{r})$?[2] Here we must return to the magnitude form of the Larmor precession, eqn 5.4. The gradients which matter then are those in the magnitude of the total field and so

[2] $B(\mathbf{r})$ means $|\mathbf{B}(\mathbf{r})|$.

$$\begin{aligned}\mathbf{G} &= \nabla|\mathbf{B}_{tot}| \\ &= \frac{(\mathbf{B}_{tot}\cdot\nabla)\mathbf{B}_{tot}}{|\mathbf{B}_{tot}|}\end{aligned} \tag{5.8}$$

and

$$\omega_0(\mathbf{r}) = \gamma|\mathbf{B}_{tot}| + \mathbf{r}\cdot\mathbf{G}. \tag{5.9}$$

Note that the vector $\mathbf{G}$ points in the direction of the variation of the magnetic field along its line, $(\mathbf{B}_{tot}\cdot\nabla)\mathbf{B}_{tot}$ [4], and this direction plays the role of the gradient of the magnetic field in a single fixed direction evident in the strong B_0 field case of eqns 5.5 and 5.7. One might reasonably ask whether migrating spins could follow the changing direction of a local magnetic field, remaining in states quantised with respect to that direction. Such an ability to track the field will depend on the adiabatic condition being fulfilled. In other words, provided the rate of precession of the spins about the local field is much greater than the rate of change of orientation of that field due to molecular motion, the local quantisation persists. Such a requirement is almost invariably satisfied.

We will revisit the condition $B_0 \sim B(\mathbf{r})$ in later chapters. But for the rest of Chapter 5, let us assume that $B_0 \gg B(\mathbf{r})$ so that eqns 5.6 and 5.7 apply.

5.2 Phase evolution of spin isochromats

5.2.1 Magnetisation phase

In Chapter 4 it was shown that the emf arising from the Faraday detection process in magnetic resonance could be quadrature mixed with an RF field oscillating at frequency, ω, close to the Larmor precession frequency ω_0, resulting in in-phase and quadrature signal components oscillating at difference frequency $\omega_0 - \omega$. In quantum mechanical terms, this detection is associated with an observable $N\gamma(I_x + iI_y)$ operating on the rotating frame density matrix ρ^{rot} as $N\gamma Tr(\rho^{rot}(I_x + iI_y))$. For any state of the rotating frame density matrix written in an orthogonal tensor basis of spin operators,[3] only I_x and I_y components can contribute to the signal. We saw in Chapter 4 how the Larmor precession following a 90°_x RF pulse led to a signal

$$N\gamma Tr([I_x + iI_y]\rho^{rot}(t)) = iM_0\exp(-i(\omega_0 - \omega)t) \tag{5.10}$$

where the minus sign is associated with clockwise precession, but the frequency scale may be arbitrarily chosen, for convenience, to be positive. The phase of the signal is determined in part by the initial RF pulse, which assigned the spins to I_y at $t = 0$ and hence the signal at $t = 0$ to the quadrature channel, and in part by the subsequent time-evolution due to the off-resonant nature of the mixing frequency, ω. Indeed, any pulse sequence will, at the final detection stage, lead to some particular absolute phase at the detection origin and some time-dependent phase depending on the detection frequency offset at that position in the NMR spectrum.

Suppose we have settled on some particular RF pulse sequence and signal detection time origin which yield, at $t = 0$, a complex signal $S(0)$. Now imagine that we carry

[3]That is, orthogonal under the trace operation.

out some variation on our NMR experiment that results in a new signal $\exp(i\phi)S(0)$. In that case the phase change $\exp(i\phi)$ may be obtained by taking a simple ratio of the two signals. Thus the concept of an absolute phase change is easily utilised by reference to the unperturbed signal. This idea applies equally to the signal contributions of sub-ensembles of spins where, as we shall see in subsequent sections, phase changes may differ.

5.2.2 Spin isochromats in an inhomogeneous field

Avogadro's number is so extraordinarily large that it allows for astonishing numerical descriptions. For example, there are more molecules of water in a glass of water than there are glasses of water in all the oceans. Or, perhaps even more remarkably, the numbers of carbon atoms removed in one revolution of a car tyre is approximately the same as the age of the universe in seconds. In short, the size of Avogadro's number means that we may consider extraordinarily small volumes of material and still have sufficient numbers of nuclear spins for a density matrix description to apply very well. Consider, for example, a very small volume of $(1\,\mathrm{nm})^3$. For typical materials this volume will contain on the order of 10^2 nuclear spins, sufficient for such a volume to be represented by a sub-ensemble obeying well-defined statistical averages.

Suppose that our spin system is subject to an inhomogeneous magnetic field. How big would the magnetic field gradient have to be to resolve the spin precession difference across 1 nm? Of course, that will be in part determined by our available frequency resolution, which in turn is limited by the transverse relaxation time. For $T_2 \sim 1\,\mathrm{s}$ we could allow for a resolution $\sim 1\,\mathrm{Hz}$. For protons, a 1 Hz frequency separation across 1 nm corresponds to a magnetic field gradient of around $25\,\mathrm{T\ m^{-1}}$, while for other nuclei this must be scaled upwards as the magnetogyric ratio, γ, reduces. A $25\,\mathrm{T\ m^{-1}}$ gradient is very large by the standards of MRI, but achievable in the highest pulsed magnetic field gradient systems used for laboratory diffusion measurement. In practice, the best resolution achieved in diffusion measurement, where the signal arises from the entire sample, is around 10 nm. For MRI however, the signal arises separately from each resolvable volume element (voxel). Hence spatial resolution is limited by the signal-to-noise available as the size of the voxel shrinks, leading to a resolution limit of around 10 microns.

Let us return to the concept of an isochromat of an inhomogeneous magnetic field, as described in Chapter 4. In MRI we might allow that the length scale for which the isochromat concept applies might be on the order of microns, whilst for very high magnetic field gradient NMR, a nanometre scale might be more appropriate. So long as this length scale is smaller than the feature to be resolved, we may treat the isochromats as part of an integrable continuum.

5.2.3 Phase evolution in the presence of a field gradient

In this section we introduce the idea of 'phase-encoding' of the spin magnetisation. In general, the ensemble of nuclear spins will be presented by a magnetisation vector (M_x, M_y, M_z). Only the $M_+ = M_x + iM_y$ components can contribute to the NMR signal, S. When a field gradient in B_0 exists, the magnetisation component M_z is

unaffected, while M_+ experiences a local phase evolution, dependent on position $\mathbf{r}$. Each isochromat evolves according to its local phase precession rate.

Behaviour of an isochromat

Let us assume the high field limit $B_0 \gg B(\mathbf{r})$, which commonly applies in MRI and in laboratory high field magnets. Then $\mathbf{G} = \nabla B_z$ and the local Larmor frequency for an isochromat of the spin system at position $\mathbf{r}$ may be written as in eqn 5.7.

In the rotating frame, with the detection frequency set on-resonance to ω_0, the isochromat contributes a transverse magnetisation $M_+(\mathbf{r}, t)d\mathbf{r}$ given by

$$M_+(\mathbf{r}, t) = M_+(\mathbf{r}, 0) \exp(-i\gamma \mathbf{r} \cdot \mathbf{G}t) \tag{5.11}$$

where $M_+(\mathbf{r}, t)$ is the local magnetisation density at $\mathbf{r}$. The minus sign in eqn 5.11 arises because under a Zeeman field $\mathbf{r} \cdot \mathbf{G}$ and hence Zeeman interaction $-\gamma \mathbf{r} \cdot \mathbf{G} I_z$, the density matrix operator, I_x, responsible for the measurement of M_x at $= 0$, precesses to $I_x \cos(\gamma \mathbf{r} \cdot \mathbf{G}t) - I_y \sin(\gamma \mathbf{r} \cdot \mathbf{G}t)$ at time t (see Fig. 4.16) . In other words, suppose we start with the transverse magnetisation along the rotating-frame x axis so that $M_+(0) = M_0$. Later in time it will have evolved to $M_0 \cos(\gamma \mathbf{r} \cdot \mathbf{G}t) - iM_0 \sin((\gamma \mathbf{r} \cdot \mathbf{G}t))$, meaning $M_x = M_0 \cos(\gamma \mathbf{r} \cdot \mathbf{G}t)$ and $M_y = -M_0 \sin(\gamma \mathbf{r} \cdot \mathbf{G}t))$.

Of course, the sign of the phase term is really a matter for arbitrary choice, since in a magnetic field gradient the offset frequency may be above or below resonance, depending on which side of the gradient field centre our isochromat is located. Consequently, we will mostly drop the minus sign, returning to it only when going back to fundamentals, as in the discussion of the Bloch–Torrey equation in Section 5.4.4.

Note that we have not allowed for T_2 relaxation over the detection period. This is easily handled by including an additional $-t/T_2$ term in the exponent, but for simplicity we will ignore the effect of relaxation here, a situation which would apply if the phase-spreading rate due to the magnetic field gradient, $\gamma \mathbf{r} \cdot \mathbf{G}$, greatly exceeds the relaxation rate T_2^{-1}.

The magnetisation helix and k-space

Let us picture our isochromats as spread along a particular axis, which for convenience, we will label z. Figure 5.2 shows a simple pulse sequence in which a 90°_x pulse is used to cause all spin isochromats to have their magnetisation vectors lying in the transverse plane along the y-axis. We will take the origin of time to be immediately following the 90°_x pulse, such that each isochromat at $t = 0$ has identical phase.

Now imagine that a magnetic field gradient of magnitude G is applied along the z-axis. In other words $\mathbf{G} = G\hat{\mathbf{k}}$ and for each isochromat the subsequent time evolution is given by

$$M_+(z, t) = M_+(z, 0) \exp(i\gamma z G t) \tag{5.12}$$

where, as discussed in the previous section, we choose for notational simplicity to use a positive argument for the gradient field precession. Figure 5.2 depicts, for each isochromat, the Argand plane in which their phase evolves.[4] Because at any time t the accumulated phase is proportional to the displacement of the isochromat along z, the

[4]The magnetisation helix concept was first introduced by Saarinen and Johnson [5].

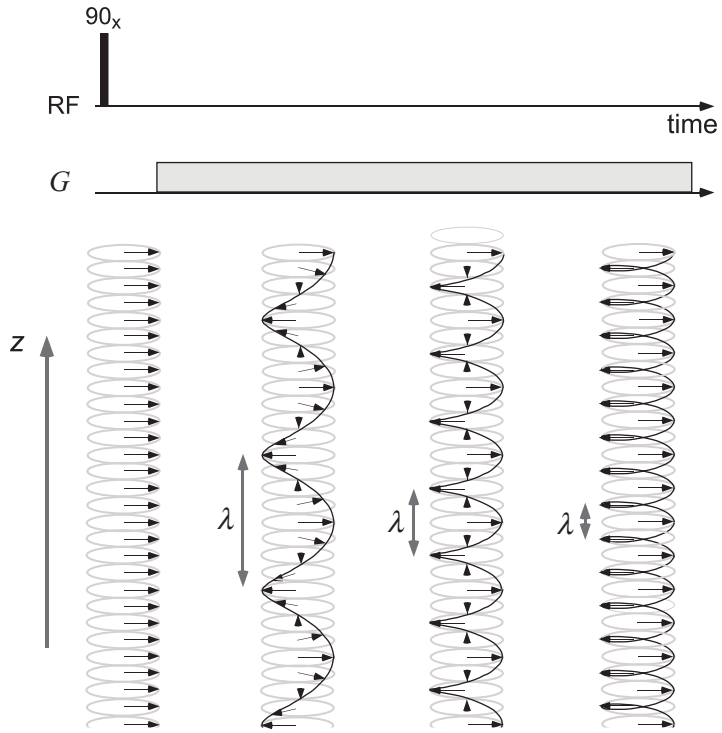

Fig. 5.2 Evolution of isochromat phase under the influence of a magnetic field gradient, G, along the z-axis following a 90°_x RF pulse. Immediately after the RF pulse the isochromats at different positions along the gradient axis start in phase. With time, a helix of magnetisation phase is gradually wound.

overall phase evolution pattern takes the form of a helix whose wavelength λ decreases with time as

$$\lambda = \frac{2\pi}{\gamma G t} \tag{5.13}$$

This magnetisation helix is extremely helpful in providing insight regarding the phase behaviour of spins under the influence of a magnetic field gradient. In analogy with the physics of diffraction, Mansfield [2] introduced the concept of a reciprocal space vector, $\mathbf{k}$, given by

$$\mathbf{k} = \gamma \delta \mathbf{g} \tag{5.14}$$

in units of angular spatial frequency, radians m^{-1} or

$$\check{\mathbf{k}} = (2\pi)^{-1} \gamma \mathbf{G} t \tag{5.15}$$

in units of cyclic spatial frequency, m^{-1}. Note that the use of the 'check' ($\check{}$) symbol is not at all standard and is introduced in this book to distinguish the two forms in

common use, for which universally, and perhaps confusingly, the symbol **k** is used. The cyclic frequency form has some advantages in providing transform symmetry as we shall see. But whether one chooses angular or cyclic frequency forms is ultimately a matter of taste.

Under such a gradient of arbitrary direction, the phase evolution of any isochromat at position **r** can be written

$$M_+(\mathbf{r},t) = M_+(\mathbf{r},0)\exp(i\mathbf{k}\cdot\mathbf{r}) \tag{5.16}$$

It is clear that **k**-space may be traversed by moving either in time or in gradient magnitude. However, the direction of this traverse is determined by the direction of the gradient **G**.

5.3 Magnetic resonance imaging

Both the NMR measurement of translational motion and the imaging of nuclear spin positions, otherwise known as magnetic resonance imaging or MRI, are based on ideas that are closely linked. Both utilise magnetic field gradients. Both draw on spatial Fourier relationships. And the two methods can be intertwined, for example in the use of sample slice selection or in the spatial localisation of translational dynamics. Consequently it is sensible that some of the essential physics of MRI is reviewed here. However, given that a more detailed description of imaging methods was the subject of an earlier book by this author [6], there seems little reason to repeat those details here and readers are referred to this and other texts dealing with MRI methods [7–10].

5.3.1 Spatial Fourier relations

Suppose that we reveal the gradient-related phase of the isochromat, by normalising with the total sample signal at $t = 0$, $M_+(0)$. Let the local normalised spin density be $\rho(\mathbf{r})$. Then $M_+(\mathbf{r},0)/M_+(0) = \rho(\mathbf{r})$ and the total normalised signal S_N is $\int M_+(\mathbf{r},t)/M_+(\mathbf{r},0)d\mathbf{r}$, where the symbol $d\mathbf{r}$ is used to represent volume integration. In the formalism of **k**-space, and using the concept of the Fourier transform and its inverse,

$$S_N(\mathbf{k}) = \int \rho(\mathbf{r})\exp(i\mathbf{k}\cdot\mathbf{r})d\mathbf{r} \tag{5.17}$$

$$\rho(\mathbf{r}) = (2\pi)^{-1}\int S_N(\mathbf{k})\exp(-i\mathbf{k}\cdot\mathbf{r})d\mathbf{k} \tag{5.18}$$

or

$$S_N(\check{\mathbf{k}}) = \int \rho(\mathbf{r})\exp(i2\pi\check{\mathbf{k}}\cdot\mathbf{r})d\mathbf{r} \tag{5.19}$$

$$\rho(\mathbf{r}) = \int S_N(\check{\mathbf{k}})\exp(-i2\pi\check{\mathbf{k}}\cdot\mathbf{r})d\check{\mathbf{k}} \tag{5.20}$$

Equations 5.17, 5.18, 5.19, and 5.20, state that the signal, $S_N(\mathbf{k})$, and the spin density, $\rho(\mathbf{r})$, are mutually conjugate. These are the fundamental relationships of NMR imaging.[5]

[5]Note that the use of cyclic rather than angular frequency units for **k** necessitates the inclusion of the 2π factor in the exponent. The advantage of this choice is that it symmetrises the forward and inverse Fourier relations and avoids the need for further 2π coefficients in front of these integrals.

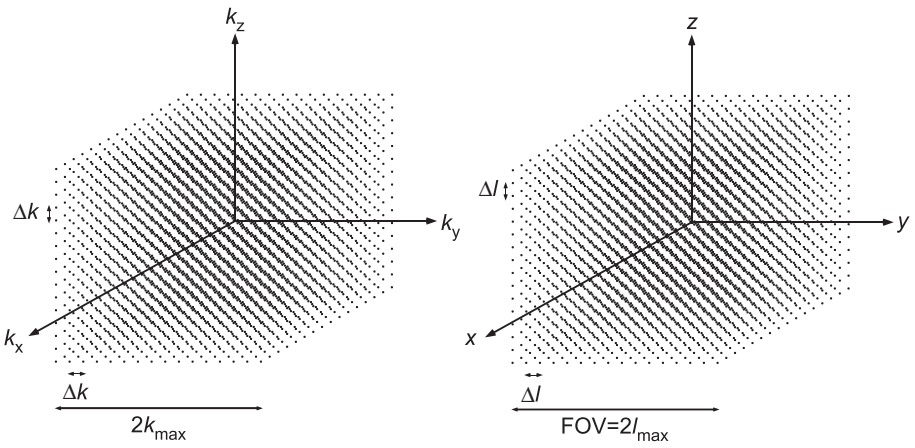

Fig. 5.3 3-D matrices for **k**-space (left) and real space (right).

The process of MRI thus requires that one samples the signal $S_N(\mathbf{k})$ in a discrete **k**-space, for example on a Cartesian grid as represented by a 3-D matrix of N^3 data points, where each dimension $\check{k}_x$, $\check{k}_y$, and $\check{k}_z$ ranges from $-\frac{1}{2}N\Delta\check{k}$ to $(\frac{1}{2}N-1)\Delta\check{k}$, with the stepping interval being $\Delta\check{k} = 2\check{k}_{max}/N$. On digital Fourier transformation this leads to a conjugate real space matrix representing the image, $\rho(\mathbf{r})$, represented by a 3-D matrix of N^3 data points, where in each dimension x, y, and z ranges from $-\frac{1}{2}N\Delta l$ to $(\frac{1}{2}N-1)\Delta l$, with the stepping intervals being $\Delta l = 2l_{max}/N$. These conjugate matrices are shown in Fig. 5.3. The Fourier relation dictates that the resolution for each component in real space is determined by the sampling range of each corresponding component in $\check{\mathbf{k}}$-space, so that

$$\Delta l = \frac{1}{2\check{k}_{max}} \tag{5.21}$$

while the field of view (FOV) for each component in real space, for example $2l_{max}$, is given by

$$\begin{aligned} FOV &= \frac{1}{\Delta\check{k}} \\ &= \frac{N}{2\check{k}_{max}} \end{aligned} \tag{5.22}$$

5.3.2 Trajectories in k-space

The manner in which **k**-space is sampled depends on the particular pulse sequence used, an almost infinitely varied range of possibilities being possible. Whether sampled on a Cartesian grid, a polar grid, or via any other coordinate system, the principles of sampling and image reconstruction are encapsulated in the Fourier relations of eqns 5.17 and 5.18. Of course, a traverse through **k**-space implies a stepping of either gradient or time variables. The former is known as phase encoding and the latter, frequency encoding. Figures 5.4 and 5.5 show examples of two different sampling schemes,

the first a purely phase-encoding approach and the second involving a combination of phase and frequency encoding [11].

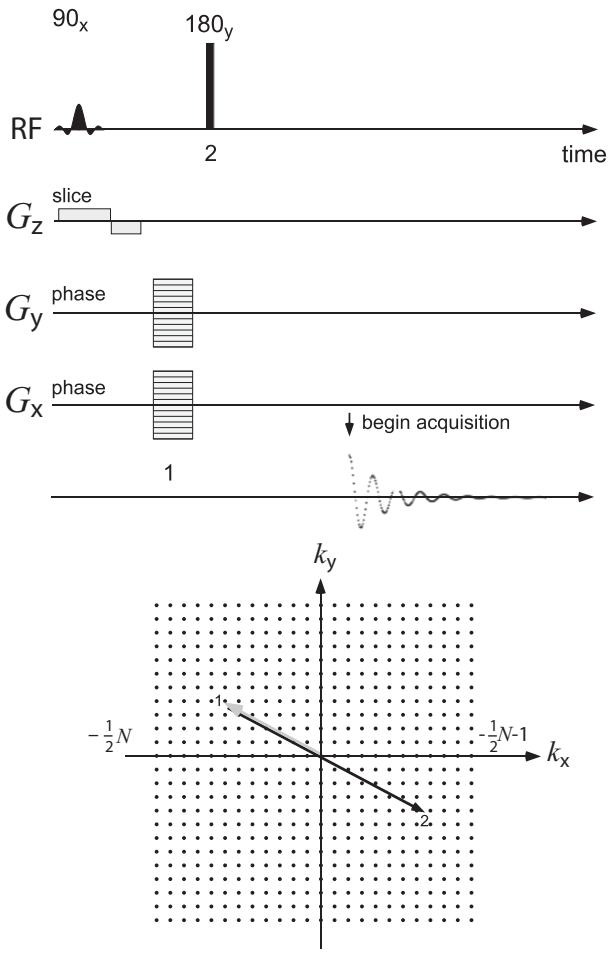

Fig. 5.4 Two-dimensional imaging pulse sequence along with **k**-space trajectory, in the case of pure phase encoding. The sequence starts with a soft RF pulse, which excites only a plane of spins normal to the z-axis. Subsequently, gradient pulses in both the x and y directions cause a phase traverse (1) to a point in the (k_x, k_y) plane determined by the particular amplitudes chosen for G_x and G_y, as well as their fixed duration. Next a 180° RF pulse inverts all the phases of the spins (2), allowing a spin echo to be formed. Acquisition of the signal begins at the centre of the echo and an FID is obtained in the absence of any magnetic field gradient, thus allowing full spectral resolution. The sequence must be repeated N^2 times to sweep out all points in **k**-space.

The frequency encoding method of using time as the variable involves sampling the signal at successive intervals under a steady 'read-out' gradient. Thus the frequency

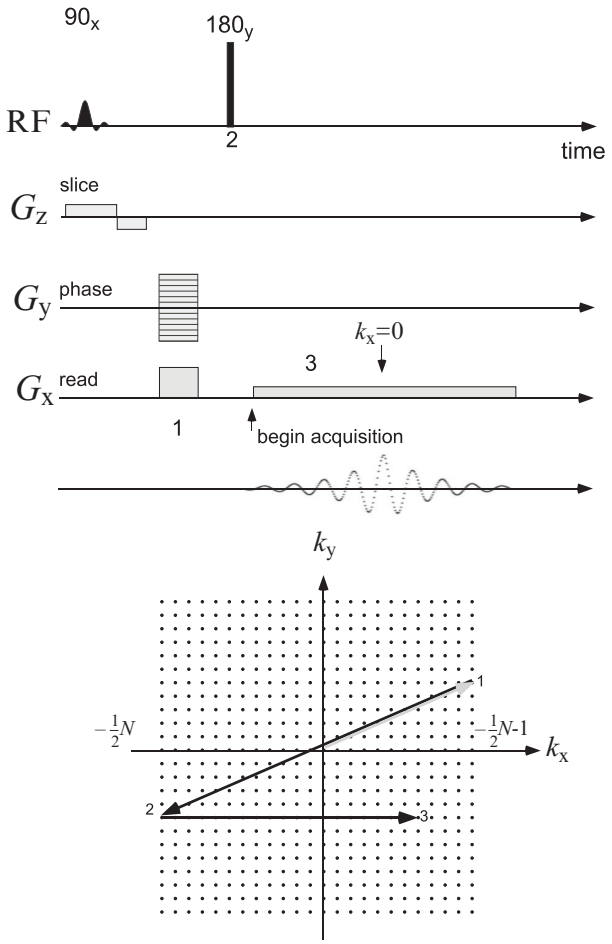

Fig. 5.5 Two-dimensional imaging pulse sequence along with **k**-space trajectory, in the case of combined phase and read encoding. The sequence starts with a soft RF pulse, which excites only a plane of spins normal to the z-axis. Subsequently, gradient pulses in both the x and y directions cause a phase traverse (1) to a point at the edge ($k_x = k_{max}$) of the (k_x, k_y) plane determined by the particular amplitudes chosen for G_x and G_y. Next a 180° RF pulse inverts all the phases of the spins (2), allowing a spin echo to be formed under an applied readout gradient (3). Acquisition of the signal takes place along a k_x line and at a k_y value set by the initial phase-encoding pulse. This signal, which is obtained right through the positive and negative k_x, is obtained in the presence of the readout magnetic field gradient, thus masking any spectral resolution. The sequence must be repeated only N times to sweep out all points in **k**-space.

encoding gradient is sometimes called the read gradient. Given that the suggested digital sampling implies a traverse through both negative and positive **k**-space, the reader may wonder how this is possible when time is the variable. The practical solution is

provided by the spin echo, in which the natural origin of time is the echo centre so that negative time corresponds to the time displacement before that origin. For frequency encoding, $S_N(\mathbf{k})$ is measured in the time domain while the Fourier transform, which yields $\rho(\mathbf{r})$, is therefore in the frequency domain. In this simple sense we can say that there is a correspondence between real space and frequency, and between reciprocal space and time.

For phase-encoding, a fixed time interval is used, during which the phase gradient is applied and the spin phases are allowed to evolve. Actually, as is clear from eqn 5.15, both $\mathbf{G}$ and t are involved in determining $\mathbf{k}$-space. For each phase gradient value shown in Fig. 5.4, one signal acquisition is possible.[6] In the case of the 2-D imaging scheme of Fig. 5.5, where a readout gradient is used, N independent phase-encoding steps are required to traverse $\mathbf{k}$-space, while in Fig. 5.4 where pure phase encoding is used, N^2 steps are required. While pure phase encoding is clearly less efficient, it does have particular virtues. First the lack of a read gradient means that the FID is available for spectral resolution, making it possible to spatially localise any feature of the NMR spectrum. Second, it is possible to use single-point ($t = 0$) time sampling, meaning that there is none of the perturbation apparent in the readout direction associated with relaxation effects, inhomogeneous broadening, or spectral interference. Thus these image-distorting contributions can be avoided when one is desirous of sampling spectral shifts due to the phase gradients alone. For that reason pure phase encoding has particular application either in chemical imaging for liquids where spectral effects are of interest, or in the imaging of solids where relaxation and spectral broadening effects are severe.

5.3.3 Selective excitation

Soft and hard pulses

Selective excitation involves applying an RF pulse that affects only a specific region of the NMR frequency spectrum. By this means, only nuclei of a certain chemical shift may be disturbed or, when the spectral properties of the spins are dominated by the spread of Larmor frequencies in the presence of a magnetic field gradient, the selective RF pulse may be used to excite only those spins within some specified layer of the sample. We shall refer to these respective uses as chemical selection and slice selection.

Efficient and precise selective excitation is a vital component of most NMR imaging techniques. The principle underlying the excitation of spins in a specified region of the spectrum is as follows. The bandwidth of frequencies contained in an excitation pulse is inversely proportional to the pulse duration. For example, if the 90° pulse has a duration, T, of order 1 ms, then only those spins with a resonant frequency within a 1 kHz bandwidth of the radiofrequency will be stimulated in an appreciable manner. In normal NMR spectroscopy the pulse duration is made sufficiently short that the associated bandwidth covers the chemical shifts of all spins of a given nuclear species. Clearly the bandwidth of the pulse is simply related to the RF amplitude. A non-selective (broadband) 90° pulse will have a very much larger magnitude, B_1, than a selective (narrowband) 90° RF pulse, since the turn angle is determined by the product $\gamma B_1 T$.

[6] In multi-echo schemes, such as echo planar imaging [12] or RARE [13], multiple phase encoding steps may be achieved in a single echo train.

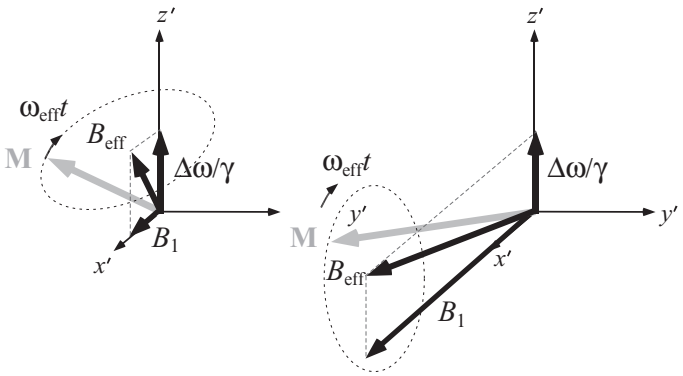

Fig. 5.6 Soft pulse effect showing different magnetisation nutation in rotating frame for spins that are off-resonant. On the left is the soft pulse, where the RF field amplitude is comparable with the field offset, and the spins are only weakly disturbed from equilibrium. On the right, the hard pulse with a much larger RF field amplitude results in a nutation that is closer to ideal for off-resonant spins.

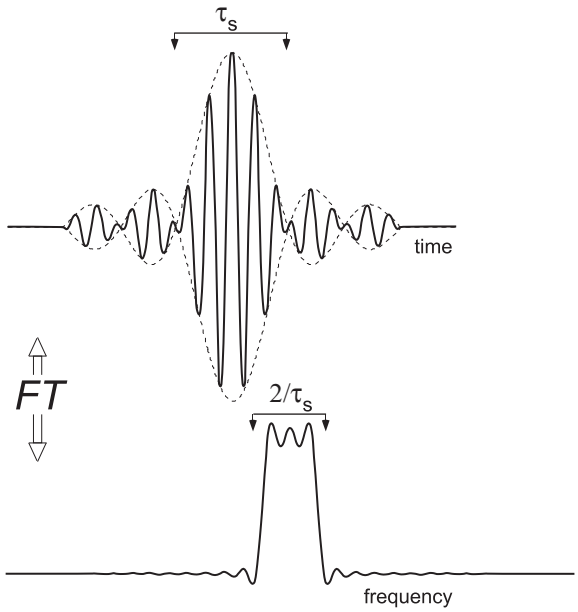

Fig. 5.7 Amplitude-modulated oscillatory waveform and its Fourier transform for the case of a double lobe sinc modulation. The spectrum shows some oscillatory deviation from the ideal rectangular response, due to the sinc lobe truncation.

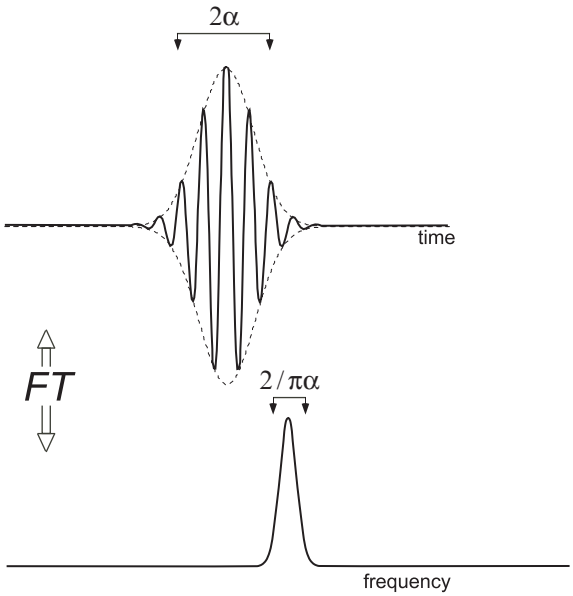

Fig. 5.8 Amplitude-modulated oscillatory waveform and its Fourier transform for the case of a Gaussian modulation. The spectrum is also Gaussian.

The crucial factor in determining the effect on other spins is the relative size of the RF field precession frequency, $\omega_1 = \gamma B_1$, and the resonance offset, $\Delta\omega_0$. Suppose that an RF pulse is applied with a reduced bandwidth, but with a magnitude and duration so as to cause 'on-resonant' spins to precess through 90° into the transverse plane. Spins with Larmor frequencies far from the RF excitation frequency ($\Delta\omega_0 \gg \omega_1$) will experience an effective field in the rotating frame considerably tilted towards the longitudinal axis as shown in Fig. 5.6. Unlike the on-resonant spins they will therefore be tipped through an angle less than 90°. Intense broadband excitation pulses are termed 'hard' pulses, while the weak, narrowband pulse is termed 'soft'.

The simplest form of soft pulse is obtained by simply reducing the amplitude and extending the duration of the usual rectangular time-domain profile. The corresponding frequency spectrum of this pulse is given by the Fourier transform, namely the sinc function shown in Fig. 5.7. Clearly the weak rectangular pulse suffers from having side lobes, so that, while the majority of the excitation is close to the central frequency, extensive excitation due to the lobes occurs over a wide bandwidth. One solution is to 'soften' the edges of the RF pulse, for example by the use of Gaussian shaping in the time domain, as shown in Fig. 5.8. Gaussian pulses are very effective in chemical shift selective excitations.

Evolution during selective excitation

Rectangular excitation requires 90° or 180° precessions for spins within a well-defined range normal to the slice plane and zero precession for spins outside. This implies that the frequency response of the RF pulse should have a rectangular profile and so, in the

time domain, should be modulated in *sinc* ($\sin(at)/(at)$) form, the Fourier transform of the hat function. However, such a model assumes that the nuclear spins behave as a linear system whereas a linear response [14] can only be true for small excitation angles. Consider a weak RF field $\omega_1(t) = \gamma B_1(t)$ applied along the rotating frame x-axis over the time period $-T < t < T$, during which a gradient G_z is applied along the z-axis. The magnetisation in this linear response approach may be written

$$M_+(z) = iM_0 \exp(-i\gamma G_z z T) \int_{-T}^{T} \omega_1(t) \exp(i\gamma G_z z dt) dt \tag{5.23}$$

The integral is simply the Fourier transform, or spectrum, of the RF pulse of finite duration. The frequency scale for this spectrum is $\gamma G_z z$, so that the integral represents the amplitude of the RF corresponding to the Larmor frequency of the spin plane labelled by z. Equation 5.23 states that the magnetisation contribution to the FID, $M_+(z)$, from isochromats at z, is proportional to the amplitude of the RF spectrum at z. If we want to excite a rectangular slice then we will need a rectangular spectrum. Second it tells us that the magnetisation for a spin plane normal to z has a net phase shift, $\gamma G_z z T$, which is a nuisance since the phase shift will vary across a slice of finite thickness. It is, however, easy to remove, since all we have to do is apply an opposite sign z gradient of magnitude $-G_z$ for a time T.[7]

Despite the bold approximations inherent in its use, the linear assumption is very helpful and moderately accurate when applied to finite turn angles, as discussed in reference [6]. There, numerical solutions to the Bloch equations suggest that for tip angles of up to 90°, the results are not too dissimilar to the linear prediction, hence justifying this rather simple but illuminating approach.

While the description of selective 90° pulses using a linear response theory is similar to the exact solution, for 180° selective pulses the effect of non-linearity distortions is far more severe and artefacts result [15, 16]. However, when a selective 180° pulse is used for phase inversion, for example as part of a spin-echo scheme, these phase errors are less severe and most out-of-slice magnetisation generated by the pulse tends to lie along the rotating frame z-axis. Hence, slice-selective 180° inversion pulses based on sinc modulation are used routinely in MRI to good effect.

5.4 Translational motion encoding

Powerful insight is provided by the evolving magnetisation helix associated with transverse magnetisation precession of spin isochromats distributed along the axis of a uniform magnetic field gradient. The helix graphically illustrates the relationship between spin phase and molecular position. It suggests an inherent wavelength λ and spatial frequency $k = 2\pi/\lambda$ associated with the distribution of spin precessions. And it allows us to visualise, in a very natural manner, the effect of the migration of spin-bearing molecules over the duration of precession.

Suppose we reverse the sign of the magnetic field gradient at some time τ following its imposition at $t = 0$, as shown in Fig. 5.9. Provided the spins remain in their original

[7] Or alternatively we can invert all the spin phases with a 180° RF pulse and then apply the identical sign gradient for this same time T.

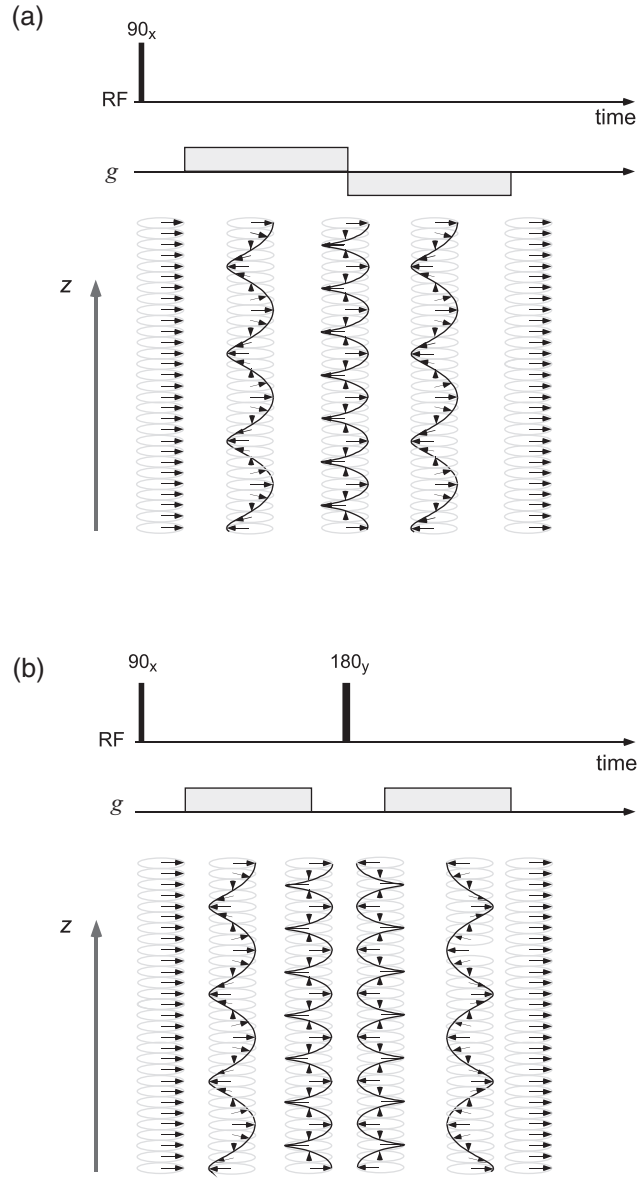

Fig. 5.9 (a) Gradient echo and (b) spin echo under the influence of gradient pulses of amplitude g. In (a), sign reversal of the gradient causes the magnetisation helix to unwind. In (b) the 180° RF pulse inverts the phase of the helix, so that a subsequent gradient pulse of the same sign has the effect of rewinding. The echo occurs when all the spin isochromats come into phase registration.

positions, the effect of the gradient reversal will be to unwind all the phases so that, once the reversed gradient has acted for an equal period τ, the isochromats will have been restored to their original states of identical phase and an echo will have been formed. That echo could take the form of the gradient echo as in Fig. 5.9(a) or the spin echo of Fig. 5.9(b). In the latter case, rather than reversing the gradient direction, the spin phases are reversed by a 180° RF pulse, so that unwinding occurs under a same-sign gradient.[8]

Figure 5.9 makes it clear that perfect echo formation is only possible if the spin-bearing molecules remain fixed in position. Any translational motion will cause perturbations to the phase evolution so that the history of the motion becomes embedded in the final phase distribution. In general we observe that the use of time-varying gradients allows insight regarding molecular translation. The key determinant of the phases embedded in the spin system following a period of motion in the presence of these field gradients depends crucially on the combined effects of the time dependence of the gradients and the time dependence of molecular translation.

Historically, the two simple variants of translational motion of interest in considering the effect of magnetic field gradients were unrestricted self-diffusion and coherent streamline flow. For these particular cases, quite simple theory is available to predict the NMR signal under the most general gradient waveforms. However, the power of NMR is that it permits in principle the elucidation of more complex motion, of restricted or timescale-dependent diffusion, of incoherent or periodic flow, of spatially inhomogeneous dynamics, or of fluid dispersion with specific spatio-temporal structure. For such applications the time dependence of the gradient waveform may need to be specially tailored to circumstance, and an appropriate theoretical treatment expressed. In the remainder of this chapter we will lay out the basics of this approach.

In embarking on this exercise, it needs to be admitted up front that there does not exist an exact theory that gives analytic closed form expressions for any motion under any gradient. However, we can come sufficiently close to such expressions that simple numerical implementations can bridge the final step. Before addressing that bridge, we first review the case where precise mathematical description is indeed possible.

5.4.1 Time-varying gradients and phase factors

The first step in writing down the phase evolution for a moving spin under the influence of time varying gradient, $\mathbf{g}(t)$, is pretty obvious. We will ignore transverse relaxation at this point, noting that it can be easily incorporated when needed. To distinguish gradients used for motion measurement from those used for imaging, we use a lower case $\mathbf{g}(t)$ for the former. The distinction is arbitrary of course, since any gradient, whether intended for imaging or motion measurement, can engender sensitivity to both. However, when $\mathbf{g}(t)$ is used we will normally be dealing with an experiment where an echo is formed at time t, which, as we shall see, will require $\int_0^t \mathbf{g}(t')dt' = 0$.

Consider a spin isochromat labelled by starting position $\mathbf{r}_0$, such that the position of the spin at later time t is $\mathbf{r}(t)$. Then the signal contribution from that isochromat is

[8]We will see later how to treat these approaches interchangeably using the idea of an 'effective gradient'.

$$M_+(\mathbf{r}_0, t) = M_+(\mathbf{r}_0, 0) \exp(i\gamma \int_0^t \mathbf{g}(t') \cdot \mathbf{r}(t') dt') \tag{5.24}$$

To estimate the total signal we would need to sum the contributions from all starting positions, $\mathbf{r}_0$. However, in the case of self-diffusion or other complex motions such as dispersive flow, there exists a distribution of possible molecular trajectories for every starting position. This requires us, even before summing over starting positions, to deal with the ensemble average implied by that. In other words, labelling each spin in the sub-ensemble by j, eqn 5.24 would need to be modified to read

$$M_+(t) = \int d\mathbf{r}_0 M_{+j}(\mathbf{r}_0, 0) \langle \exp(i\gamma \int_0^t \mathbf{g}(t') \cdot \mathbf{r}_j(t') dt') \rangle_{j-ensemble} \tag{5.25}$$

The evaluation of ensemble averages of phase factors is a central theme in physics. We saw this earlier in Chapter 4 in dealing with the Anderson–Weiss treatment of relaxation caused by time-varying fields. In that case the use of a Gaussian phase approximation (GPA) allowed for easy evaluation and such an approach has direct application in helping us deal with a number of problems associated with molecular motion under magnetic field gradients. For the moment however, it is enough to make the point that exact evaluation of eqn 5.25 is not trivial.

Effective gradients, the spin echo and gradient echo

The phase shift experienced at time t by a nuclear spin j following the path $\mathbf{r}_j(t')$ in a gradient $\mathbf{g}(t')$ is

$$\phi_j(t) = \gamma \int_0^t \mathbf{g}(t') \cdot \mathbf{r}_j(t') dt' \tag{5.26}$$

This simple relation takes no account of the influence of RF pulses on the spin phase. For example, a 180°_y pulse inverts all prior phase shifts, an effect which is equivalent to that which would result if we had used a negative value of gradient up to the time of the RF pulse. This suggests that we can take account of RF pulses by defining an 'effective gradient', $\mathbf{g}^*(t)$, which has the actual sign at the current time t, but is historically inverted by all prior 180°_y pulses. In the case of 90°_y RF pulses, the value of $\mathbf{g}^*$ is transformed to zero since such RF pulses leave magnetisation along the z-axis are immune to precession. The effect is illustrated in Fig. 5.10. More generally, $\mathbf{g}^*$ is defined by the equivalence of its Hamiltonian,

$$\begin{aligned} \mathcal{H}(t) &= -\gamma \mathbf{g}^*(t) \cdot \mathbf{r}_j(t) I_{jz} \\ &= -\gamma \mathbf{g}(t) \cdot \mathbf{r}_j(t) U_{RF}^\dagger I_{jz} U_{RF} \end{aligned} \tag{5.27}$$

where U_{RF} is the ordered product of evolution operators associated with the history of prior RF pulses.

Let us try to simplify eqn 5.25 so that we can see how it applies in some special cases. First, let's allow that the spin does not move, whence $\mathbf{r}_j(t) = \mathbf{r}_0$. Then

$$M_+(t) = \int d\mathbf{r}_0 M_+(\mathbf{r}_0, 0) \exp(i\gamma \mathbf{r}_0 \cdot \int_0^t \mathbf{g}^*(t') dt') \tag{5.28}$$

At any time t such that $\int_0^t \mathbf{g}^*(t') dt' = 0$, $M_+(t) = M_+(0)$ and an echo is formed. Thus the condition for the echo is that the time integral of the effective gradient is

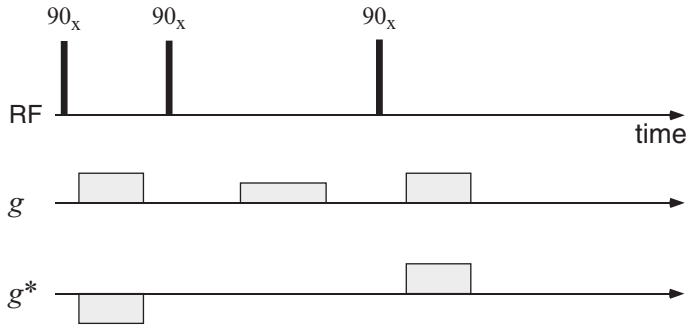

Fig. 5.10 A stimulated-echo sequence in which magnetic gradient pulses appear in the dephasing period before the second (90°_x) RF pulse, in the rephasing period after the third (90°_x) RF pulse, and as a homospoiling gradient between the second and third RF pulses. Note the effective gradient, g^*, which is only sensitive to gradient applied when the spins have transverse magnetisation.

zero. In the case of the gradient echo, no RF pulses are used and $\mathbf{g}^*(t) = \mathbf{g}(t)$, while for the spin echo, the role of RF pulses must be accounted for in determining $\mathbf{g}^*(t)$.

The normalised echo signal

Up to this point we have been accounting for the total signal by summing over isochromats as $\int d\mathbf{r}_0 M_+(\mathbf{r}_0, 0)$. Such an integral can be used to allow for non-uniform spin density across $\mathbf{r}_0$. We could also allow for relaxation effects by incorporating appropriate decays $\exp(-t/T_2)$ and $\exp(-t/T_1)$ during periods when the spin magnetisation resides in the transverse plane or along the longitudinal axis. But in many cases we are only concerned to understand the role of the applied gradient $\mathbf{g}^*(t')$, in its ability to impart phase shifts to the total magnetisation as a result of spin translational motion. The easiest way to demonstrate that is to use a signal normalised to the case $\mathbf{g}^*(t') = 0$, namely

$$E(t) = \frac{M_+(t)_{\mathbf{g}^*(t')\neq 0}}{M_+(t)_{\mathbf{g}^*(t')=0}} \tag{5.29}$$

This signal, when used to measure motion instead of position, will be ideally sampled when all phase shifts due to starting position alone will be zero, in other words the echo condition $\int_0^t \mathbf{g}^*(t')dt' = 0$. Hence we may refer to $E(t)$ as the *normalised echo amplitude*.

Note that this normalisation of relaxation, such that all translational motion is associated with gradient-induced phase shifts, is only true if relaxation effects are not correlated with position. In other words we require that relaxation is a uniform process intrinsically associated with each nuclear spin and not related to where the spin-bearing molecule resides within the sample. An example of a positional correlation where relaxation is coupled with geometry would be where additional relaxation mechanisms occur at surfaces bounding the fluid. The effects of such surface relaxation will be considered in the next chapter. For the rest of Chapter 5, however, the uniform relaxation assumption will apply so that relaxation normalisation is straightforward.

5.4.2 Coherent spin motion: velocity, acceleration, and jerk

In the special case that the molecules all have a common motional behaviour (which specifically precludes Brownian motion), eqn 5.26 yields a simple result.[9] For example, suppose that the motion comprises some constant velocity, $\mathbf{v}$, then $\mathbf{r}_j(t')$ is $\mathbf{r}_j(t')+\mathbf{v}t'$. Where an acceleration term is present, then $\mathbf{r}_j(t')$ is $\mathbf{r}_j(t') + \mathbf{v}t' + \frac{1}{2}\mathbf{a}t'^2$.

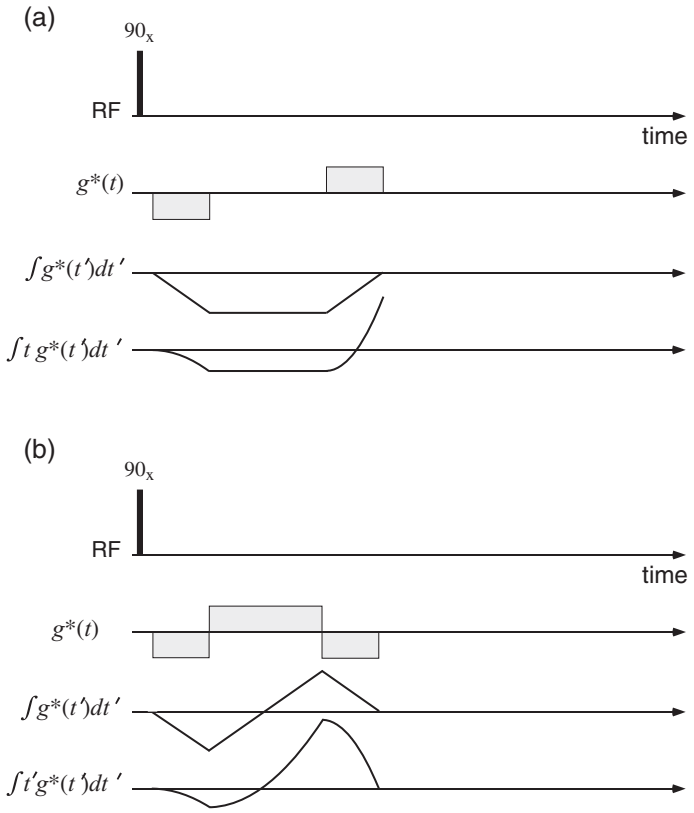

Fig. 5.11 Effective gradient sequences resulting in the echo condition $\int_0^t g^*(t')dt' = 0$, but with first moment $\int_0^t t'g^*(t')dt'$ non-zero in (a) and zero in (b).

It is clear that the resulting phase shifts involve successively higher moments of $\mathbf{g}^*(t)$. The zeroth moment, $\int_0^t \mathbf{g}^*(t')dt'$, is required to be zero if the final phase shift is to depend only on the motion and not on the starting positions of the spins. This is, of course, the condition for a spin echo to be formed! Furthermore, by choosing a specific time dependence for $\mathbf{g}^*(t)$, we can make the echo sensitive to either velocity, acceleration, or the next higher time derivative of displacement (sometimes known as 'jerk'). In particular, the final phase modulation of the spin echo will consist, in the case of the moment expansion, of

[9]Here we use the effective gradient $\mathbf{g}^*(t)$ to apply to any gradient waveform and RF pulse sequence.

$$E(t) = \exp(i\gamma\mathbf{v} \cdot \int_0^t t'\mathbf{g}^*(t')dt' + i\gamma\mathbf{a} \cdot \int_0^t t'^2\mathbf{g}^*(t')dt' + ...) \tag{5.30}$$

Examples of pulse sequences in which the effective gradient obeys the echo condition are shown in Fig. 5.11. In Fig. 5.11(a) the echo will be sensitive to velocity while in (b) it is sensitive to acceleration but produces no phase shift for steady flow.

5.4.3 The Carr–Purcell analysis of diffusion effects

We now turn to the problem of Brownian motion. One of the earliest attempts to deal with the effect of molecular self-diffusion in the presence of time-varying gradients was provided by Carr and Purcell [17]. In their treatment, unrestricted self-diffusion is pictured as a succession of discrete hops with motion resolved in one dimension, the direction of the field gradient. The independence of motion in other directions means that we treat dimensions separately, obtaining total displacements where necessary by adding quadratically according to the Pythagoras theorem. The method is ideally suited to piecewise-constant gradient waveforms. In the following section we meet a treatment more suited to continuously varying gradients. Nonetheless, the Carr–Purcell approach is sufficiently illuminating to warrant our interest.

The particle hopping model

The principle behind the Carr–Purcell approach is the definition of a fundamental diffusion jump with mean time τ_s and rms displacement in one dimension, ξ. A molecule has equal probability of jumping to the left or right so that the distance travelled after n jumps at time $t = n\tau_s$ is given by

$$Z(n\tau_s) = \sum_i^n \xi a_i \tag{5.31}$$

where a_i is a random number equal to ± 1. Z represents the z-axis displacement of molecules from their respective origins. Thus

$$\overline{Z^2(n\tau_s)} = \sum_i^n \sum_j^n \xi^2 \overline{a_i a_j} \tag{5.32}$$

where the over bar represents an ensemble average. Because a_i randomly varies between ± 1, $\overline{a_i a_j} = 0$ unless $i = j$, so that all cross terms cancel. Thus

$$\overline{Z^2(n\tau_s)} = \sum_i^n \xi^2 \overline{a_i^2} = \xi^2 \sum_i^n 1 = n\xi^2 \tag{5.33}$$

Defining the self-diffusion coefficient as

$$D = \xi^2/2\tau_s \tag{5.34}$$

we obtain

$$\overline{Z^2(t)} = 2Dt \tag{5.35}$$

and for three dimensions,

$$\overline{R^2(t)} = 6Dt \tag{5.36}$$

Signal attenuation under a steady gradient

Next we calculate the influence of this motion on the coherence of transverse magnetisation in the case where a steady magnetic field gradient, $g = \partial B/\partial z$, is present, following the method originally used by Carr and Purcell in their classic paper on spin echoes [17]. The only motion that will concern us is that along the field gradient axis, z. For convenience we consider the influence of diffusion on the transverse magnetisation of spins originating at z. Then the local Larmor frequency after m jumps is

$$\omega(m\tau_s) = \gamma B_0 + \gamma g z + \gamma g \sum_{i=1}^{m} \xi a_i \tag{5.37}$$

so that the cumulative phase angle after time $t = n\tau_s$ is

$$\phi(t) = \gamma B_0 t + \gamma g z t + \gamma \sum_{m=1}^{n} g\tau_s \sum_{i=1}^{m} \xi a_i \tag{5.38}$$

The first term in eqn 5.38 represents the constant average Larmor precession and is of no particular interest here. The second is the phase spread due to starting positions of spins. We shall return to that effect later. But for the moment we shall only be concerned with the third, phase deviation term, which varies randomly across the ensemble and so causes irreversible dephasing. Note that it contains two parts. The second (outer) sum tells us the local Larmor frequency after m hops. The first sum adds the cumulative precessions resulting from that local frequency with local dwell time τ_s. The dephasing part of eqn 5.38 may be rewritten

$$\Delta\phi(t) = \gamma g \tau_s \xi \sum_{i=1}^{n} (n + 1 - i) a_i \tag{5.39}$$

The proof of this relationship is best demonstrated pictorially, as in Fig. 5.12, where each row in the triangle indicates the successive, random, value of a_i up to time $m\tau_s$, and the horizontal sum of these elements gives the phase shift that occurs in the interval τ_s, while the spin is at the current location. The total phase shift accumulating at time t is given by the area of the triangle multiplied by $\gamma g \tau_s \xi$.

What we wish to calculate is $\overline{\exp(i\Delta\phi)}$, the coefficient by which the ensemble-averaged transverse magnetisation will be phase modulated as a result of the diffusional motion in the presence of the gradient. Of course $\Delta\phi(t)$ varies randomly over the ensemble. We will assume that its distribution, $P(\Delta\phi)$, is Gaussian, a good assumption when dealing with the sum of very many randomly varying quantities, a result known as the 'central limit theorem' [18]. Thus

$$\overline{\exp(i\Delta\phi)} = \int_{-\infty}^{\infty} P(\Delta\phi) \exp(i\Delta\phi) d(\Delta\phi) \tag{5.40}$$

Since $P(\Delta\phi)$ is given by the normalised Gaussian function, $(1/2\pi\overline{(\Delta\phi)^2})^{1/2} \exp(-\Delta\phi^2/2\overline{(\Delta\phi)^2})$, eqn 5.40 yields

$$\overline{\exp(i\Delta\phi)} = exp(-\overline{(\Delta\phi)^2}/2) \tag{5.41}$$

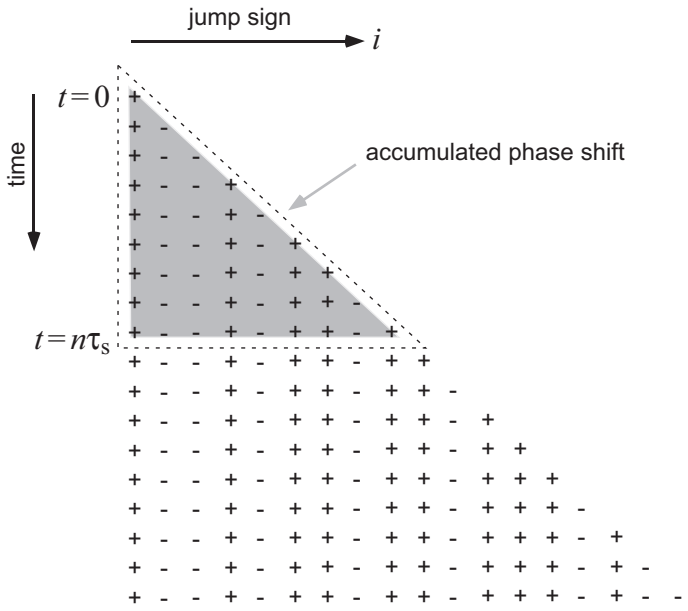

Fig. 5.12 Cumulative phase diagram in which the sign at the end of each row indicates whether the jump in the current τ_s interval is positive or negative with respect to the gradient direction. The precessional phase shift that results during that interval is determined by the net position along the gradient axis and is therefore calculated by summing jumps along the row. The cumulative phase shift at time t is given by the sum within the shaded triangle.

This coefficient represents a simple attenuation of the magnetisation and hence the signal at time t. In order to evaluate $\overline{\Delta\phi^2}$, we square eqn 5.39 and take an ensemble average. Once again, cross terms disappear. Thus

$$\begin{aligned}\overline{(\Delta\phi)^2} &= \gamma^2 g^2 \tau_s^2 \xi^2 \sum_{i=1}^{n} (n+1-i)^2 \\ &= \gamma^2 g^2 \tau_s^2 \xi^2 \sum_{j=1}^{n} j^2 \\ &= \tfrac{1}{3}\gamma^2 g^2 \tau_s^2 \xi^2 n^3 \end{aligned} \tag{5.42}$$

where the last sum is evaluated assuming that n is large. (Note that this is the standard mean-squared phase shift for a triangular section of steps, as shown in Fig. 5.12, where n represents the numbers of steps in the orthogonal sides.) Substituting eqn 5.34, we find that the signal attenuation due to diffusion is expressed by the coefficient

$$\overline{\exp(i\Delta\phi)} = \exp(-\tfrac{1}{3}\gamma^2 g^2 D t^3) \tag{5.43}$$

This t^3 dependence is characteristic of self-diffusion in the presence of a steady gradient.

Of course eqn 5.43 only tells us about phase spreading due to migrations of molecules, based on a common displacement from $z = 0$, and ignoring the second term in eqn 5.38. In practice, our sample is of finite size and so starting positions for molecules are distributed as $\rho(z)$ along the gradient axis.[10] Hence the total signal phase will need to account for this initial distribution as

$$\begin{aligned}\overline{\exp(i\phi)} &= \left(\int_{-\infty}^{\infty} \rho(z)\exp(i\gamma gzt)dz\right)\overline{\exp(i\Delta\phi)} \\ &= \left(\int_{-\infty}^{\infty} \rho(z)exp(i\gamma gzt)dz\right)\exp(-\tfrac{1}{3}\gamma^2 g^2 Dt^3) \end{aligned} \tag{5.44}$$

The term in brackets is the decay known as T_2^*, and arises from the field inhomogeneity (in this case imposed by gradient g) across the sample. It merely serves to mask the underlying attenuation due to diffusion alone. The means of removing this dephasing associated with the starting position of spins is of course, the echo.

Before moving on, it is worth noting that the decay of the signal caused by the positional phase spread, $\int_{-\infty}^{\infty} \rho(z)\exp(i\gamma gzt)dz$, can be used to good effect in suppressing unwanted signals, a process known as 'homospoiling'.

Signal attenuation under an echo with steady gradient

Suppose we now consider the dephasing effect that remains at the time of formation of an echo at time $t = 2\tau$ when a steady gradient is present. Because of the echo formation we may ignore all phase shifts associated with starting position z and deal only with phase shifts $\Delta\phi$.

The phase step diagram for this is shown in Fig. 5.13. Here, the 180°_y pulse has reversed all phase shifts that existed before time $t = \tau$, where τ is the separation of the first and second RF pulses. Clearly the second evolution period contains a section that completely cancels the net phase shift that occurred before the 180° pulse. The residual phase shift at the time of the echo is given by the sum of the shaded triangular region. This region now involves two uncorrelated triangular segments, each with orthogonal sides of n steps. Using our previous observation concerning $\overline{(\Delta\phi)^2}$ in such triangular sections, we can see that the value of $\overline{(\Delta\phi)^2}$ that applies in the case of the echo is exactly double that which applied in Fig. 5.13 (and twice that which occurs during the period t between the first two RF pulses.) Consequently, for the echo at $t = 2\tau$,

$$\begin{aligned}\overline{\exp(i\Delta\phi)} &= \exp(-\tfrac{2}{3}\gamma^2 g^2 D\tau^3) \\ &= \exp(-\tfrac{1}{12}\gamma^2 g^2 D(2\tau)^3) \end{aligned} \tag{5.45}$$

where the second form expresses this attenuation in terms of the total time 2τ from the first RF pulse to the echo centre. This constant gradient spin-echo method has been used to obtain self-diffusion coefficients in simple liquids with an accuracy of order 0.1 [19].

[10] In Chapter 1, the notation $p(\mathbf{r}, 0)$ was used to signify the initial probability density of finding a molecule at position $\mathbf{r}$. Here we use $\rho(\mathbf{r})$ to describe the density of molecules in the sample. Normally these will be identically the same quantities.

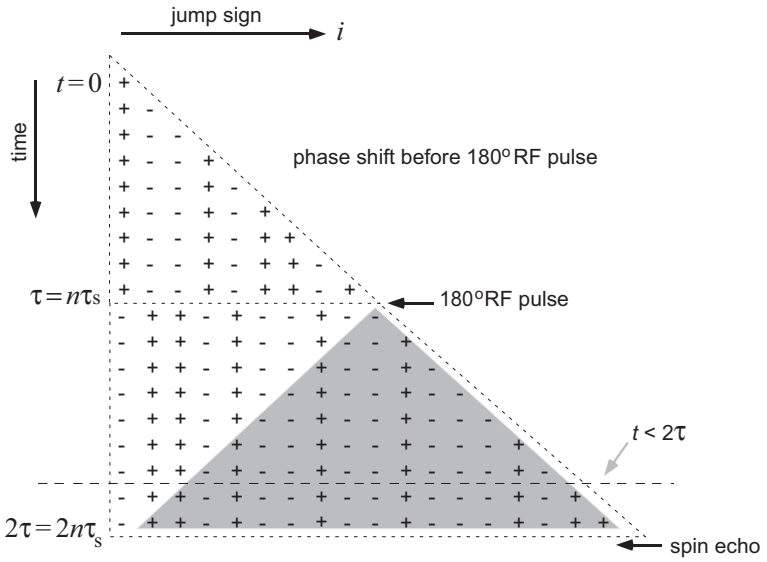

Fig. 5.13 Cumulative phase diagram for spin echo formation in a steady magnetic field gradient. Note that the 180° RF pulse inverts all prior phase shifts. The net phase shift is the sum of that occurring before and after the 180° RF pulse and corresponds to the shaded area.

Signal attenuation due to diffusion leading up to the echo

Note that eqn 5.45 is valid only at the echo centre. It is interesting to recalculate the diffusive attenuation factor during the time $\tau < t < 2\tau$ leading up to the echo. We can easily do this by reference to Fig. 5.13. Instead of the shaded double triangular region being of height τ, it has the lesser height $t - \tau$. Furthermore, the phase cancellation between the upper and lower regions on the left is incomplete, leaving a small uncompensated triangle of phase of height $2\tau - t$ on the bottom left. Note that these two residual triangular regions are uncorrelated and contribute to the signal attenuation independently. Using the arguments of the previous section concerning $\overline{(\Delta\phi)^2}$, we can see that

$$\begin{aligned}\overline{\exp(i\Delta\phi)} &= \exp\left(-\tfrac{1}{3}\gamma^2 g^2 D[(2\tau - t)^3 + 2(t-\tau)^3]\right) \\ &= \exp\left(-\gamma^2 g^2 D(2\tau^3 - 2\tau^2 t + \tfrac{1}{3}t^3)\right) \end{aligned} \quad (5.46)$$

Equation 5.46, as required, reproduces the correct result at the echo centre, at $t = 2\tau$. However, this attenuation function has the remarkable property that its maximum is at $t = \sqrt{2}\tau$ and not $t = 2\tau$. What can this mean?

Of course the signal envelope that is conventionally used to define the echo is based on the refocusing of static dephasing effects. In this perspective, the echo is defined by the dephasing and rephasing associated with the starting positions z in the magnetic field gradient. For the case of the steady gradient, the effect of the dephasing due to starting positions was given by the factor $\left(\int_{-\infty}^{\infty} \rho(z)\exp(i\gamma g z t)dz\right)$. For an echo, we

may rewrite that term in eqn 5.44 using the idea of a phase reversal at $t = \tau$, so that the time variable t in the interval $\tau < t < 2\tau$ may be replaced by $(t - 2\tau)$, and

$$\begin{aligned}\overline{\exp(i\phi)} &= \left(\int_{-\infty}^{\infty} \rho(z)\exp(i\gamma g z[t-2\tau])dz\right)\overline{\exp(i\Delta\phi)} \\ &= \left(\int_{-\infty}^{\infty} \rho(z) exp(i\gamma g z[t-2\tau])dz\right)\exp\left(-\gamma^2 g^2 D(2\tau^3 - 2\tau^2 t + \tfrac{1}{3}t^3)\right)\end{aligned} \tag{5.47}$$

If the first term dominates the signal attenuation away from $t = 2\tau$, then of course the echo maximum will occur at time $t = 2\tau$. But if, for whatever reason, the static dephasing term produces only a small phase spread, for example if the molecules are confined in a small region of space of size d such that $\gamma g d[t - 2\tau] \ll \pi$, while D is sufficiently large that the diffusive attenuation term dominates, then indeed an echo will be seen at $t = \sqrt{2}\tau$ rather than at $t = 2\tau$. Such an effect has been noted by Zanker *et al.* [20] for diffusion of gases contained in small sample tubes.

Signal attenuation under a steady gradient CPMG sequence

Equation 5.45 is easily generalised to a multiple, Carr–Purcell–Meiboom–Gill, echo sequence. For m echoes there are m such triangular phase step regions in the diagram equivalent to Fig. 5.13. Consequently the attenuation coefficient is

$$\begin{aligned}\overline{\exp(i\Delta\phi)} &= \exp(-\frac{2m}{3}\gamma^2 g^2 D t^3) \\ &= \exp(-\tfrac{2}{3}\gamma^2 g^2 D t^2 (mt))\end{aligned} \tag{5.48}$$

Now the dependence of the attenuation on the total time mt is linear rather than cubic as in the case of the simple spin echo. This means that the attenuation effect at some total time, mt, may be arbitrarily reduced by decreasing the interval t between echoes and increasing m, the number of echoes. This was the method suggested by Carr and Purcell to eliminate additional relaxation of the transverse magnetisation due to diffusive motion occurring in the presence of field inhomogeneities.

Note that in all these expressions for $\overline{\exp(i\Delta\phi)}$, no account is taken of relaxation effects. Provided, however, we divide our magnetisation by that which applies when no magnetic field gradients are applied, then we may identify $\overline{\exp(i\Delta\phi)}$ with the normalised signal, $E(t)$.

5.4.4 The Bloch–Torrey equation for diffusion and flow

A later and more general approach to providing a description of spin phase evolution under any time-dependent gradient was made by Torrey [21]. The effect of molecular self-diffusion and velocity advection was accounted for by introducing an additional term in the Bloch equations (4.31), so that self-diffusion and flow is represented as a 'transport of magnetisation'. The magnetisation is effectively treated as fluid, and represented in an Eulerian sense by a vector $\mathbf{M}(\mathbf{r}, t)$. Using the substantive derivative

to relate the rate of change of transverse magnetisation to precession, transverse relaxation, and diffusive replenishment in a magnetisation gradient, the equation for the x-component contains additional terms as,

$$\frac{DM_x}{Dt} = \gamma M_y(B_0 - \omega/\gamma) - \frac{M_x}{T_2} + \nabla \cdot \underline{\underline{D}} \cdot \nabla M_x \tag{5.49}$$

or

$$\frac{\partial M_x}{\partial t} = \gamma M_y(B_0 - \omega/\gamma) - M_x/T_2 + \nabla \cdot \mathbf{D} \cdot \nabla M_x - (\mathbf{v} \cdot \nabla)M_x \tag{5.50}$$

Note that the diffusion tensor is used in this description. We will have occasion to return to anisotropic diffusion later but for the moment, we will, for simplicity, assume a common diffusion scalar coefficient, D, and evaluate eqn 5.50 in the rotating frame, where the Zeeman Hamiltonian, on resonance, arises from the magnetic field gradient terms alone and

$$\frac{\partial M_+}{dt} = -i\gamma \mathbf{r} \cdot \mathbf{g}^*(t)M_+ - \frac{M_+}{T_2} + D\nabla^2 M_+ - (\mathbf{v} \cdot \nabla)M_+ \tag{5.51}$$

where $M_+ = M_x + iM_y$.

It is clear that M_+ is a function of both $\mathbf{r}$ and t, and eqn 5.51 is solved by making the substitution [21, 22]

$$M_+(\mathbf{r}, t) = A(t) \exp\left(-i\gamma \mathbf{r} \cdot \int_0^t \mathbf{g}^*(t')dt'\right) \exp(-t/T_2) \tag{5.52}$$

We will see that $A(t)$ is a (generally complex) modulation factor with a modulus less than unity, determined by the spreading motion of the spin-bearing molecules, and an argument that derives from net translational displacement. The phase factor term $\exp\left(-i\gamma \mathbf{r} \cdot \int_0^t \mathbf{g}^*(t')dt'\right)$ arises from the helical phase distribution 'burned into' the spin system by the magnetic field gradient, and under the condition for a gradient echo at time t, $\int_0^t \mathbf{g}^*(t')dt' = 0$, so that, at the echo centre, this term becomes unity. Finally, the term $\exp(-t/T_2)$ accounts for the relentless spin–spin relaxation experienced by the spins while the magnetisation is resident on the transverse plane. Consequently, at the echo centre $M_+(\mathbf{r}, t)$ reduces to $A(t)\exp(-t/T_2)$, independent of the local coordinates.

Substitution of eqn 5.52 in eqn 5.51 leads to

$$\frac{\partial A(t)}{\partial t} = -\left[D\gamma^2 \left(\int_0^t \mathbf{g}^*(t')dt'\right)^2 - i\gamma \mathbf{v} \cdot \int_0^t \mathbf{g}^*(t')dt'\right] A(t) \tag{5.53}$$

with solution [21, 22]

$$A(t) = \exp\left[-D\gamma^2 \int_0^t \left(\int_0^{t'} \mathbf{g}^*(t'')dt''\right)^2 dt'\right] \exp\left[i\gamma \mathbf{v} \cdot \int_0^t \int_0^{t'} \mathbf{g}^*(t'')dt''dt'\right] \tag{5.54}$$

Under the echo condition $\int_0^t \mathbf{g}^*(t')dt' = 0$, $A(t)$ is simply the normalised echo attenuation $E(t)$. We will use the Bloch–Torrey result to evaluate a number of echo-attenuation expressions for cases where the motion comprises simple diffusion and flow.

At any time other than the echo condition, the Bloch–Torrey factorisation of eqn 5.52 contains a time-dependent term in addition to $A(t)$, namely the phase factor $\exp\left(-i\gamma\mathbf{r}\cdot\int_0^t \mathbf{g}^*(t')dt'\right)$. This term is akin to a structure factor, a Fourier phase factor rising from the effect of gradient dephasing due to the spin positions in the magnetic field gradient, and one which must be evaluated by averaging over all $\mathbf{r}$. In that sense we might regard it as being similar to the structure factor seen in the bracketed terms of eqns 5.44 and 5.47, but note the subtle difference. The spin positions in the exponent of eqns 5.44 and 5.47 are *starting* positions. Crucially, $\mathbf{r}$ in the Bloch–Torrey factor, $\exp\left(-i\gamma\mathbf{r}\cdot\int_0^t \mathbf{g}^*(t')dt'\right)$, represents, by contrast, the local position vector in the Eulerian fluid, for which any density function, $\rho(\mathbf{r})$, over which this phase factor is integrated to represent the whole sample, will depend on the time of evaluation. Only at the echo centre will the expressions coincide. When $\int_0^t \mathbf{g}^*(t')dt' = 0$ this troublesome, time-dependent, exponential term is unity, and the distribution of the values of $\mathbf{r}$ irrelevant. But at any other time, the ensemble average of this exponential term contributes an additional time-dependent attenuation. For example, if the Bloch–Torrey expression for $A(t)$ is used to estimate the diffusion attenuation component in advance of the echo, eqn 5.47 is not reproduced. So long as we use Bloch-Torrey to evaluate our signal only at the echo centre, we are safe.

5.5 Pulsed gradient spin-echo NMR: diffusion and flow

In each of the cases analysed using the Carr–Purcell particle hopping model, the gradient was considered to be time-independent. Clearly the attenuation of the spin echo or CPMG train that arises from diffusive dephasing under the influence of a steady gradient may be conveniently used to measure molecular self-diffusion. This method has been effective in providing very precise self-diffusion coefficients in a variety of simple liquids. However, the method is inconvenient where the motion is slow. This is because the steady gradient spreads the Larmor spectrum at all times, and in particular during the period of RF pulse transmission and during the period of signal detection. This means that the maximum gradient that can be applied is limited by the transmitter and receiver bandwidths. McCall, Douglass, and Anderson [23] suggested in 1963 that the gradient might be applied in the form of rectangular pulses inserted respectively in the dephasing and rephasing parts of the echo sequence, but gated off during RF pulse transmission and signal detection. This pulsed gradient spin-echo (PGSE) sequence was first demonstrated by Stejskal and Tanner in 1965 [24].[11]

5.5.1 The Stejskal–Tanner experiment

The basic pulse sequence for the Stejskal and Tanner experiment is shown in Fig. 5.14, first as a spin echo in (a) and then as a stimulated echo in (b). From the perspective of

[11]The pulsed gradient method for measuring spin translational motion is sometimes referred to as pulsed field gradient NMR (PFG NMR). Given that pulsed magnetic field gradients are variously used in magnetic resonance applications for imaging and for coherence selection purposes, we prefer the name pulsed gradient spin echo, with its acronym PGSE NMR, where the role of the echo, however formed, and so central to the measurement of dynamics, is explicit. The name pulsed gradient spin-echo NMR was originally suggested by Stilbs and Moseley [25, 26].

motion-induced phase shifts, the two sequences are equivalent, but the way that relaxation acts to attenuate the echo signal is clearly different, the spin echo experiencing T_2 throughout the evolution of magnetisation in the transverse plane, and the stimulated echo allowing for a slower T_1 relaxation during the period in which magnetisation is stored along the longitudinal axis. There is no universally agreed nomenclature for the acronyms describing these methods. To this author, PGSE seems to present a convenient label for both types of echo.

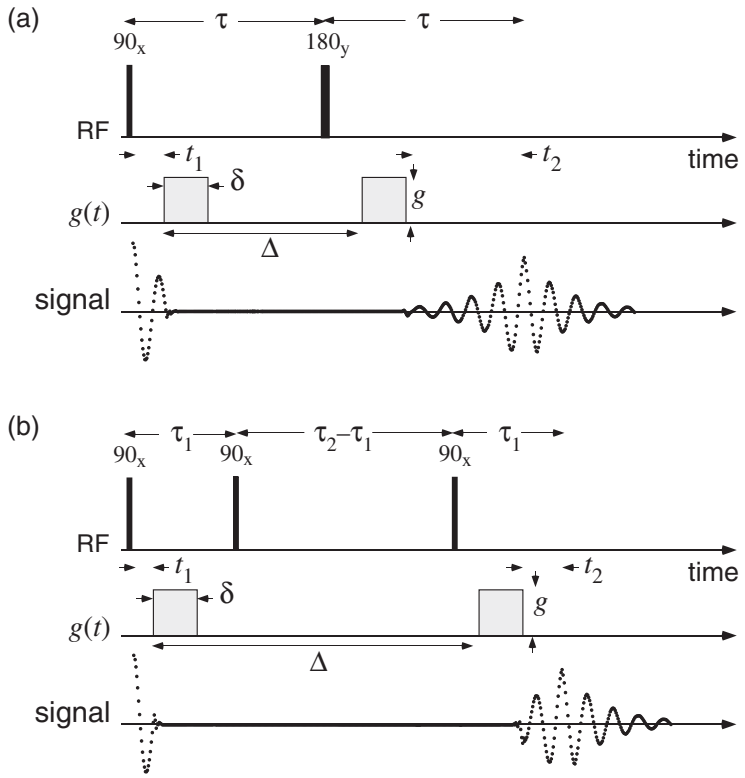

Fig. 5.14 (a) Pulsed gradient spin-echo (PGSE) sequence, with gradient amplitude g, pulse duration δ, and gradient pulse spacing Δ. τ is the time between the 90° and 180° RF pulses and corresponds to half the spin-echo formation time, T_E. (b) stimulated-echo version of PGSE sequence.

One of Stejskal's important contributions was the use of a propagator description of generalised motion [27]. As we shall see later, this allows a very natural and insightful formalism in the special circumstance that the gradient pulse duration is short. For the moment though, we will outline the effect of simple self-diffusion and flow under the condition of finite duration gradient pulses.

Carr–Purcell derivation

The cumulative phase step diagram for the PGSE experiment in the spin echo version is shown in Fig. 5.15, where $\delta = m\tau_s$ and $\Delta = p\tau_s$.

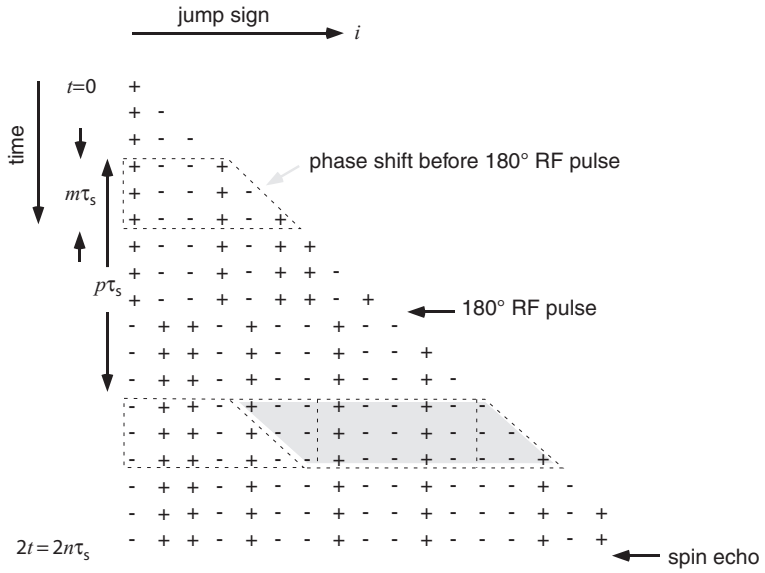

Fig. 5.15 Cumulative phase diagram for spin-echo formation in the PGSE experiment. The net phase shift is the sum of that occurring before and after the 180° RF pulse and corresponds to the shaded area. Note that $\delta = m\tau_s$ and $\Delta = p\tau_s$.

The effect of the 180° RF pulse is to cause the inversion of prior phase shifts, leading to cancellation of phase shifts associated with the unshaded areas. The net phase shift is therefore obtained by summing two uncorrelated triangular regions, each with mean square phase shift $\frac{1}{3}\gamma^2 g^2 \tau_s^2 \xi^2 m^3$, along with one uncorrelated rectangular region with mean square phase shift $\gamma^2 g^2 \tau_s^2 \xi^2 m^2 (p-m)$. The net mean square phase shift is therefore

$$\begin{aligned} \overline{\Delta\phi^2} &= \gamma^2 g^2 \tau_s^2 \xi^2 m^2 (p - m + \tfrac{2}{3}m) \\ &= 2\gamma^2 g^2 \delta^2 D(\Delta - \delta/3). \end{aligned} \tag{5.55}$$

Using eqn 5.41, we obtain the well-known Stejskal–Tanner relation [24] for the attenuation of the echo amplitude,

$$S(g)/S(0) = \exp(-\gamma^2 g^2 \delta^2 D(\Delta - \delta/3)) \tag{5.56}$$

where, as before, we label the ratio of the echo amplitude at gradient g to that at zero gradient, as the normalised echo attenuation, $E(g)$. Note that the chosen variable here is the gradient amplitude g. In fact, a very convenient experimental procedure is to keep all the experimental times fixed, and to vary the magnetic field gradient amplitude. In this way, $E(g)$ has relaxation effects removed, except in as much as

overall signal attenuation due to relaxation reduces the available signal to noise ratio. Of course, the timescale over which diffusion occurs is set by the period, Δ, separating the start of the gradient pulses, a parameter to be varied if the time dependence of diffusion is to be probed. Even where $E(g, \delta)$ is measured, care in arranging the pulse sequence can allow for normalisation of relaxation effects.

Equation 5.56 provides a precise description of the influence of self-diffusion in the PGSE experiment and is the basis of a considerable literature pertaining to this technique [24, 28–32]. An example of self-diffusion measurement is shown in Fig. 5.16, in which spectrally separated molecular species in the same liquid mixture have their respective echo attenuations plotted as a function of squared gradient amplitude. The spectral separation is possible because the echo signal is sampled in the absence of the magnetic field gradient. The PGSE method may be used to precisely measure diffusion down to 10^{-14} m^2 s^{-1}, some five orders of magnitude slower than that exhibited in Fig. 5.16.

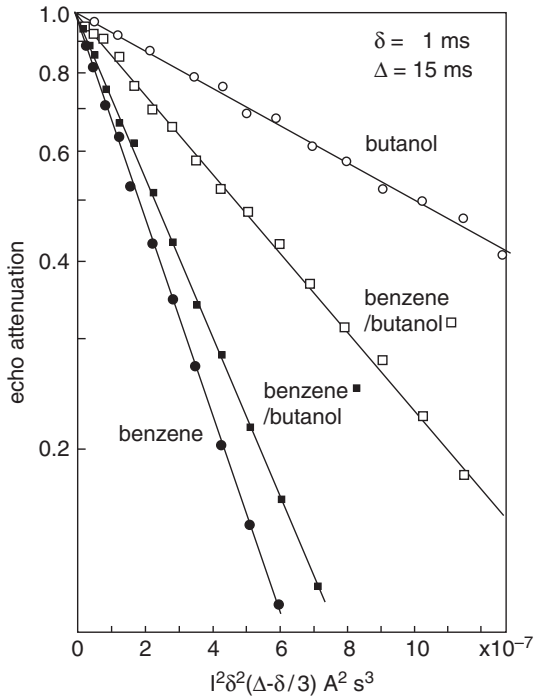

Fig. 5.16 Echo-attenuation data for pure benzene, pure butanol, and for the benzene and butanol components in an equimolar mixture. The self-diffusion coefficients are, respectively, $(2.23\pm0.02)\times10^{-9}$, $(0.43\pm0.01)\times10^{-9}$, $(1.83\pm0.02)\times10^{-9}$, and $(0.90\pm0.01)\times10^{-9}$ m^2 s^{-1}. (From reference [33].)

Note that the exponent in the Stejskal–Tanner equation is proportional to the mean-squared displacement of the molecules over an effective timescale $(\Delta - \delta/3)$. The attenuation of the echo arises because of the incoherent nature of the phase shifts

across the nuclear ensemble. Suppose by contrast that there is an additional coherent motion due to each molecule being additionally displaced by an identical amount. This of course corresponds to the superposition of a uniform velocity $\mathbf{v}$, so that the extra displacement moved per incremental step is $\mathbf{v}\tau_s$. The effect is easy to calculate. Consider the PGSE phase step diagram of Fig. 5.15. The shape of the diagram which allows for a constant velocity component will be exactly the same. However, all steps will now have an additional, identical magnitude contribution, with negative sign before the 180° RF pulse and positive sign after. The mean phase shift corresponds to the sum in the shaded area. This is $\gamma\tau_s\mathbf{g}\cdot(\mathbf{v}\tau_s)pm$ or $\gamma\delta\mathbf{g}\cdot\mathbf{v}\Delta$. Consequently a phase shift of $\exp(i\gamma\delta\mathbf{g}\cdot\mathbf{v}\Delta)$ is common to all spins in the ensemble, and may be factorised out of the signal, leaving the diffusive contribution exactly as before. The combined effect of diffusion and flow is therefore a phase shift due to flow and an attenuation due to diffusion given by

$$E(\mathbf{g}) = \exp(i\gamma\delta\mathbf{g}\cdot\mathbf{v}\Delta - \gamma^2 g^2\delta^2 D(\Delta - \delta/3)) \tag{5.57}$$

Equation 5.57 is an idealisation. It makes no allowance for the interfering effects of steady background gradients, nor for the effects of finite rise times in the gradient pulses, instead assuming perfect rectangular pulse shapes. Later we will address these perturbing effects. But for the moment, let us see how the Bloch–Torrey result yields the idealised Stejskal–Tanner relation.

Bloch–Torrey derivation

We return to the simple spin-echo version of the PGSE experiment shown in Fig. 5.14 (a), whose gradient echo equivalent, based on effective gradient g^*, is shown in Fig. 5.17. Note that if there are small residual gradients due to polarising magnet inhomogeneity then the centre of this echo will be at a time τ after the 180°_y pulse, the rephasing time being equal to the dephasing period separating the 90°_y and 180°_y pulses.

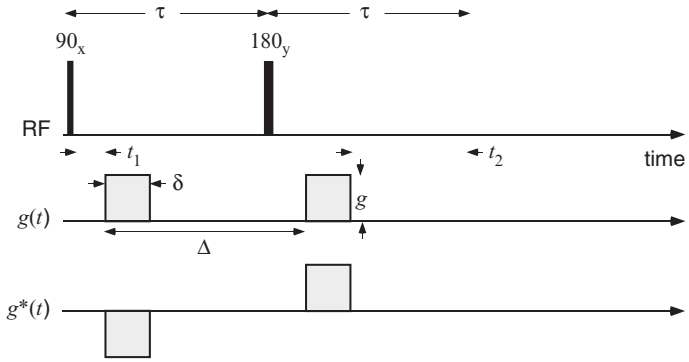

Fig. 5.17 As in Fig. 5.14(a), but showing the effective gradient $g^*(t)$.

To evaluate the spin phase distributions we need to evaluate a number of Bloch–Torrey integrals using the timings indicated. Note that we call the time delay before the first gradient pulses t_1. We will also assume a vector gradient, though at this

stage we will be dealing with isotropic diffusion and only the squared magnitude of $\mathbf{g}^*$ will enter the diffusive contribution to the phase spread. At this point any weak background gradients will be ignored. The relevant integrals are

$$\int_0^{2\tau} \mathbf{g}^*(t')dt' = 0 \tag{5.58}$$

and

$$\begin{aligned}\int_0^t \int_0^{t'} \mathbf{g}^*(t'')dt''dt' &= -\int_{t_1}^{t_1+\delta} \mathbf{g}(t'-t_1)dt' - \int_{t_1+\delta}^{t_1+\Delta} \mathbf{g}\delta dt' \\ &\quad + \int_{t_1+\Delta}^{t_1+\Delta+\delta} [-\mathbf{g}\delta + \mathbf{g}(t'-t_1-\Delta)]dt' \\ &\quad + \int_{t_1+\Delta+\delta}^{2\tau} [-\mathbf{g}\delta + \mathbf{g}\delta]dt' \\ &= -\mathbf{g}\delta\Delta\end{aligned} \tag{5.59}$$

and

$$\begin{aligned}\int_0^t \left(\int_0^{t'} \mathbf{g}^*(t'')dt''\right)^2 dt' &= -\int_{t_1}^{t_1+\delta} g^2(t'-t_1)^2dt' - \int_{t_1+\delta}^{t_1+\Delta} g^2\delta^2 dt' \\ &\quad + \int_{t_1+\Delta}^{t_1+\Delta+\delta} [g^2\delta^2 - 2g^2(t'-t_1-\Delta) + g^2(t'-t_1-\Delta)^2]dt' \\ &= g^2\delta^2(\Delta - \delta/3)\end{aligned} \tag{5.60}$$

Equation 5.58 is simply the condition for the formation of an echo. Equations 5.59 and 5.60 taken together with eqn 5.58 reproduce the earlier expression for the velocity-induced echo phase shift and diffusion-induced echo attenuation given in eqn 5.56. Because we chose to make the effective gradient negative for the first pulse, the sign of the velocity phase shift term is negative. By contrast, in the Carr–Purcell derivation we chose to negate the phases after the 180° pulse, so that the velocity term was positive. So long as we understand the consequences of these phase conventions, we should be able to understand the absolute sign of the phase shift.

Phase evolution during the pulse sequence

Before leaving the Bloch–Torrey analysis it is instructive to plot the evolution of the phase shift integrals that generate sensitivity to position (eqn 5.58) and velocity (eqn 5.59), as well as the evolution of the phase-spreading integrals associated with diffusion (eqn 5.60). These are shown in Fig. 5.18.

The effect of finite gradient pulse rise and fall times

Perfectly rectangular gradient pulses are an idealisation hard to achieve in practice. The changing magnetic field associated with the rising gradient pulse can act to induce

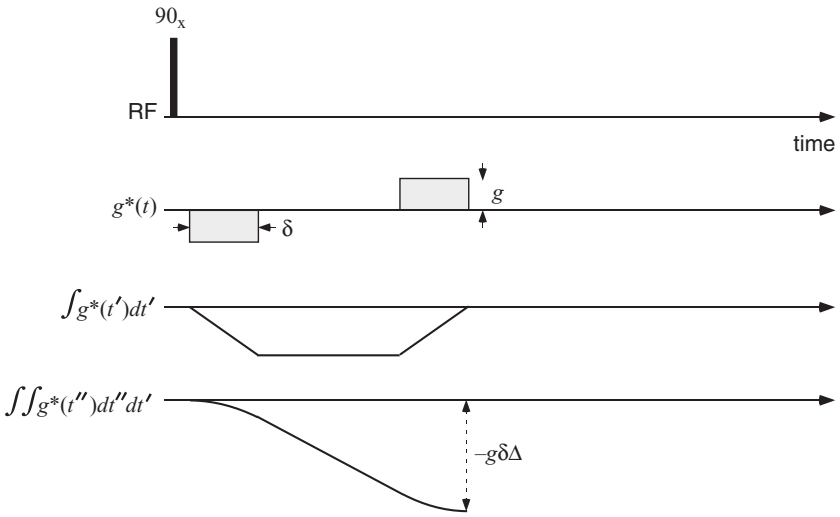

Fig. 5.18 Effective gradient sequence for Stejskal–Tanner experiment resulting in the echo condition $\int_0^t g^*(t')dt' = 0$, along with the velocity phase term $\int_0^t \int_0^{t'} g^*(t'')dt''dt'$.

eddy currents in the conductors surrounding the NMR sample space, for example the room temperature bore or cooled surfaces in the vicinity of a superconducting magnet. These eddy currents themselves produce magnetic fields and gradients that act back on the sample. By using a self-screened design for the gradient coil, such effects may be reduced, but in practice a significant reduction in eddy currents can be achieved just by switching the gradient pulse on and off at a controlled rate, for example by using a linear ramp.

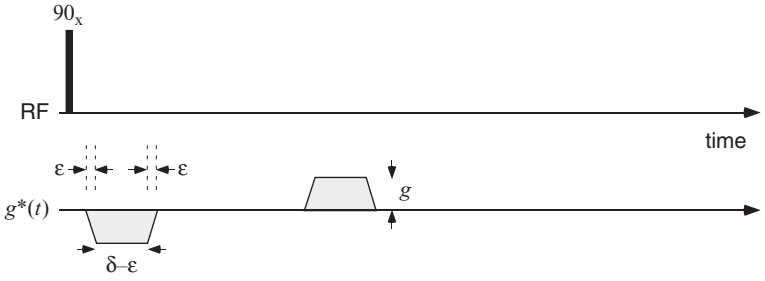

Fig. 5.19 Effective gradient sequence for Stejskal–Tanner experiment with finite rise and fall times.

Again the Bloch–Torrey approach may be easily used to generate the normalised echo signal when such a ramp is used [34, 35]. A useful timing nomenclature is to allow for a gradient pulse whose total area is $g\delta$, with rise and fall times ϵ, and hence constant gradient duration $\delta - \epsilon$, as shown in Fig. 5.19. The phase shift due to flow is unaffected by this variation in pulse shape, depending only on pulse area, while the attenuation due to diffusion is slightly modified as

$$E(\mathbf{g}) = \exp(i\gamma\delta\mathbf{g}\cdot\mathbf{v} - \gamma^2 D g^2\delta^2(\Delta-\delta/3)[1+\frac{\epsilon}{\Delta-\delta/3}(\frac{\epsilon^2}{30\delta^2}-\frac{\epsilon}{6\delta})]) \qquad (5.61)$$

The correction term in the square brackets is so weak as to be practically negligible, except where high-precision diffusion measurements are required. For example, even for a slow ramp comprising 20% of the pulse duration along with a relatively short $\Delta \sim 2\delta$, $\epsilon/\delta \sim 0.2$ and $\epsilon/\Delta \sim 0.1$, yields a correction term of around 0.3 %.

5.5.2 The role of background gradients

The influence of a steady background gradient

The Bloch–Torrey method is ideal for calculating the subtle perturbations to the Stejskal–Tanner relation that arise from gradient artifacts. Here we consider the effect of a weak steady background gradient, $\mathbf{G}_0$. The derivation is tedious but straightfor-

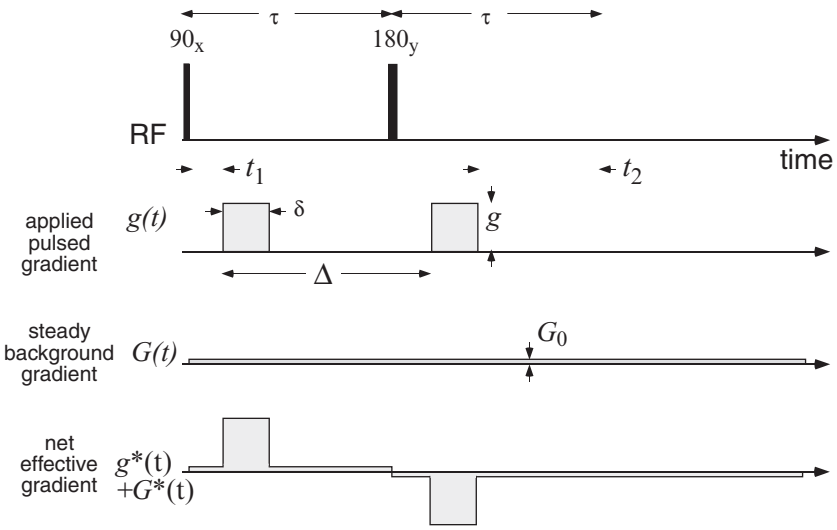

Fig. 5.20 As in Fig. 5.14(a), but showing the effective gradient $\mathbf{g}^*(t)$. Also shown is a weak background gradient G_0. Because $\mathbf{g}^*(t)$ and $\mathbf{G}_0$ and may act in different directions, the two gradients are shaded different colours.

ward and the exact form of the signal is given by [24, 27]

$$\begin{aligned} E(\mathbf{g}) \;=\; & \exp(i\gamma\delta\mathbf{g}\cdot\mathbf{v}\Delta + i\gamma\tau^2\mathbf{G}_0\cdot\mathbf{v} \\ & -\gamma^2 D[g^2\delta^2(\Delta-\delta/3) + \tfrac{2}{3}G_0^2\tau^3 \\ & -\mathbf{g}\cdot\mathbf{G}_0\delta\{t_1^2+t_2^2+\delta(t_1+t_2)+\tfrac{2}{3}\delta^2-2\tau^2\}]) \end{aligned} \qquad (5.62)$$

with t_1 again being the delay between the 90°_x RF pulse and the start of the first gradient pulse, and t_2 being the delay between the end of the second gradient pulse

and the centre of the echo. This result is useful in dealing with an apparatus where the residual gradients are poorly shimmed or where a steady background gradient is deliberately used to stabilise the echo.[12]

Stimulated echo

The measurement of self-diffusion by PGSE NMR is limited by the loss of phase coherence due to transverse relaxation. One nice method of avoiding this problem is to store the spatially-encoded magnetisation along the longitudinal axis by means of a second 90° pulse, as shown in Fig. 5.14(b). The magnetisation is recalled at a later time and rephased in a stimulated echo. Over the storage period the spins are subject to T_1 relaxation, which is generally slower than T_2. The expression equivalent to eqn 5.62 for the case of the stimulated echo is [36]

$$\begin{aligned} E(\mathbf{g}) \;=\; & \exp(i\gamma\delta\mathbf{g}\cdot\mathbf{v}\Delta + i\gamma\tau_1\mathbf{G}_0\cdot\mathbf{v}\Delta \\ & -\gamma^2 D[g^2\delta^2(\Delta-\delta/3) + G_0^2\tau_1^2(\tau_2-\tfrac{1}{3}\tau_1) \\ & -\mathbf{g}\cdot\mathbf{G}_0\delta\{t_1^2+t_2^2+\delta(t_1+t_2)+\tfrac{2}{3}\delta^2-2\tau_1\tau_2\}]) \end{aligned} \tag{5.63}$$

For small background gradients this expression is entirely equivalent to that of the spin-echo expression, the only penalty paid being the loss of a factor of 2 in the signal intensity due to projection of only half the transverse magnetisation along the z-axis during the storage period. Comparison of eqns 5.62 and 5.63 illustrates the reduced influence of $\mathbf{G}_0$ in the latter expression because of the replacement of τ^3 and τ^2 by $\tau_1^2(\tau_2-\frac{1}{3}\tau_1)$ and $\tau_1\tau_2$, respectively. The stimulated-echo method thus has the additional advantage that the magnetisation is not only protected from T_2 relaxation during the storage period but is also experiences reduced precessional dephasing caused by residual gradients.

5.5.3 Echo schemes to reduce the effect of background gradients

When measuring molecular diffusion in porous media, the diamagnetic susceptibility difference between the matrix and the imbibed fluid can lead to quite large inhomogeneous magnetic fields in the pore space. This has the effect of significantly perturbing the measurement of diffusion using pulsed gradients, both because of the cross terms apparent in eqns 5.62 and 5.63, and because diffusion in these inhomogeneous fields may lead to additional spin relaxation and loss of signal intensity.[13] Note that in an experiment where the diffusive attenuation is measured by incrementing the pulsed gradient amplitude g, only the cross terms bother us, since the quadratic (G_0^2) term in the echo-attenuation exponent arising from the background gradient alone contributes a fixed attenuation.

CPMG and spin-locking

One approach to the reduction of residual gradient influence is to employ a CPMG echo train but with a single pair of gradient pulses inserted in appropriately spaced locations between the 180° RF pulses [37]. While the CPMG train method does not

[12] See Chapter 12.

[13] This effect is discussed in detail in Section 6.4.

suffer from the factor-of-two signal-to-noise ratio loss of the stimulated echo, it does suffer T_2 relaxation. An alternative method of retaining the full signal amplitude while avoiding transverse relaxation is to employ spin-locking pulses over the waiting period between the two gradient pulses in a normal spin echo [38]. Under a sustained spin-lock pulse the magnetisation decays as $T_{1\rho}$, which, for sufficiently powerful RF fields, can be made much longer than T_2.

13-interval sequence

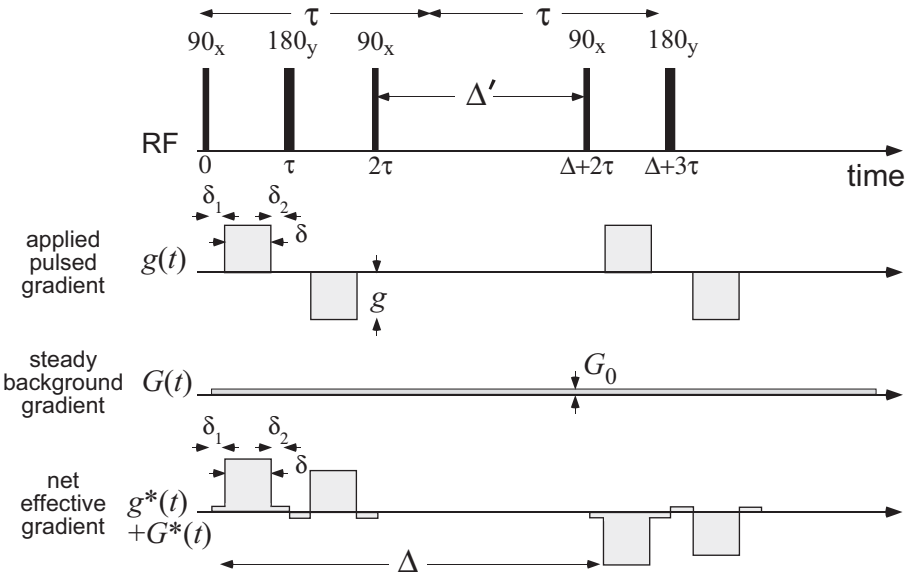

Fig. 5.21 13-interval gradient pulse scheme of Cotts *et al.*, designed to minimise the effect of background gradients. Note that Δ' as shown in eqn 5.64 differs from the conventional definition of Δ.

The role of spin echoes in reducing the effect of background gradients was analysed in detail by Karlicek and Low and led to a suggestion that the pulsed magnetic field gradients be applied with alternating sign in respective dephasing and rephasing spin-echo segments [39]. This idea was followed by the best known of the schemes to reduce the effect of background gradients, the so-called '13-interval' sequence of Cotts *et al.* [40]. The pulse sequence is based on a stimulated echo, as shown in Fig. 5.21, but with the diffusion encoding period divided into a spin-echo dephasing and rephasing segment, with bipolar gradients. The latter have the effect of refocusing background gradient dephasing at the point of both the 90° RF storage pulse and the stimulated echo, but cumulatively adding the desired dephasing of the pulsed gradients, thanks to the use of bipolar pulses. The effective gradients also shown in Fig. 5.21 make clear how the sequence works. Ignoring the influence of flow, diffusive effect of the background gradients is given by

$$E(\mathbf{g}) = \exp\left(-\gamma^2 D\left[g^2\delta^2(4\Delta' + 6\tau - 2\delta/3) + \frac{4\tau^2}{3}G_0^2 - \mathbf{g}\cdot\mathbf{G}_0 2\delta\tau(\delta_1 - \delta_2)\right]\right)$$

implying that the cross term vanishes under the condition $\delta_1 = \delta_2$.

Compensating a changing background field

Of course this cancellation depends on the background gradients being the same in the two encoding intervals separated by Δ'. Given that Δ' may be quite long and, as a consequence, in a heterogeneous medium, spin-bearing molecules may diffuse to regions of differing local background field, the cancellation may be imperfect. This problem is discussed by Sun *et al.* [41] and Seland *et al.* [42], who propose the use of asymmetric bipolar pulses designed to correct for this effect.

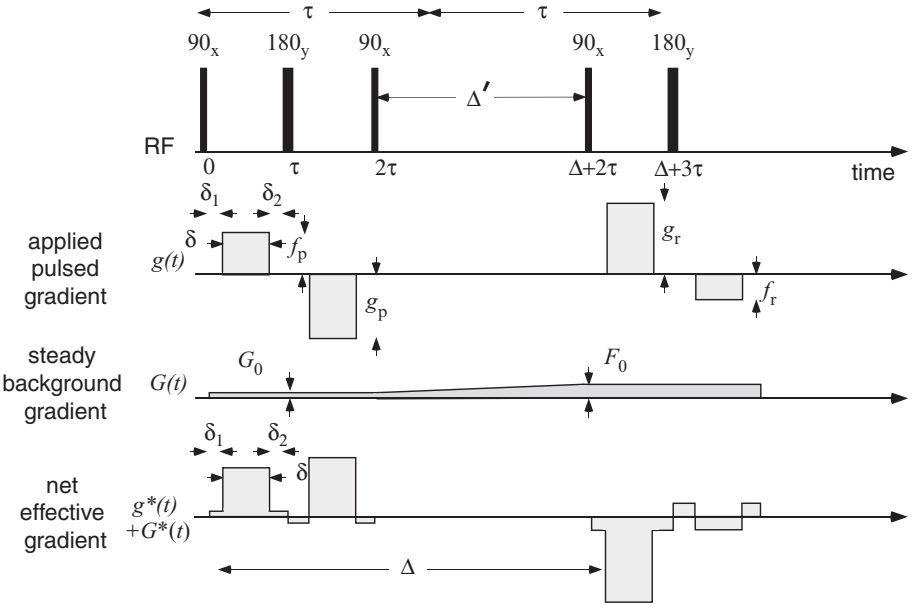

Fig. 5.22 Generalised 13-interval gradient pulse scheme of Cotts *et al.*, with four unequal pulsed field laboratory gradients, with the intensities $f_{p,r}$ and $g_{p,r}$, respectively, along with a background gradient, which changes value from G_0 to F_0 during the storage period Δ'. $f_{p,r}$ and $g_{p,r}$ can be adjusted to cancel the effect of the background field. (Adapted from Galvosas *et al.* [43].)

An exact solution has been provided by Galvosas *et al.* based on the parametrisation of Fig. 5.22 [43]. First, the pulsed gradients must obey the echo condition, namely

$$f_p + g_p = f_r + g_r \tag{5.64}$$

where the subscripts refer to the 'prepare' and 'read' segments of times 2τ when the magnetisation is in the transverse plane. In their analysis, the normalised echo attenuation at the echo centre ($t = t_e$) may be written

$$E = \exp(-\gamma^2 D[I_p + I_c + I_b]) \tag{5.65}$$

where I_p, I_c, and I_b are Bloch–Torrey-type integrals associated with the pulsed gradients, the cross term, and the background effective gradients as

$$\begin{aligned} I_p &= \int_0^{t_e} dt' \left(\int_0^{t'} \mathbf{g}^*(t'')dt'' \right)^2 \\ I_c &= \int_0^{t_e} dt' \int_0^{t'} \mathbf{g}^*(t'')dt'' \int_0^{t'} \mathbf{G}^*(t'')dt'' \\ I_1 &= \int_0^{t_e} dt' \left(\int_0^{t'} \mathbf{G}^*(t'')dt'' \right)^2 \end{aligned} \tag{5.66}$$

The result of the integrations is

$$\begin{aligned} I_p = \delta^2 \{ &(\Delta' + \tau)(g_r + f_r)^2 + \tau \left[2(f_r)^2 - (f_p + f_r)(g_p - g_r) \right] \\ &- \frac{1}{3}\delta \left[(g_p)^2 + f_p f_r + g_r(f_p - f_r) \right] \} \end{aligned} \tag{5.67}$$

$$\begin{aligned} I_c = \delta \{ &G_0[a(g_p - f_p) + 2\tau^2 f_p + \tau(\delta_2 - \delta_1)g_p] \\ &- F_0[a(g_r - f_r) + 2\tau^2 f_r - \tau(\delta_2 - \delta_1)f_r] \} \end{aligned} \tag{5.68}$$

$$I_b = \frac{2}{3}\tau^3(F_0^2 + G_0^2) \tag{5.69}$$

where $a = \delta_1^2 + \delta_1\delta + \delta^2/3$. Galvosas *et al.* show that the cross term can always be eliminated ($I_c = 0$) if the ratios of the pulsed gradients are set to obey [43]

$$\frac{g_p}{f_p} = \frac{a - 2\tau^2}{a + \tau(\delta_2 - \delta_1)} \tag{5.70}$$

and

$$\frac{g_r}{f_r} = 1 - \frac{2\tau^2 - \tau(\delta_2 - \delta_1)}{a} \tag{5.71}$$

Further details regarding the practical setting of ratios in an easy manner are given in reference [43].

5.5.4 More efficient encoding schemes

DIFFTRAIN

A useful variant of the stimulated-echo sequence, which allows for repeated sampling at different diffusion times Δ, has been proposed by Buckley *et al.* [44]. The key idea

behind their 'DIFFTRAIN' method, shown in Fig. 5.23, is the replacement of the final 90° RF pulse by a small tip-angle (α) pulse, so that only a fraction, $\sin\alpha$, of the stored magnetisation is recalled for echo sampling, leaving a fraction $\cos\alpha$ remaining along the z-axis for subsequent recall. This allows a range of Δ values to be explored in a single excitation process,[14] thus significantly improving the efficiency of the experiment. Of course there is a price to be paid. So long as we are only interested in the echo amplitude as sampled by a single point in the time domain, the method works well. But should we wish to sample the FID following the echo, an essential requirement if spectral resolution is desired, then we must trade away the acquisition time (and hence the spectral resolution) against the fineness of the Δ stepping interval.

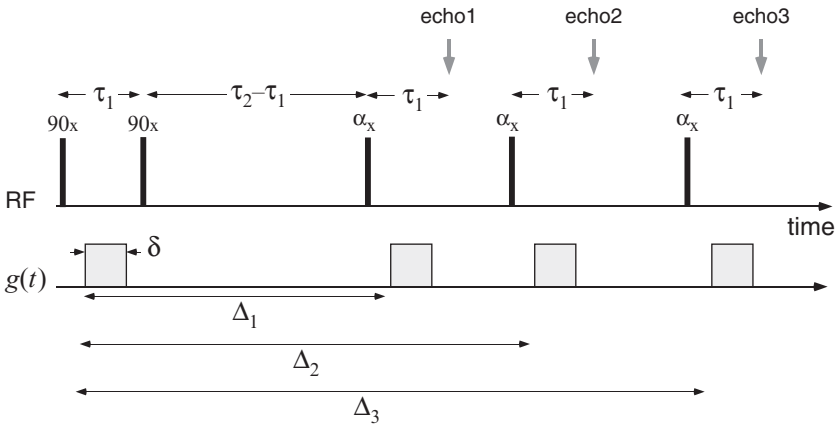

Fig. 5.23 DIFFTRAIN stimulated-echo pulse sequence in which a small tip angle-pulse α_x is used to successively recall magnetisation already encoded by the first gradient pulse. By this means, multiple echoes corresponding to different values of Δ may be obtained in a single shot.

Multiple-modulation multiple-echo

The downside of DIFFTRAIN is the sacrifice of signal-to-noise ratio inherent in the use of small tip angles. In many signal-rich applications this is a small price to pay. But in applications where signal-to-noise ratio is inherently poor, for example in borehole NMR well-logging operations, maximisation of available signal is paramount. A comparison familiar in MRI is to be found in the relative performance of fast low angle shot (FLASH) imaging [45], where multiple recall of magnetisation via low tip-angle pulses is used, and the echo planar imaging (EPI) [12] or rapid acquisition relaxation enhanced imaging (RARE) techniques, [13] where full signal recall is made using gradient of spin-echo trains. These comparisons are further discussed in Chapter 10.

By analogy, Y-Q Song and co-workers [46, 47] have suggested the use of echo train recycled magnetisation with large tip angle RF pulses to provide a multiple gradient

[14]Note that the fraction of magnetisation that remains after n recall events is $\cos^n\alpha$, so that for small tip angles, the available stored magnetisation decays quite slowly with increasing n.

step encoding in diffusion and flow measurements, an experiment termed multiple-modulation multiple-echo (MMME). However, unlike RARE or EPI, MMME uses unequal time spacings that generate a maximal number of spin echoes. For example, as discussed in Section 4.6.2, the stimulated-echo pulse sequence generates two additional spin echoes, the echo of the initial pulse FID caused by the second pulse, and the echo of that echo caused by the third pulse. Using a formalism developed by Hürlimann [48], it is possible to account for the effect of relaxation, diffusion (or flow) on multiple echo amplitudes in more complex RF and gradient pulse trains. First, however, it is helpful to design an RF sequence that generates a large number of echoes, all nicely separated. An example is shown in Fig. 5.24, the so-called '1-3-9' sequence, in which the four RF pulses of turn angles α_1 to α_4 are spaced by τ, 3τ, and 9τ. The generation of such equally spaced echoes was first pointed out by Hennig [49]. The series can be adjusted by factors of 3, as in MMME3 '1-3', MMME5 '1-3-9-27' and so on.

Under the influence of a constant gradient, the RF pulses are slice-selective, and the spatial modulation of the frequency can lead to complex echo shapes. Song and co-workers have shown that these effects can be minimised, and that echoes of nearly equal magnitude can be achieved in the MMM4 sequence by using $\alpha_1 = 54.74°$, $\alpha_2 = \alpha_3 = 70.53°$, and $\alpha_4 = 109.47°$. The use of this large turn angle compromise ensures that the echo amplitudes, while reduced somewhat (about a quarter of the full Hahn echo), are larger than achievable by low turn angle recall.

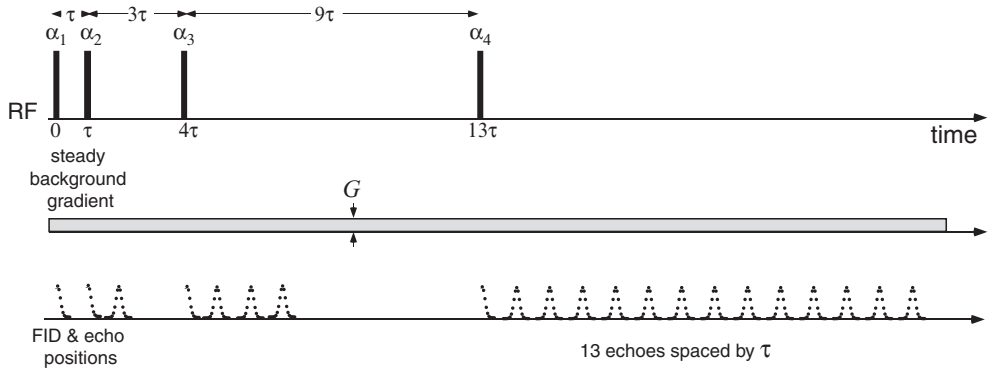

Fig. 5.24 MME4 pulse sequence in which the pulse spacings are set so as to generate 13 equally spaced echoes after the fourth RF pulse. The figure shows the positions of FIDs and echoes, though their relative amplitudes in practice depend on the RF pulse turn angles, α_1 to α_4. Each echo has its own relative sensitivity to relaxation and diffusion, factors which need to be calculated from an analysis of each coherence pathway. (Adapted from Song *et al.* [47].)

The diffusion sensitivity for each echo can be defined by a factor $b_{\mathbf{Q}}$, where $\mathbf{Q}$ is a vector that describes the apparent precession states of the magnetisation component contributing to that echo at each interval during the echo sequence, $Q = \pm 1$ referring to transverse magnetisation components of opposite sign precession and 0 indicating magnetisation in z-storage. Note that the natural state of precession in the transverse

Table 5.1 Diffusion sensitivity of MME4 sequence. The Q value indicates the sense of precession for magnetisation components in the transverse plane, where 0 indicates magnetisation in z-storage. The starting condition prior to α_1 is of course 0. (From Song *et al.* [47].)

Echo number	**Q**					$b_{\mathbf{Q}}$
1	0	1	0	0	−1	38/3
2	0	−1	1	0	−1	42
3	0	0	1	0	−1	99
4	0	1	1	0	−1	560/3
5	0	−1	−1	1	−1	126
6	0	0	−1	1	−1	162
7	0	1	−1	1	−1	704/3
8	0	−1	0	1	−1	345
9	0	0	0	1	−1	486
10	0	1	0	1	−1	2009/3
11	0	−1	1	1	−1	888
12	0	0	1	1	−1	1152
13	0	1	1	1	−1	4394/3

plane is a clockwise $Q = -1$. This is apparent in our complex number representation of transverse plane precession by the factor $\exp(-i\phi) = \exp\left(-i\gamma\mathbf{r}\cdot\int_0^t \mathbf{g}^*(t')dt'\right)$. However, subsequent RF pulses can invert phases of transverse magnetisation so as to make them appear later as $Q = 1$, the idea of 180° RF pulses causing the prior effective gradient to be reversed, being an example of that. The crucial point to understand is that, just as with the effective gradient idea, the successive states of the **Q**-vector are viewed from the perspective following the final α_4 RF pulse.

The easiest way to appreciate the notation is to start with echo 13. Here α_1 generates a transverse plane component of magnetisation, with a clockwise precession $Q = -1$. The successive components after α_2 and α_3 are those remaining in the transverse plane and continuing as $Q = -1$. Then α_4 performs an inversion, all previous Q values are inverted to $+1$, and it is left to the natural -1 precession after α_4 to reverse the accumulated phases of 13 τ intervals preceding. When a component is stored along z, as denoted by $Q = 0$, the phase is stored as a $\cos\phi$ or $\sin\phi$ component, in other words a superposition of $\exp(-i\phi)$ and $\exp(i\phi)$. Thus z-storage generates the phase reversal necessary to make possible an echo after α_4. Using these simple ideas, the echo number analysis is easily performed by accumulating phase based on local Q-value weighted by the relevant duration between RF pulses.

Because the intrinsic echo amplitudes in the absence of diffusion differ, the easiest way to use MMME is to perform two experiments with two different τ values, so that the intrinsic amplitudes (provided relaxation is negligible) will be identical. Then the echo attenuation may be written in terms of the ratios of corresponding echoes as

$$\frac{E(\tau)}{E(\tau')} = \exp\left(-b_{\mathbf{Q}}\gamma^2 DG^2\left[\tau^3 - \tau'^3\right]\right). \tag{5.72}$$

The MMME method may be extended to multiple dimensions by inclusion of pulsed gradients in other directions, retaining the steady gradient component to properly space the echoes. Examples of this approach to measure the diffusion tensor, or to combine diffusion measurements with imaging, are given in reference [47].

DANTE 'one shot' methods

Another approach to rapid diffusion measurement is to use multi-frequency magnetisation gratings, generated by pulse sequences that excite a discrete spectrum of frequencies in the presence of a magnetic field gradient. Principal among these is the DANTE sequence proposed by Morris and Freeman [50]. The sequence name (Delays alternating with nutations for tailored excitation) alludes to the repetitive circular journeys by Dante and Virgil in Dante Alighieri's *Purgatorio*, akin to the trajectories undergone by off-resonant spins. B_1 value.

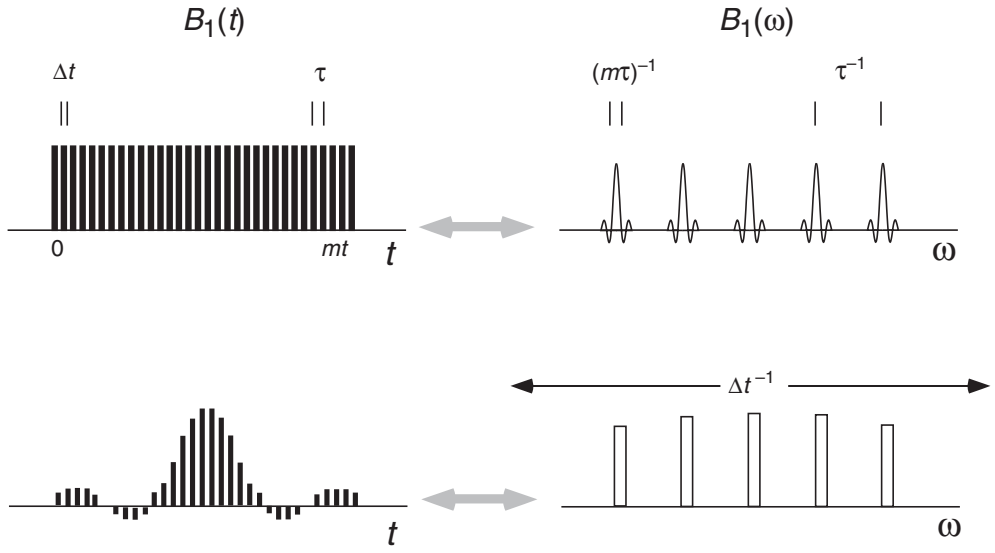

Fig. 5.25 DANTE train of RF pulses with corresponding frequency spectra. In the upper part of the diagram the RF modulation takes the form of a series of m equally spaced rectangular pulses. Because the train is finite, this is equivalent to multiplication by a Heaviside window, causing each frequency-domain spike to be convoluted with a sinc profile. In the lower part, the use of an overall sinc window implies that the local spike profile will be rectangular. Note that the spectrum has a finite extent, Δt^{-1}, determined by the width of the RF pulses.

A simple explanation is obtained by using linear response theory. Figure 5.25 shows a series of m RF pulses, of duration Δt and spacing τ, for which a spin isochromat on-resonance experiences a total flip angle $m\gamma B_1 \Delta t$. The frequency response of this train is shown alongside and consists of a comb of sidebands spaced by τ^{-1}, with each spike in the comb having the form of a sinc function of width $(mt)^{-1}$, the total comb width being of order $(\Delta t) - 1$. For a specific total turn angle, such as $\pi/2$, B_1 can

be made arbitrarily large by making Δt sufficiently short, within the constraints set by the transmitter bandwidth. By choosing τ sufficiently short that the off-resonant sidebands are outside the spectral range of the spins, the selective excitation will be confined to the central on-resonant comb element, with an excitation bandwidth given by $(m\tau)^{-1}$. Because of the sharp discrete nature of the spin precession steps, it is possible to use a value of B_1 that is larger by a factor of $\tau/\Delta t$ than that used in continuous RF excitation, thus avoiding the non-linear transmission problem that is so severe at low levels of B_1. The additional transmitted power is, of course, dissipated in the outer sidebands and, for a specific total turn angle θ, represents no more in total than would be applied to the coil in a hard θ pulse at the same B_1 value. It is not necessary to restrict the DANTE sequence to equal amplitude (or phase) RF pulses. Indeed, where an ideal rectangular frequency spread is desired in the selective excitation, the train can be sinc modulated as shown in the lower part of Fig. 5.25.

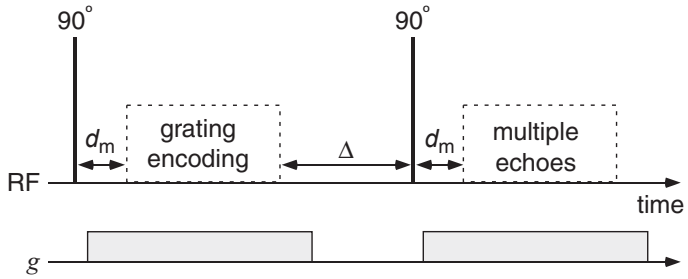

Fig. 5.26 Schematic grating-based diffusion pulse sequence in which the grating block consists of RF pulses with small tip angles. The magnetisation grating created by the excitation decays during the period Δ, and the remaining pattern is detected as a train of echoes. (Adapted from Szutkowski and Furó [51].)

Szutkowski and Furó [51] have developed an effective method for the measurement of diffusion using one-shot magnetisation grating methods, based on an earlier sequence by Zha and Lowe [52]. The principle is shown schematically in Fig. 5.26. The DANTE RF pulse sequence is applied during the 'grating encoding' period and results in a multiple echo train during the time domain of the detection period, the amplitude of each echo being proportional to the corresponding component of the grating. The delay period Δ allows molecules to diffuse, thus blurring the grating and resulting in echo attenuation. The echo train readout is sensitive to Stejskal–Tanner-like attenuation as $g^2(n\tau)^2$, where τ is the DANTE (and echo) pulse spacing. In a single-shot measurement of echo attenuation vs $g^2(n\tau)^2$, for a sample comprising both protonated water and polyethylene glycol (M_w=6000), Szutkowski and Furó were able to clearly identify bi-exponential diffusion decay [51].

5.5.5 Using pulsed gradients to measure the diffusion tensor

We now rewrite the Bloch–Torrey equation when the diffusive behaviour of the spin ensemble is represented by the tensor $\underline{\underline{D}}$,

$$\frac{\partial M_+}{\partial t} = -i\gamma \mathbf{r}\cdot\mathbf{g}^*(t)M_+ - \frac{M_+}{T_2} + \nabla\cdot\underline{\underline{D}}\nabla M_+ - (\mathbf{v}\cdot\nabla)M_+ \tag{5.73}$$

with solution

$$\begin{aligned} A(t) &= \exp(-\gamma^2\int_0^t\left[\int_0^{t'}\mathbf{g}^*(t'')dt''\right]^T\underline{\underline{D}}\left[\int_0^{t'}\mathbf{g}^*(t'')dt''\right]dt') \\ &\quad\times\exp(i\gamma\mathbf{v}\cdot\int_0^t\int_0^{t'}\mathbf{g}^*(t'')dt''dt') \end{aligned} \tag{5.74}$$

where $\mathbf{g}^*(t) = \left(g_x^*(t), g_y^*(t), g_z^*(t)\right)^T$. The normalised echo attenuation for the idealised Stejskal–Tanner pulse sequence is therefore

$$E(\mathbf{g}) = \exp(i\gamma\delta\mathbf{g}\cdot\mathbf{v}\Delta - \gamma^2\delta^2\mathbf{g}^T\underline{\underline{D}}\mathbf{g}(\Delta-\delta/3)), \tag{5.75}$$

$\mathbf{g}$ being the vector description of the magnetic field gradient pulse amplitude. Expressions for echo attenuation in the case of isotropic diffusion continue to apply by simply replacing g^2D by $\mathbf{g}^T\underline{\underline{D}}\mathbf{g}$. Note that a commonly used shorthand notation is $\underline{\underline{g}} : \underline{\underline{D}}$ where $\underline{\underline{g}}$ is formed by the outer product $\mathbf{g}^T\mathbf{g}$. In an experiment in which the gradients have components along all three axes, the diffusive attenuation is

$$\begin{aligned} E(\mathbf{g}) &= \exp(-\gamma^2\delta^2[g_{xx}D_{xx} + g_{yy}D_{yy} + g_{zz}D_{zz} \\ &\quad +(g_{xy}+g_{yx})D_{xy} + (g_{yz}+g_{zy})D_{yz} + (g_{zx}+g_{xz})D_{zx}](\Delta-\delta/3)). \end{aligned} \tag{5.76}$$

For self-diffusion $\underline{\underline{D}} = \underline{\underline{D}}^T$ so that there exist six independent elements of the diffusion tensor to be determined. In a typical experiment, seven independent gradient directions are used to determine the six independent $D_{\alpha\beta}$ elements along with the echo amplitude at zero gradient, $E(0)$. A suitable combination is

$$\mathbf{g} = g_0\{(1,0,0),(0,1,0),(0,0,1),(1,0,1),(1,1,0),(0,1,1),(1,1,1)\}. \tag{5.77}$$

The $\underline{\underline{D}}$ matrix is then diagonalised by a similarity transformation to find the eigenvalues corresponding to the diagonal elements in the principal axis frame. This similarity transformation of course represents the rotation required to take the lab-frame coordinates to the principal-axis frame and, as a consequence, the process of measuring the diffusion tensor not only reveals the underlying diffusion anisotropy, but also the direction of the axis corresponding to the most rapid diffusion coefficient. As a consequence the method has proven particularly useful a contrast in medical imaging [53], where the fast diffusion axis direction enables one to track the orientation of nerve fibres or other aligned tissue structure.

5.6 Pulsed gradient spin-echo NMR: general motion

Of course, diffusion and flow represent an important but nonetheless specific type of molecular motion. For more general motions it is not possible to obtain a closed form

expression for the echo amplitude under all possible effective gradients, $\mathbf{g}^*(t)$ using the Bloch–Torrey approach. However, there does exist a variant of the PGSE experiment for which general analytic expressions are available. E.O. Stejskal pointed out [27] that for the particular case of narrow gradient pulses, in the limit as $\delta \to 0$, it is possible to use the propagator formalism for molecular translational dynamics, introduced in Chapter 1.

5.6.1 Narrow gradient pulse approximation and q-space

The principle underlying this description is that gradient pulses must be sufficiently narrow that we may neglect motion over their duration. In the case of unrestricted diffusion, the narrow pulse condition might naively translate to $\delta \ll \Delta$, although, as we have seen, we know how to handle unrestricted diffusion when the pulse width is finite. The meaning of narrow in this context really hinges on the existence of any characteristic times for the motion. For unrestricted steady flow there is no characteristic length or time scale, and likewise for self-diffusion, at time intervals beyond the molecular collision time. But where boundaries to motion exist, as in a porous medium or lyotropic liquid crystal, or when translational dynamics differ across a hierarchy of timescale regimes, as in the case of segmental self-diffusion for entangled polymers, then characteristic lengths and timescales play a significant role in determining the characteristics of the propagator for translational motion, and the allowed conditions for narrow pulse approximation will be so-determined.

Using the narrow pulse approach, we can see that the effect of the first gradient pulse is to impart a phase shift $\gamma\delta\mathbf{g}\cdot\mathbf{r}$ to a spin located at position $\mathbf{r}$ at the instant of the pulse, as shown in Fig. 5.27. This phase shift is subsequently inverted by the 180°_y RF pulse. Suppose that the molecule containing the spin has moved to $\mathbf{r}'$ at the time of the second gradient pulse. The net phase shift following this pulse will be $\gamma\delta\mathbf{g}\cdot(\mathbf{r}'-\mathbf{r})$. If the spins are stationary then, of course, a perfectly refocused echo will occur. Any motion of the spins will cause phase shifts in their contribution to the echo. The size of this shift is a product of two vectors, the dynamic displacement $(\mathbf{r}'-\mathbf{r})$ and a vector $\gamma\delta\mathbf{g}$.

The conditional probability and q-space

Again we define our 'echo signal' , $E(\mathbf{g},\Delta)$, as the amplitude of the echo at its centre and, as important as these may be in determining the actual signal-to-noise ratio of our experiment, we neglect relaxation effects, which are removed by the normalisation process. We handle the ensemble average of individual spin contributions by taking each phase term $\exp(i\gamma\delta\mathbf{g}\cdot[\mathbf{r}-\mathbf{r}'])$ weighted by the probability for a spin to begin at $\mathbf{r}$ and move to $\mathbf{r}'$ at later time Δ. Using the Markovian propagator definition of Section 1.3.3, this probability is identically $p(\mathbf{r},0)P(\mathbf{r}|\mathbf{r},t)$. Of course, in NMR the probabilities we are interested in concern molecules existing at a particular location along with their spin magnetisation having survived. In experiments where the magnetisation is freshly prepared, for example transverse magnetisation following a 90° RF pulse being applied to an ensemble of spins in thermal equilibrium, there is no distinction to be made, so that $M(\mathbf{r},0)$ and $p(\mathbf{r},0)$ are synonymous, and both will be simply equal to the molecular density function, $\rho(\mathbf{r})$ that characterises the sample, the

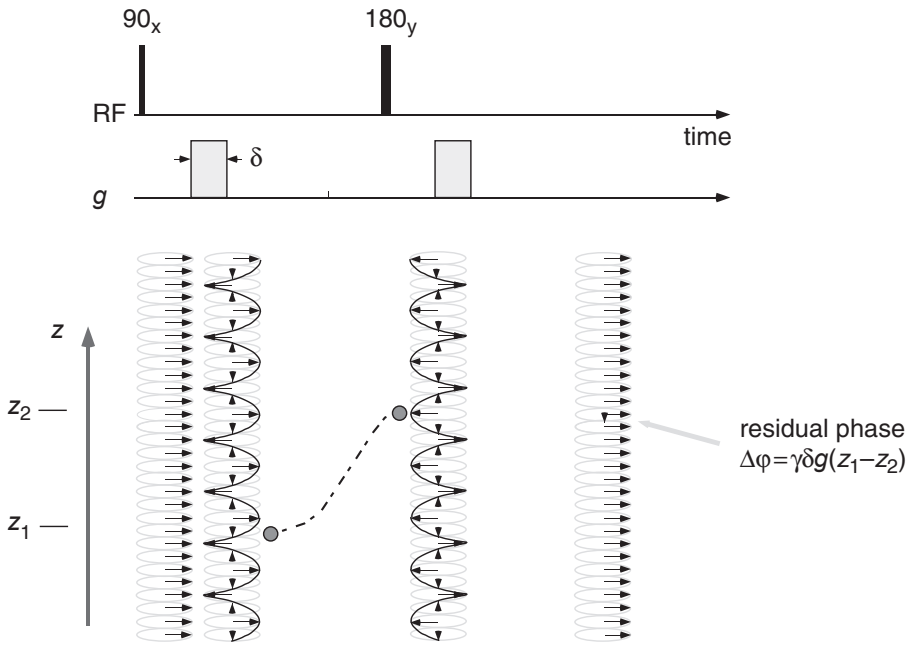

Fig. 5.27 The effect of displacement along the gradient direction in the narrow pulse depiction of the Stejskal–Tanner PGSE experiment. A spin-bearing molecule migrating by a displacement $Z = z_2 - z_1$ over the time between the gradient pulses results in a residual phase shift $\gamma\delta g Z$.

same density we measure in NMR imaging. For the rest of this chapter, we shall write the starting density condition as $\rho(\mathbf{r})$ and treat $\rho(\mathbf{r})P(\mathbf{r}|\mathbf{r},t)$ as the probability for a spin to begin at $\mathbf{r}$ and move to $\mathbf{r}'$ at later time Δ. Thus

$$E(\mathbf{g},\Delta) = \int \rho(\mathbf{r}) \int P(\mathbf{r}|\mathbf{r},\Delta) \exp(i\gamma\delta\mathbf{g}\cdot[\mathbf{r}-\mathbf{r}'])d\mathbf{r}'d\mathbf{r} \tag{5.78}$$

In fact eqn 5.78 bears a close resemblance to the expressions (such as eqn 5.17) that were used to describe the signal in **k**-space imaging. We will pursue this analogy by defining a reciprocal space q, where[15]

$$\mathbf{q} = \gamma\delta\mathbf{g} \tag{5.79}$$

in units of angular spatial frequency, radians m^{-1}, or

$$\check{\mathbf{q}} = \frac{1}{2\pi}\gamma\delta\mathbf{g} \tag{5.80}$$

in units of cyclic spatial frequency, m^{-1}.

[15]This **q**-space notation, which follows in an obvious manner from a neutron scattering analogy, was first introduced in reference [54], while the connection with neutron scattering was originally outlined in reference [28].

The reader will find in the literature both versions, both written simply as $\mathbf{q}$. Therein lies a dilemma for the remainder of this book. Use of the angular frequency leads to simpler mathematical expressions, avoiding factors of 2π in the exponents of phase factors. Use of the cyclic frequency leads to a better comparison of structural features, $1/\check{q} = 2\pi/q$ being the relevant wavelength. In practice, one needs to be fluent with both forms, and for the rest of the book, we simplify the mathematics by using the angular frequency version. But we retain the symbol $\check{q}$ to explicitly identify cyclic frequency when desired.

Now eqn 5.78 can be rewritten

$$E(\mathbf{q}, \Delta) = \int \rho(\mathbf{r}) \int P(\mathbf{r}|\mathbf{r}', t) \exp(i\mathbf{q} \cdot [\mathbf{r}' - \mathbf{r}]) d\mathbf{r}' d\mathbf{r} \tag{5.81}$$

The neutron scattering analogy

The Pulsed Gradient Spin Echo NMR signal attenuation expression is akin to a scattering function which applies in inelastic neutron scattering where $\mathbf{q}$ is the scattering wavevector, as illustrated in Fig. 5.28. Eqn 5.81 is akin to the scattering function that applies in neutron scattering, where $\mathbf{q}$ is the scattering wavevector. PGSE and neutron scattering are closely analogous, as illustrated in Fig. 5.28, the main differences being the scale of temporal and spatial regimes sampled, and the detection of $E(\mathbf{g}, \Delta)$ in the time domain of Δ in the case of PGSE and in the frequency domain in the case of neutron scattering.

Neutron scattering results in a q-dependent signal which comprises two components. The first, known as the *coherent* part, is sensitive to relative displacements between nuclear scattering centres, and yields a diffraction pattern related to the average sample structure. The second, known as the *incoherent* part, is sensitive to time-dependent displacements of individual nuclear scattering centres, and so provides information regarding dynamics, revealed as a change in the outgoing neutron energy. Incoherent scattering is associated with spin-flips, which provide the ability in principle to localise scattering and so 'collapse the wavefunction' so that interference effects disappear.

Equation 5.81 is equivalent to the neutron scattering function for the incoherent fraction,

$$S_{incoherent} = \overline{N^{-1} \sum_{i=1} \exp(i\mathbf{q} \cdot [\mathbf{r}_i(t) - \mathbf{r}_i(0)])} \tag{5.82}$$

where the sum is taken over all N scattering centres. By contrast, the coherent neutron scattering is described by

$$S_{coherent} = \overline{N^{-2} \sum_{i=1} \sum_{j=1} \exp(i\mathbf{q} \cdot [\mathbf{r}_j(t) - \mathbf{r}_i(0)])} \tag{5.83}$$

This sensitivity to relative motion, $\mathbf{r}_j(t) - \mathbf{r}_i(0)$, makes the interpretation of coherent neutron scattering and quasi-elastic light scattering more difficult. The direct measurement of self-motion is a major advantage in PGSE NMR.

While PGSE NMR and incoherent inelastic neutron scattering are formally analogous in their mathematical expression, there exist a number of significant differences.

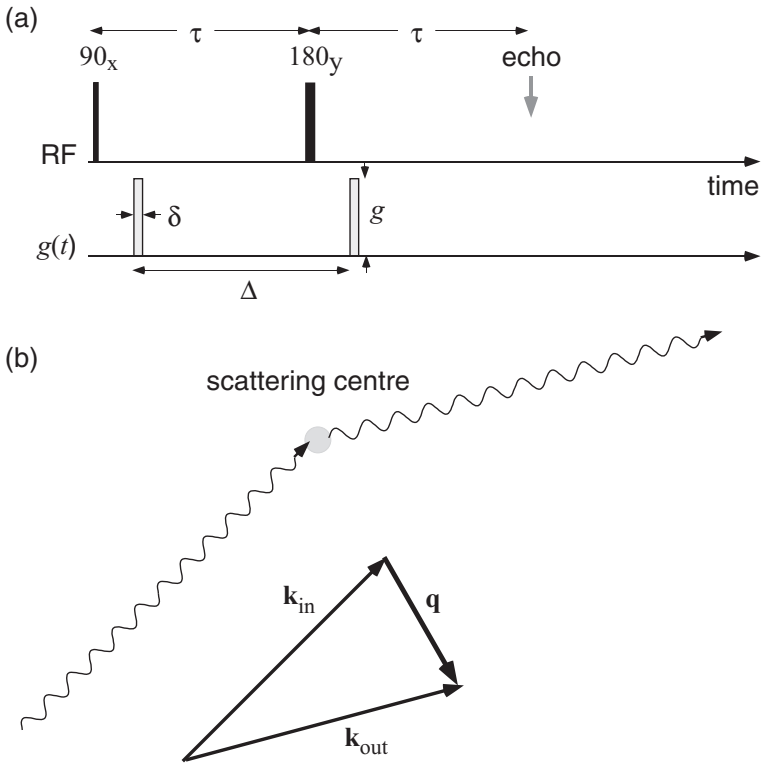

Fig. 5.28 (a) Narrow pulse approximation PGSE NMR and (b) scattering analogy in which the scattering wavevector, $\mathbf{q}$, has magnitude $\gamma\delta g$ (in angular spatial frequency units) and orientation given by the gradient direction.

Most obvious are the very scales of temporal and spatial regimes sampled, and the detection of $E(\mathbf{g}, \Delta)$ in the time domain of Δ in the case of PGSE and in the frequency domain in the case of neutron scattering. But in a more fundamental sense, the reader should not be tempted to identify Fig. 5.28 b) with the process of applying two magnetic field gradient pulses in PGSE NMR. In no sense are the incoming and outgoing $\mathbf{k}$ vectors equivalent to the actions of the first and second gradient pulses,[16] the underlying physics of the two methods being fundamentally different. Nonetheless, it has become customary to refer to PGSE NMR as 'scattering', and this practice is harmless unless actually believed.

The averaged propagator and q-space

Clearly the phase shifts appearing in the integrand of eqn 5.81 depend only on the dynamic displacement, $\mathbf{R} = \mathbf{r}' - \mathbf{r}$. Using the definition of the averaged propagator [55] given in eqn 1.81,

[16]The reader will see this immediately by noting that such an assumption would imply that PGSE NMR corresponds to $\mathbf{k}_{\text{out}} = -\mathbf{k}_{\text{in}}$, in which case $\mathbf{q} = 2\mathbf{k}$, in violation of eqn 5.79.

$$\overline{P}(\mathbf{R},t) = \int \rho(\mathbf{r}) P(\mathbf{r}|\mathbf{r}+\mathbf{R},t) d\mathbf{r}, \tag{5.84}$$

it is easy to see that eqn 5.81 may be rewritten[17]

$$E(\mathbf{q},\Delta) = \int \overline{P}(\mathbf{R},\Delta) \exp(i\mathbf{q}\cdot\mathbf{R}) d\mathbf{R}, \tag{5.85}$$

or, taking Z as the component of $\mathbf{R}$ along $\mathbf{q}$,

$$E(q,\Delta) = \int_{\infty}^{\infty} \overline{P}(Z,\Delta) \exp(iqZ) dZ \tag{5.86}$$

Equation 5.85 expresses a simple Fourier relationship between $E(\mathbf{q},\Delta)$ and $\overline{P}(\mathbf{R},\Delta)$. The meaning of the narrow pulse PGSE experiment is now transparent. Acquisition of the signal in q-space permits us to image $\overline{P}(\mathbf{R},\Delta)$, just as acquisition in $\mathbf{k}$-space permitted us to image $\rho(\mathbf{r})$. PGSE is an imaging experiment in its own right, probing the dynamic displacement space, $\mathbf{R}$, rather than the static displacements, $\mathbf{r}$. Note that while the echo attenuation, E, is implicitly a function of the PGSE pulse separation Δ, we shall often omit the argument Δ for simplicity.

For completeness it is helpful to write the normalised echo signals for diffusion and flow in this simple narrow pulse, $\mathbf{q}$-space perspective, that is

$$E(q,\Delta) = \exp(-q^2 D\Delta) \tag{5.87}$$

and

$$E(\mathbf{q},\Delta) = \exp(i\mathbf{q}\cdot\mathbf{v}\Delta) \tag{5.88}$$

5.6.2 Low q limit

An especially useful simplification occurs in the low q limit, that is,

$$E(\mathbf{q},\Delta) \approx 1 + iq\int \overline{P}(Z,\Delta) Z dZ - \tfrac{1}{2}q^2 \int \overline{P}(Z,\Delta) Z^2 dZ + \ldots \tag{5.89}$$

where Z is the projection of $\mathbf{R}$ along $\mathbf{q}$ and q is $|\mathbf{q}|$. The leading term linear in q represents a phase shift in the signal that informs on the mean displacement. For Brownian motion, or any other motion with no net flow, the linear term disappears and

$$E(\mathbf{q},\Delta) \approx 1 - \tfrac{1}{2}q^2 \langle Z^2(\Delta)\rangle \tag{5.90}$$

When the low q echo-attenuation data is plotted against q^2, the initial linear decay allows $\langle Z^2(\Delta)\rangle$ to be measured directly. This represents the simplest of all possible signal analysis in the case of the narrow gradient pulse PGSE experiment. In the study of hindered and restricted diffusion, such an analysis provides a useful guide to interdependence of length and time scales.

[17]The use of the average propagator formalism was introduced to description of the PGSE NMR experiment by Kärger and Heink [55].

5.6.3 The meaning of k-space and q-space for time-varying gradients

In the case of a magnetic field gradient, $\mathbf{G}(t)$, that varies with time, the naive definition of **k**-space given in eqn 5.15 needs revisiting. Of course, **k** provides a means of determining what phase has been acquired by a spin isochromat remaining stationary at position **r**. If the gradient is time-dependent then that phase will be given by the cumulation of incremental precessions, as described by the integral

$$\begin{aligned}\phi(t) &= \gamma \int_0^t \mathbf{g}(t') \cdot \mathbf{r} dt' \\ &= \gamma \left(\int_0^t \mathbf{g}(t') dt' \right) \cdot \mathbf{r}\end{aligned} \tag{5.91}$$

which tells us that

$$\mathbf{k}(t) = \gamma \left(\int_0^t \mathbf{G}(t') dt' \right) \tag{5.92}$$

where we use angular frequency units.

For q-space, where we used eqn 5.80 to define **q** pertaining to a pair of narrow gradient pulses, the redefinition is more subtle when a general time-varying effective gradient, $\mathbf{g}^*(t)$, is used over an experimental interval ranging from $t' = 0$ to the echo centre at $t' = t$. Of course, at the echo centre where the signal is to be acquired, $\int_0^t \mathbf{g}^*(t') dt' = 0$. And in the experiment where we encode for motion, we might expect that a definition of **q** will be provided by the requirement that the acquired phase is given by $\gamma \mathbf{q} \cdot \mathbf{R}$, where $\mathbf{R} = \mathbf{r}(t) - \mathbf{r}(0)$. But that phase is given by

$$\phi(t) = \gamma \int_0^t \mathbf{g}^*(t') \cdot \mathbf{r}(t') dt' \tag{5.93}$$

and it is clear that any definition of **q** will depend on a detailed knowledge of the trajectory $\mathbf{r}(t')$! Let us take a simple example where we know that trajectory, namely when the spin-bearing molecules are translating at a constant velocity **v** such that $\mathbf{R}(t') = \mathbf{v}t'$. Then

$$\phi(t) = \mathbf{v} \cdot \gamma \int_0^t t' \mathbf{g}^*(t') dt' \tag{5.94}$$

and, we may define for this special case,

$$\mathbf{q} = t^{-1} \gamma \int_0^t t' \mathbf{g}^*(t') dt' \tag{5.95}$$

For example, if we apply eqn 5.95 to the case of gradient pulses of width δ and amplitude g, then it is easy to show by this definition that q is simply given by the area under the gradient pulse, $q = \gamma g \delta$.

But in general, where the motion is unknown in advance, no simple definition of **q** is possible, except in the limit when $\mathbf{g}^*(t')$ takes the form of delta functions of opposite sign, applied at times $t' = 0$ and $t' = t$. In other words, only in the narrow gradient pulse approximation is the scattering analogy truly meaningful.

5.7 Finite gradient pulses and generalised motion

We now turn our attention to the problem of how to describe the spin echo attenuation under quite general conditions of motion. Clearly some generally modulated effective gradient, obeying the echo condition $\int_0^t \mathbf{g}^*(t')dt' = 0$ at some time t, will not be amenable to an exact description provided by the Bloch–Torrey relations unless the motion is unbounded diffusion or flow. For example, when the gradient pulse widths of a PGSE experiment are finite in comparison with some characteristic dynamical timescale, eqn 5.78 breaks down. Such a timescale might be the time, τ_{pore}, for liquid or gas molecules in a porous medium to diffuse across a pore space. τ_{pore} provides a measure for crossover from free Brownian motion at short times to restricted motion, with strong boundary influences, at long times. Clearly the narrow gradient pulse assumptions inherent in the derivation of eqn 5.78 no longer apply if $\delta \sim \tau_{pore}$.

In the next two sections we outline two different approaches to the problem. The first, which retains the language of conditional probabilities, provides a time-domain approach to a closed form analytic expression for generalised motion. The second utilises the frequency domain and provides expressions based on the analysis of the spectrum of the velocity autocorrelation function.

5.7.1 Multiple propagator approach

The multiple propagator approach is a method by which the language of the propagator may be generalised to handle any gradient waveform, and not just the two-impulse experiment. One motivation for this approach is to decouple the physics of the restricted diffusion from that of the NMR pulse sequence employed. Ideally we would like a general expression for the echo attenuation that satisfies the following two conditions. First, the propagator description should be retained and the nature of the restricted diffusion should be embedded entirely within the mathematical form of that propagator. Second, the gradient waveform should appear within a closed form expression in a natural and obvious manner, so that the time sequence of the waveform evolution is explicit.

The method is based on a suggestion by Caprihan, Wang, and Fukushima [56], who postulated that the case of restricted diffusion under general gradient waveforms could be handled by breaking the gradient pulse into successive intervals, writing a propagator for each stage of the evolution. Their method involved quite a complex sum over a large number of independent terms. Here we adopt a similar philosophy, but using a different approach which leads to much simpler, and quite general, closed-form expressions. The chosen approach [57] explicitly demonstrates the succession of spin phase evolutions at each step of the gradient waveform and the evolutions are expressed in terms of a product of matrix operators, between which are sandwiched time-evolution terms associated with the diffusive motion. Note that the mathematical description is developed in terms of motion that is fundamentally diffusive, albeit restricted, although in principle it could be generalised to any motion where a conditional probability description was possible.

Discretising the effective gradient waveform

In order to retain the language of propagators when dealing with generalised gradient waveforms, the translational motion must be sub-divided into a sequence of discrete time intervals, with all spin phase evolution taking place at well-defined times at the boundaries of those intervals. In other words we will require the narrow pulse approximation of eqn 5.78 to apply over each evolutionary step, if not over the entire waveform duration. This means, in effect, that we must approximate the gradient waveform by a succession of impulses, such that the time integral function, $\mathbf{F}(t) = \int_0^t \mathbf{g}^*(t')dt'$, is represented by a stepwise progression. The basic scheme is shown in Fig. 5.29.

Suppose that we break the waveform into N time intervals τ, each bounded by impulses $\mathbf{q}_n$, $\mathbf{q}_{n+1}$ etc. We may discretise the waveform amplitude $\mathbf{g}^*(n\tau)$ into units of dimension $\mathbf{g}_{step}$. At time $n\tau$ the impulse will be $\mathbf{q}_n = m_n\mathbf{q}$, where $\mathbf{q} = \gamma\delta\mathbf{g}_{step}$ and m_n is some positive or negative integer, depending on the local magnitude and sign of $\mathbf{g}^*(n\tau)$, and given by

$$m_n = integ(\mathbf{g}^*(n\tau))/\mathbf{g}_{step} \tag{5.96}$$

We may write the echo amplitude at the end of the sequence as

$$\begin{aligned} E(t) \;=\; & \int d\mathbf{r}_1 \int d\mathbf{r}_2 \ldots \int d\mathbf{r}_{N+1} \\ & \rho(\mathbf{r}_1)\exp(i\mathbf{q}_1\cdot\mathbf{r}_1)P(\mathbf{r}_1|\mathbf{r}_2,\tau)\exp(i\mathbf{q}_2\cdot\mathbf{r}_2)P(\mathbf{r}_2|\mathbf{r}_3,\tau) \\ & \ldots\exp(i\mathbf{q}_N\cdot\mathbf{r}_N)P(\mathbf{r}_N|\mathbf{r}_{N+1},\tau) \end{aligned} \tag{5.97}$$

Multiple propagators expressed in the eigenfunction expansion

Using the eigenmode expansion $P(\mathbf{r}|\mathbf{r}',\tau) = \sum_{k=0}^{\infty} u_k(\mathbf{r})u_k^*(\mathbf{r}')\exp(-\lambda_k\tau)$,

$$\begin{aligned} E(t) \;=\; & \int d\mathbf{r}_1 \int d\mathbf{r}_2 \ldots \int d\mathbf{r}_{N+1} \\ & \rho(\mathbf{r}_1)\exp(i\mathbf{q}_1\cdot\mathbf{r}_1)\sum_{k_1} u_{k_1}(\mathbf{r}_1)u_{k_1}^*(\mathbf{r}_2)\exp(-\lambda_{k_1}\tau) \\ & \exp(i\mathbf{q}_2\cdot\mathbf{r}_2)\sum_{k_2} u_{k_2}(\mathbf{r}_2)u_{k_2}^*(\mathbf{r}_3)\exp(-\lambda_{k_2}\tau) \\ & \ldots\exp(i\mathbf{q}_N\cdot\mathbf{r}_N)\sum_{k_N} u_{k_N}(\mathbf{r}_N)u_{k_N}^*(\mathbf{r}_{N+1})\exp(-\lambda_{k_N}\tau) \end{aligned} \tag{5.98}$$

Regrouping the summations, a succession of matrix products emerges as

$$\begin{aligned} E(t) \;=\; & \int d\mathbf{r}_1 \int d\mathbf{r}_2 \ldots \int d\mathbf{r}_{N+1} \\ & \rho(\mathbf{r}_1)\exp(i\mathbf{q}_1\cdot\mathbf{r}_1)\sum_{k_1,k_2,k_3\ldots k_N} u_{k_1}(\mathbf{r}_1)u_{k_1}^*(\mathbf{r}_2)\exp(-\lambda_{k_1}\tau) \\ & \exp(i\mathbf{q}_2\cdot\mathbf{r}_2)u_{k_2}(\mathbf{r}_2)u_{k_2}^*(\mathbf{r}_3)\exp(-\lambda_{k_2}\tau) \\ & \ldots\exp(i\mathbf{q}_N\cdot\mathbf{r}_N)u_{k_N}(\mathbf{r}_N)u_{k_N}^*(\mathbf{r}_{N+1})\exp(-\lambda_{k_N}\tau) \end{aligned}$$

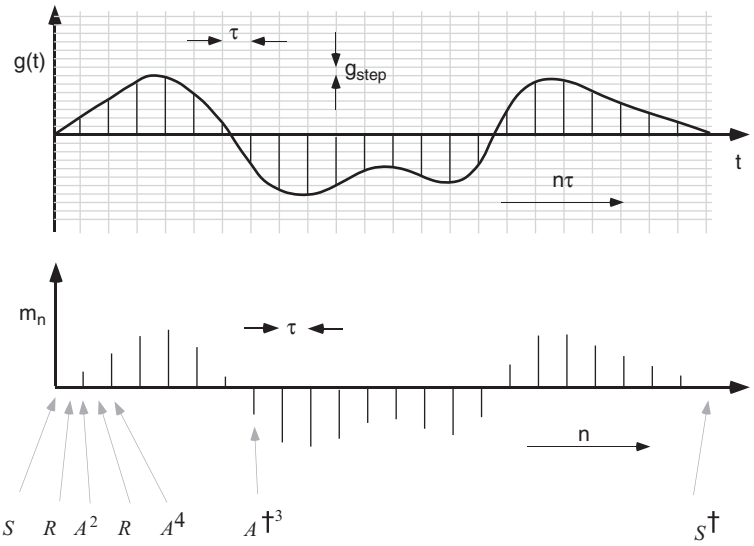

$$SRA^2RA^4RA^6RA^6RA^4RA^2RA^{\dagger 3}RA^{\dagger 6}RA^{\dagger 7}RA^{\dagger 6}RA^{\dagger 4}RA^{\dagger 4}RA^{\dagger 3}RA^{\dagger 4}RA^{\dagger 5}RA^{\dagger 4}RA^3RA^6RA^6RA^5RA^4RA^3RA^2RA^{\dagger}$$

Fig. 5.29 Schematic decomposition of a generalised gradient waveform into a sequence of equally time-separated impulses, the magnitudes of each of which are expressed as integer multiples, m_n, of the basic digitisation unit, g_{step}. From this train the succession of matrix operators may be written directly, starting and finishing with the S row and column vectors. The effect of the diffusive evolution is contained within the diagonal R matrices, while that of the phase evolutions is contained in the A matrices, each of which is raised to the power m_n, the integer corresponding to the impulse strength at the nth step. Negative gradients are represented by using the Hermitian transpose of A. The entire sequence shown is indicated in the matrix product below the diagram.

$$\begin{aligned} = \sum_{k_1,k_2,k_3\ldots k_N} & S_{k_1}(\mathbf{q}_1)R_{k_1k_1}A_{k_1k_2}(\mathbf{q}_2))R_{k_2k_2}A_{k_2k_3}(\mathbf{q}_3) \\ & \ldots R_{k_{N-1}k_{N-1}}A_{k_{N-1}k_N}(\mathbf{q}_N))R_{k_Nk_N}S^*_{k_N}(\mathbf{q}_{N+1}) \end{aligned} \tag{5.99}$$

where

$$S_k(\mathbf{q}) = V^{-1/2}\int d\mathbf{r}u_k(\mathbf{r})\exp(i\mathbf{q_k}\cdot\mathbf{r}), \tag{5.100}$$

$$R_{kk} = \exp(-\lambda_k\tau), \tag{5.101}$$

and

$$A_{kk'} = \int d\mathbf{r}u^*_k(\mathbf{r})u_{k'}(\mathbf{r})\exp(i\mathbf{q_{k'}}\cdot\mathbf{r}) \tag{5.102}$$

and the initial density, $\rho(\mathbf{r}_1)$, may be set to the inverse of the pore volume (V), provided that the eigenfunctions are appropriately normalised.

Equation 5.99 describes a matrix multiplication process. For the moment, let us note a helpful result which follows from the orthogonality condition $\delta(\mathbf{r}' - \mathbf{r}) = \sum_k u_k(\mathbf{r})u_k^*(\mathbf{r}')$, namely

$$A_{kk''}(\mathbf{q}_A + \mathbf{q}_B) = \sum_{k'} A_{kk'}(\mathbf{q}_A)A_{k'k''}(\mathbf{q}_B) \tag{5.103}$$

From this we obtain the result that $A(n\mathbf{q}) = A(\mathbf{q})^n$.

The matrix product

With these results we may write our echo-attenuation scheme using the simple matrix product

$$E = S(\mathbf{q}_1)RA(\mathbf{q}_2)RA(\mathbf{q}_3).....RA(\mathbf{q}_N)RS^\dagger(-\mathbf{q}_{N+1}) \tag{5.104}$$

It is the recognition of the matrix algebra inherent in eqns 5.99 to 5.104 that represents the key simplifying step in the formulation of the problem. Because of the emergence of mathematical tools such as Matlab and Mathematica, the matrix product is very easy and very rapid to evaluate, and so the expression presented here provides a practical tool for rapid computation.

To illustrate how the method works, consider the case of an effective gradient waveform $\mathbf{g}^*(t)$, which begins and ends with zero amplitude and which has zero time integral at the sampling time in order to satisfy the echo condition. As shown in Fig. 5.29, the waveform may be represented by a series of equally spaced impulses. While this may seem a rather crude approximation in the domain of $\mathbf{g}^*(t)$, it provides a stepwise approximation to the more important time-integral waveform, $\mathbf{F}(t)$. Setting, for convenience, the initial and final impulses to the minimum value $\mathbf{q}$ (an unimportant requirement if N is sufficiently large),

$$E = S(\mathbf{q})R[A(\mathbf{q})]^{m_2}.....R[A(\mathbf{q})]^{m_n}.....R[A(\mathbf{q})]^{m_N}RS^\dagger(-\mathbf{q}) \tag{5.105}$$

Thus we find that, in general, any waveform may be handled, provided that we calculate just three matrices, $R(\tau)$, $S(\mathbf{q})$, and $A(\mathbf{q})$, where $\mathbf{q}$ is the smallest impulse used to digitise the waveform. Equation 5.105 is so straightforward that it can be immediately adapted to any sequence by organising the matrices as required.

Dimensions of the matrices

The matrix elements of S, R, and A are calculated, in the case of restricted diffusion within a pore, using the fundamental eigenfunction expansion for the particular geometry under study. The R matrix, which is diagonal, comprises the temporal solutions to the Fick's law differential equation, typically of the form $\exp(-\alpha_k^2 D_0\tau/a^2)$, where α_k is an eigenvalue dependent on the boundary conditions and a gives a measure of the pore dimension. These elements rapidly decay with increasing k and hence limit the required dimension of our matrices. The size $k_{max} \times k_{max}$ of our desired matrices will thus be determined by the exponents of the elements of the R-matrix, and our wish that matrix element sums converge when we multiplying out the products. Suppose we take the example of diffusion between parallel planes.[18] For $k \times k$ matrices the R-matrix elements will decay as $\exp(-k^2\pi^2 D_0\tau/a^2)$. Provided $k^2 D_0\tau/a^2 \sim 1$,

[18]This case, along with those of cylinders and spherical pores are treated in Chapter 7.

this convergence condition should be reasonably satisfied and 15 × 15 matrices are sufficiently accurate for calculating any gradient waveform response for plane parallel pore-restricted diffusion. The relatively small size of these matrices makes multiplication of large numbers of matrices extremely rapid, particularly using software such as Matlab™.

Application to standard gradient pulse schemes

Equation 5.105 can be easily evaluated for some cases of special interest shown in Fig. 5.30. The sequences are shown using a small number of impulses simply for clarity. In practice one may calculate the echo attenuation quite rapidly using on the order of 100 impulses.

(i) Steady gradient spin echo.
The effective gradient is as shown in Fig. 5.30(a). The waveform is subdivided into $2N + 1$ intervals and $2N + 2$ impulses, so that the total effective scattering wave vector amplitude is $q_{net} = (N + 1)q$, with the pulse spacing and pulse duration identical and given by $\Delta = \delta = (N + \frac{1}{2})\tau$ and

$$E = S(q)[RA(q)]^N[RA(q)]^N RS^\dagger(q) \tag{5.106}$$

Note that the final and initial impulses have opposite sign q amplitudes, so that for this case the initial and final vectors are, respectively, $S(q_1) = S(q)$ and $S^\dagger(-q_{2N+2}) = S^\dagger(q)$.

(ii) Finite gradient pulse spin echo.
The effective gradient is as shown in Fig. 5.30(b). In this case we break the entire waveform into $2N + 1$ intervals, so that the total effective scattering wave vector amplitude is $q_{net} = (M + 1)q$, with $\Delta = (N + \frac{1}{2})\tau$ and $\delta = (M + \frac{1}{2})\tau$. Hence

$$E = S(q)[RA(q)]^M R^{N-M}[RA^\dagger(q)]^M RS^\dagger(q) \tag{5.107}$$

Note that in the narrow gradient pulse approximation, $M = 0$ and

$$E = S(q)R^{N+1}S^\dagger(q) \tag{5.108}$$

precisely consistent with eqn 5.81.

(iii) CPMG spin-echo train.

Consider the effective gradient train shown in Fig. 5.30(c). It comprises $2N$ impulses and N periods of the gradient time integral waveform. This series of impulses may be represented by the relation

$$E = S(q)[RA^\dagger(q)A^\dagger(q)RA(q)A(q)]^M RA^\dagger(q)A^\dagger RS^\dagger(-q) \tag{5.109}$$

where $M = N - 1$. This CPMG train has a square wave time-integral waveform, with period $T = 2\tau$, where τ is the time-evolution step interval. Here the final and initial impulses have equal sign so that in this case the initial and final operators are, respectively, $S(q_1) = S(q)$ and $S^\dagger(-q_{2N+1}) = S^\dagger(-q)$.

The matrix method provides a completely general way to deal with the problem of restricted diffusion, including the effects of wall relaxation, under any gradient

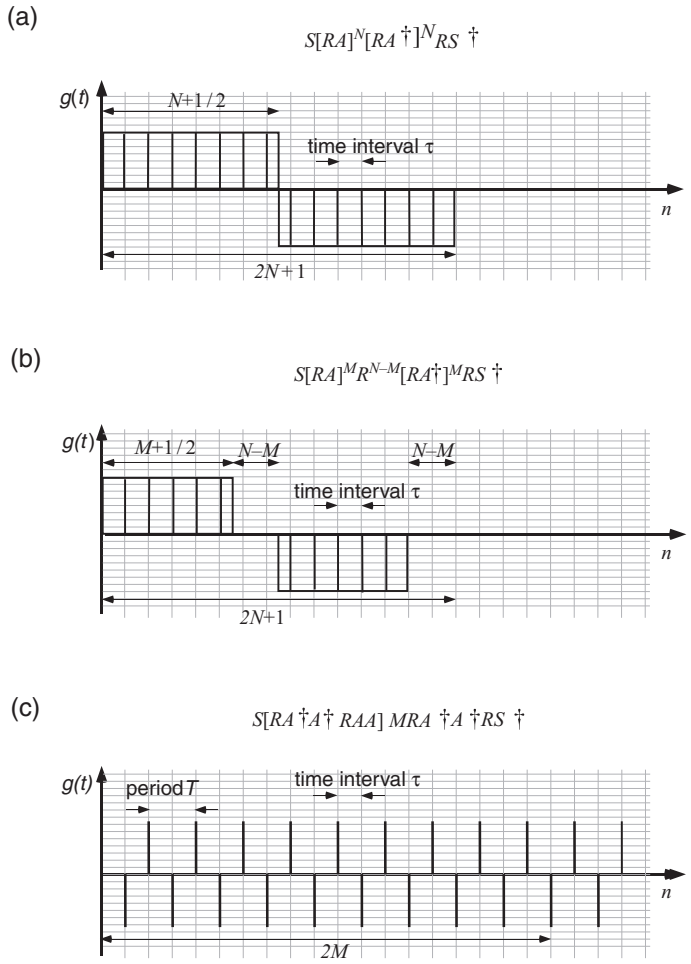

Fig. 5.30 Schematic illustration of impulse decomposition for different pulse sequences. In each case the evolution matrix product corresponding to the sequence is shown above. (a) The steady gradient spin echo (or pulsed gradient spin echo with $\delta = \Delta$) represented by a train of constant magnitude impulses, q. Note that $\Delta = (N + 1/2)\tau$ while the wave vector value corresponding to the area under the complete gradient pulse is $q_{net} = (N + 1)q$. (b) Finite pulse-width PGSE experiment in which $q_{net} = (M+1)q$, $\Delta = (N+1/2)\tau$, and $\delta = (M+1/2)\tau$. (c) CPMG PGSE sequence.

waveform, provided one can obtain an eigenfunction expansion for the propagator. As regards the finite gradient pulse-width problem in PGSE NMR, the matrix expression allows for the ready calculation of echo-attenuation expressions in a few lines of computer code. In Chapter 6, where we investigate restricted diffusion in some detail, we shall return to these matrix expressions to evaluate the PGSE NMR experiment in specific restriction geometries.

5.7.2 Generalised gradients and the frequency domain

The narrow pulse requirement of the two pulse PGSE NMR method severely limits the ability of the method to access information about motion for which the characteristic times are very short. As δ is decreased, so the scattering wavevector q decreases, making the method less and less sensitive to shorter translational displacements, an inconvenient contradiction to say the least. Even if the multiple propagator matrix method is used to allow for a theoretical description under the condition of finite duration gradient pulses, the shortest practical length of time scale Δ accessed by two-pulse PGSE is on the order of a few milliseconds. Of course if gradient amplitudes were able to increase in compensation, q values could be maintained, but higher amplitude gradient pulses bring with them greater eddy current effects and the need for finite pulse rise time.[19]

Notice that the depiction of dynamics in the PGSE description is time-domain in nature. A quite different approach to the use of gradients to measure motion was proposed in the 1980s by Janez Stepišnik [58, 59], in which the frequency domain provides the natural description. In consequence the Stepišnik method is formulated in terms of gradient waveforms of long duration but well-defined frequency characteristics. In this approach, one treats the effect of the gradient via the time dependence of the accumulated spin phase. The mathematical treatment lends itself to analogy with the measurement of rotational dipolar auto-correlation spectral density [22, 60] via the 'probe' of the spin relaxation times, where T_1 samples at positions ω_0 and $2\omega_0$, while $T_{1\rho}$ samples at ω_1 and $2\omega_1$.

The frequency-domain method, which is termed here frequency-domain modulated gradient NMR (FDMG-NMR), was first demonstrated experimentally in 1995 [61]. It has been used to great effect in the elucidation of quite complex dynamics in problems concerning restricted diffusion and fluid dispersion. But it does suffer from two 'Achilles heels'. First, it is based on the use of multiple echoes. In particular the fundamental period defining the measurement frequency results in a net stationary spin phase migration of zero. In the CPMG sequence, such a cyclic process minimises sensitivity to diffusion, and this is also the case for FDMG-NMR. Of course the use of a long echo train duration helps restore sensitivity and better define the frequency, but nonetheless the constraint remains. In consequence the most effective application of the method is for examining restricted diffusion of small molecules (for example, water) or the fluctuation dynamics of flow-driven fluid dispersion. That constitutes a fairly large area of application!

The second weakness in the method concerns the problem of how to deal with an ensemble average of phase factors, and the need to use a Gaussian phase approximation. While stochastic processes often lend themselves to this step, in the case of restricted diffusion, where highly non-Gaussian propagators result, such a simplification is controversial. As always in science, the usefulness of the theory will be determined by its

[19]The use of large steady gradients in a stimulated-echo sequence does allow a means of controlling the effective pulse duration by the bracketing of the 90° RF pulses. This method is discussed in Chapter 12. However, a disadvantage of this approach is the loss of signal amplitude due to the RF pulses being able to stimulate only a narrow slice of the sample under the frequency-spreading effect of the gradient and the loss of spectral information during detection.

ability to represent the data. As we will see in this and later chapters, judged by such a criterion, the method is very useful indeed.

Time interval of the effective gradient

The key idea that underpins the use of magnetic field gradients to measure the translational motion of spin-bearing molecules is that the individual spins acquire a phase factor, $\exp(i\phi)$, due to precession in the local magnetic field $\mathbf{B}_0(\mathbf{r}, t)$. In the presence of a uniform effective magnetic field gradient $\mathbf{g}^*(t)$, this phase is position-dependent,

$$\phi(t) = \gamma \int_0^t \mathbf{g}^*(t') \cdot \mathbf{r}(t') dt' \tag{5.110}$$

In the case of a signal acquired in a spin echo, the time integral of the effective gradient $\mathbf{g}^*(t')$ is zero at the point of echo formation, so that integrating by parts, we may rewrite the integral in eqn 5.110 in terms of the local spin velocity $\mathbf{v} = \mathbf{r}/t$ as $\mathbf{g}^*(t)$,

$$\phi(t) = -\int_0^t \mathbf{F}(t') \cdot \mathbf{v}(t') dt' \tag{5.111}$$

where

$$\mathbf{F}(t) = \gamma \int_0^t \mathbf{g}^*(t') dt' \tag{5.112}$$

To evaluate the normalised amplitude E, of the spin-echo signal arising from the entire spin ensemble, one must calculate the ensemble average

$$E(t) = \langle \exp(-i \int_0^t \mathbf{F}^*(t') \cdot \mathbf{v}(t') dt' \rangle \tag{5.113}$$

Note that the concept of q-space no longer has any meaning, since the Fourier dependence of E on $\mathbf{R}$ is no longer apparent.

The Gaussian approximation

The problem now is to evaluate the ensemble average. This can be performed by expanding the exponential function in a power series and taking ensemble averages of each term as

$$\langle \exp(iA) \rangle = \sum_{r=0}^{\infty} \frac{(i)^r}{r!} \langle A^r \rangle \tag{5.114}$$

where

$$\langle A^r \rangle = \int P(A) A^r dA \tag{5.115}$$

$P(A)$ being the ensemble probability distribution over A.

The power series, eqn 5.114, can be converted back to exponential form by a method known as the cumulant expansion. To obtain this result it is helpful to introduce the characteristic function,

$$\langle \exp(ikA) \rangle = \int \exp(ikA) P(A) dA \tag{5.116}$$

It can be shown that this function may be written

$$\langle \exp(ikA) \rangle = \exp(\sum_{r=1}^{\infty} \frac{(ik)^r}{r!} \Xi_r) \tag{5.117}$$

where

$$\begin{aligned}
\Xi_1 &= \langle A \rangle \\
\Xi_2 &= \langle (A - \langle A \rangle)^2 \rangle = \langle A^2 \rangle - \langle A \rangle^2 \\
\Xi_3 &= \langle (A - \langle A \rangle)^3 \rangle = \langle A^3 \rangle - 3\langle A^2 \rangle \langle A \rangle + 2\langle A^3 \rangle \\
\Xi_4 &= \langle (A - \langle A \rangle)^4 \rangle - 3\langle (A - \langle A \rangle)^2 \rangle^2 = \langle A^4 \rangle - 4\langle A^3 \rangle \langle A \rangle - 3\langle A^2 \rangle^2 \\
&\quad +12\langle A \rangle^2 \langle A^2 \rangle - 6\langle A^4 \rangle
\end{aligned} \tag{5.118}$$

Equation 5.117 is easily verified term by term by taking successive derivatives $\partial^n / \partial k^n$, with $n = 0, 1, 2 \ldots$, then setting $k = 0$. With $k = 1$, eqn 5.117 yields the cumulant expansion

$$\langle \exp(iA) \rangle = \exp(\sum_{r=1}^{\infty} \frac{(i)^r}{r!} \Xi_r) \tag{5.119}$$

Condensing the expression is easily done, provided the assumption is made that the probability distribution $P(A)$ is Gaussian, namely

$$P(A) = (2\pi \Xi_2)^{-1/2} \exp(-\frac{(A - \langle A \rangle)^2}{2\Xi_2}) \tag{5.120}$$

In this case the Fourier transform of the Gaussian $P(A)$ represented by eqn 5.116 reduces to

$$\langle \exp(ikA) \rangle = \exp(i\langle A \rangle k - \tfrac{1}{2}\Xi_2 k^2) \tag{5.121}$$

and setting $k = 1$ we have

$$\langle \exp(iA) \rangle = \exp(i\langle A \rangle - \tfrac{1}{2}(\langle A^2 \rangle - \langle A \rangle^2)) \tag{5.122}$$

That the Ξ_r terms for $r \geq 3$ disappear in the cumulant expansion under the normalised Gaussian distribution is not immediately obvious. For the $r = 3$ term

$$\begin{aligned}
\Xi_3 &= \int (A - \langle A \rangle)^3 P(A) dA \\
&= -\Xi_2 \int (A - \langle A \rangle)^2 \frac{\partial P(A)}{\partial A} dA.
\end{aligned} \tag{5.123}$$

and integrating by parts we find

$$\Xi_3 = 2\Xi_2 \int (A - \langle A \rangle) P(A) dA. \tag{5.124}$$

$(A - \langle A \rangle)$ is antisymmetric about $A = \langle A \rangle$, while $P(A)$ is symmetric and so the integral is zero. For $n = 4$, and again integrating by parts,

$$\begin{aligned}\Xi_4 &= \int (A-\langle A\rangle)^4 P(A)dA - 3\left[\int (A-\langle A\rangle)^2 P(A)dA\right]^2 \\ &= -\Xi_2 \int (A-\langle A\rangle)^3 \frac{\partial P(A)}{\partial A} dA - 3\Xi_2^2 \\ &= 0, \end{aligned} \tag{5.125}$$

and so on.

The delicate question concerns the validity of the Gaussian phase approximation. Of course, our relevant moments Ξ_1 and Ξ_2 will be derived from $\langle \int_0^t \mathbf{F}(t')\cdot\mathbf{v}(t')dt'\rangle$ and $\langle[\int_0^t \mathbf{F}(t')\cdot\mathbf{v}(t')dt']^2\rangle$. It is immediately obvious that eqn 5.122 cannot possibly represent any PGSE NMR experiment in which the dependence of the echo decay on the gradient amplitude g is other than Gaussian. In the next chapter we will see that such non-Gaussian behaviour is very apparent in the case of restricted diffusion where the q-vector in the two gradient pulse Stejskal–Tanner experiment is sufficiently large. However, if we look at the FDMG NMR experiment from its intended standpoint as a frequency-domain analysis of motion, we will quickly come to the conclusion that the two gradient pulse Stejskal–Tanner experiment is not its ideal vehicle. On the contrary, to have a well-defined frequency we will want to use an $\mathbf{F}(t)$ waveform that is oscillatory and which comprises many periods. In effect then, each period of the cycle will contribute only small phase excursions, these gradually accumulating to generate the final signal attenuation. It is precisely under these cumulatively averaging conditions that the central limit theorem suggests the likelihood of a Gaussian distribution of phase.

FDMG signal phase shift and attenuation

Equations 5.113 and 5.122 lead directly to

$$E(t) = \exp(i\alpha(t) - \beta(t)) \tag{5.126}$$

where

$$\alpha(t) = -i\int_0^t \mathbf{F}(t')\cdot\langle\mathbf{v}(t')\rangle dt' \tag{5.127}$$

and

$$\beta = \tfrac{1}{2}\langle[\int_0^t \mathbf{F}(t')\cdot\mathbf{v}(t')dt']^2\rangle - [\int_0^t \mathbf{F}(t')\cdot\langle\mathbf{v}(t')\rangle dt']^2 \tag{5.128}$$

These relations are simplified if we decompose $\mathbf{v}(t)$ into its ensemble mean $\langle\mathbf{v}(t)\rangle = \langle\mathbf{v}\rangle$ and variable component $\mathbf{u}(t)$ as

$$\mathbf{v}(t) = \mathbf{u}(t) + \langle\mathbf{v}\rangle. \tag{5.129}$$

whence

$$\alpha(t) = -i\int_0^t \mathbf{F}(t')\cdot\langle\mathbf{v}\rangle dt' \tag{5.130}$$

and

$$\beta(t) = \tfrac{1}{2}\int_0^t\int_0^t \mathbf{F}(t')\cdot\langle\mathbf{u}(t')\mathbf{u}(t'')\rangle\cdot\mathbf{F}(t'')dt'dt'' \tag{5.131}$$

Note that the simplification that reduces eqn 5.128 to 5.131 arises from the uncorrelated nature of $\mathbf{u}(t)$ and the mean flow $\langle \mathbf{v} \rangle$ such that $\langle \mathbf{u}(t) \cdot \langle \mathbf{v} \rangle \rangle = 0$. $\alpha(t)$ represents the phase shift due to the mean flow of the spin-bearing molecules, while $\beta(t)$ gives the signal attenuation due to the fluctuations in displacement about this mean. It involves a tensor of velocity correlation functions.

In Chapter 2 we defined the diffusion spectrum by

$$\underline{\underline{D}}(\omega) = \tfrac{1}{2} sym \int_{-\infty}^{\infty} \langle \mathbf{u}(\tau)\mathbf{u}(0) \rangle \exp(i\omega\tau) d\tau \tag{5.132}$$

with inverse transform

$$sym\langle \mathbf{u}(\tau)\mathbf{u}(0) \rangle = \frac{1}{\pi} \int_{-\infty}^{\infty} \underline{\underline{D}}(\omega) \exp(-i\omega\tau) d\omega \tag{5.133}$$

or, equivalently

$$sym\langle \mathbf{u}(t')\mathbf{u}(t'') \rangle = \frac{1}{\pi} \int_{-\infty}^{\infty} \underline{\underline{D}}(\omega) \exp(i\omega(t'' - t')) d\omega, \tag{5.134}$$

Taking the (half) Fourier transform of the time-integral effective gradient

$$\mathbf{F}(\omega, t) = \int_0^t \mathbf{F}(t') \exp(i\omega t') dt', \tag{5.135}$$

and noting the factor $\frac{1}{2}$ in eqn 5.131, one obtains the spin-echo-attenuation exponent [58]

$$\begin{aligned} \beta(t) &= \frac{1}{2\pi} \int_{\infty}^{\infty} \mathbf{F}(\omega, t) \cdot \underline{\underline{D}}(\omega) \cdot \mathbf{F}(-\omega, t) d\omega \\ &= \frac{1}{\pi} \int_{0}^{\infty} \mathbf{F}(\omega, t) \cdot \underline{\underline{D}}(\omega) \cdot \mathbf{F}(-\omega, t) d\omega \end{aligned} \tag{5.136}$$

where the symmetry of $\underline{\underline{D}}(\omega)$ is assumed.

$\mathbf{F}(\omega, t)$ extracts only the diagonal components of the diffusion tensor. Suppose we apply the effective gradient along some axis z. Then in this case we will measure the element $D_{zz}(\omega)$ as

$$\beta(t) = \frac{1}{\pi} \int_0^{\infty} |F(\omega, t)|^2 D_{zz}(\omega) d\omega \tag{5.137}$$

The meaning of eqn 5.137 is clear. The product of $|F(\omega, t)|^2$ and $D_{zz}(\omega)$ in the integral means that the diffusion spectrum is sampled by the squared spectrum of the time-integral effective gradient. Figure 5.31 illustrates this schematically. As in the multiple propagator approach, the FDMG NMR method manages to decouple the description of the motion ($D_{zz}(\omega)$) from the description of the gradient waveform ($|F(\omega, t)|^2$), thus greatly simplifying the analysis.

For a precise frequency sampling, $|F(\omega, t)|^2$ should be as close to a delta function as possible and in the next section we show how this can be achieved. For the moment,

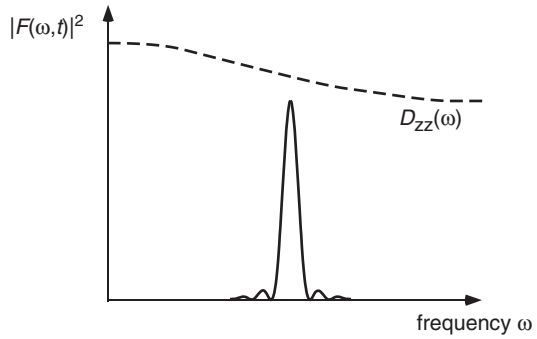

Fig. 5.31 Schematic effective gradient spectrum, $|F(\omega,t)|^2$ used to sample the diffusion spectrum $D(\omega)$.

however, it useful to touch base with an earlier result. Suppose that the fluctuation correlation time for molecular velocities is very short compared with the characteristic time ω^{-1} able to be sampled by $|F(\omega,t)|^2$. This would be the case for unrestricted Brownian motion of small molecules, where $\tau_c \sim 10^{-12}s$. For an exponential correlation function, the diffusion spectrum would feature a constant Lorentzian plateau out to 10^{12} Hz, so that in eqn 5.137, $D_{zz}(\omega)$ reduces to a constant $D_{zz}(0)$, and

$$\beta(t) = \frac{1}{\pi} D_{zz}(0) \int_0^\infty |F(\omega,t)|^2 d\omega \tag{5.138}$$

From the Parceval identity

$$\beta(t) = D_{zz}(0) \int_0^t |F(t')|^2 dt' \tag{5.139}$$

in precise agreement with the Bloch–Torrey relation 5.54.

FDMG signal for pulse sequences of interest

Let us start with the two-gradient pulse Stejskal–Tanner PGSE NMR experiment, comprising finite gradient pulses of amplitude g, width δ, separated by Δ, and with echo formation at time t . The phase spectrum follows from eqns 5.112 and 5.135 as

$$\mathbf{F}(\omega,t) = \gamma \mathbf{g} \frac{(1-\exp(i\omega\Delta))(1-\exp(i\omega\delta)}{\omega^2} \tag{5.140}$$

with

$$|\mathbf{F}(\omega,t)|^2 = \gamma^2\delta^2\Delta^2|\mathbf{g}|^2 \left[\frac{\sin(\omega\delta/2)\sin(\omega\Delta/2)}{(\omega\Delta/2)(\omega\delta/2)}\right]^2 \tag{5.141}$$

Figure 5.32(a) shows the spectrum. Again for free diffusion of small molecules, $D_{zz}(\omega)$ is essentially constant (with value $D = D_{zz}(0)$ over the frequency range of interest. Using the standard integral $\int_0^\infty \sin^2(ax)\sin^2(bx)/x^4 dx = a^2\pi(3b-a)/6$, one obtains the Stejskal–Tanner result

$$\alpha(t) = \gamma^2\delta^2|\mathbf{g}|^2 D(\Delta - \delta/3) \tag{5.142}$$

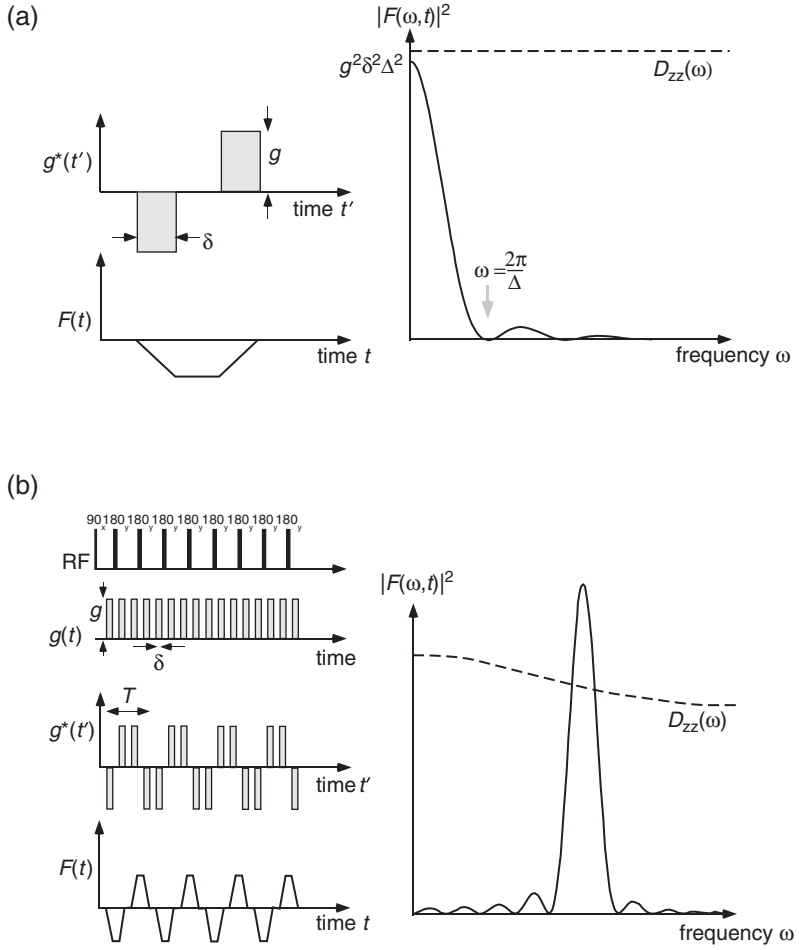

Fig. 5.32 Frequency-domain modulated gradient NMR RF and gradient pulse sequences, showing the (actual) gradient modulation waveform $g(t')$, the time integral of the effective gradient waveform $F(t)$, and the spectrum of $F(t)$. $|F(,\omega,t)|^{2}$, directly samples the diffusion spectrum. The wave forms and spectra are for (a) Stejskal–Tanner PGSE sequence, with a constant diffusion spectrum as discussed in eqn 5.138 and (b) single lobe/ac rectangular modulation. Note that pulse sequence (b) samples the diffusion spectrum at a single frequency.

The spectrum of the two pulse PGSE gradient is dominated by the zero frequency lobe, with frequency width of order Δ^{-1}. It is therefore unsuitable for extracting high-frequency information concerning $D_{zz}(\omega)$. It would be very useful to have available a gradient modulation sequence whose frequency spectrum contained a high-frequency peak that could be adjusted in position, in order to trace out the frequency dependence of $D_{zz}(\omega)$. Such a measurement could in principle locate 'edges' in the spectrum at the inverse motional correlation time, τ_c^{-1}. Our ideal gradient modulation sequence would

possess a frequency spectrum that contained a single peak whose frequency could be adjusted in position in order to trace out the frequency dependence of $D(\omega)$.

Figure 5.32(b) shows a suitable gradient modulation wave form, based on a CPMG sequence with repeated gradient pulses. Also shown is the associated spectrum. Equally effective is the CPMG train using a constant gradient. The dominant sampling lobe of these idealised sequences is at $\omega = 2\pi/T$, where T is the time-integral gradient repeat period. This lobe has width of order $2\pi/NT$, where N is the total number of periods employed. With $N \geq 4$, a reasonably narrow peak can be achieved and with such a train, given gradient pulse durations $\delta \geq 10\mu$s, it is possible in principle to probe spectral densities in the frequency range 10–100 kHz. This becomes possible because, rather than using two gradient pulses, for which the attenuation effect disappears as the gradient pulse duration δ is shortened, the repetitive pulse train employs an increasing number of gradient pulses in any time interval t as the frequency is increased and T is reduced. Thus the frequency-domain analysis extends the effective timescale of the PGSE experiments downward to the sub-millisecond range.

The exact behaviour of the CPMG train of 180° RF pulses, interspaced by $T/2$, in the presence of a constant magnetic field gradient, is easily described. If the first 180° pulse follows the excitation at time $T/4$, the $F(t)$ time dependence is a sawtooth-shaped function oscillating about zero. From eqn 5.135 it can be shown that its spectrum is

$$|\mathbf{F}(\omega, t)|^2 = 4\gamma^2|\mathbf{g}|^2 \frac{8\sin^2(\omega T/8)\sin^2(N\omega T/2)}{\omega^4 \cos^2(\omega T/4)} \tag{5.143}$$

Note that the number of 180° RF pulses must be a multiple of two. This spectrum has only one frequency peak at $\omega = 2\pi/T$, with a width depending on N. Figure 5.32(b) shows that even $N = 4$ gives a reasonably narrow peak, which can be approximated by

$$|\mathbf{F}(\omega, t)|^2 = NT\gamma^2|\mathbf{g}|^2 T^2 \delta(\omega - 2\pi/T) \tag{5.144}$$

The expected echo-attenuation factors for the pulsed gradient CPMG wave form shown in Fig. 5.32(b), along with its constant gradient counterpart, are, respectively,

$$\beta(t) = \tfrac{1}{2} NT\gamma^2|\mathbf{g}|^2\delta^2 D(2\pi/T) \tag{5.145}$$

and

$$\beta(t) = \tfrac{1}{2} NT\gamma^2|\mathbf{g}|^2 T^2 D(2\pi/T) \tag{5.146}$$

where $t = NT$.

By varying T it is possible to probe the frequency spectrum of the molecular translational dynamics, adjusting N as necessary to retain sufficient attenuation as T is reduced. Of course, the dependence of β on NT^3 shows the price paid in using many (N) periods in which the applied gradient pulse duration, which would be potentially $\sim NT$ in a two-pulse experiment, is subdivided into into durations on the order T. The dephasing factor for the two-pulse experiment is $\sim (NT)^3$ whereas for the CPMG train it is smaller by N^2. This, of course, was the very reason for which the CPMG trains was developed: to decrease sensitivity to diffusion! Hence we see that FDMG NMR comes at the price of a restriction to relatively fast moving molecules.

Of course the really interesting question concerns the way in which complex molecular translational dynamics are manifest in the spectral density $D(\omega)$. This topic we cover in the next chapter.

5.8 Phase effects of RF pulses and homospoiling

Dealing with the combined effects of gradient pulses and RF pulses is relatively straightforward in the case of the spin echo. The idea that a 180° RF pulse simply inverts spin phase, and hence negates prior effective gradients, is a helpful idea. But when dealing with multiple combinations of RF pulses, as found in the double PGSE NMR sequences discussed in Chapter 8, alternative approaches can prove useful. Here we introduce a means of tracking the effect of RF pulses on spin coherence encoded by magnetic field gradient pulses. The idea is based on the Argand plane depiction of transverse magnetisation, introduced in Chapter 4. Suppose, for convenience, we regard the first 90° RF pulse of our sequence as having a phase x. Its effect is to induce a magnetisation along the y-axis of the rotating frame. We would detect this magnetisation with arbitrary phase, depending on our receiver setting and our subsequent 'phasing of the signal' by $\exp(i\theta)$ multiplication. So we can simply choose to define y as the real axis of our Argand plane.

5.8.1 Rules for RF pulses

Now consider the effect of our first gradient pulse on a single-spin isochromat. It will induce a phase change factor $\exp(i\phi)$ depending on the position of those spins. What happens with the subsequent RF and gradient pulses follows very simply once we work out the basic rules. For example, what do various RF pulses do to a pre-existing magnetisation of $\exp(i\phi)$?

Let us take a very simple example: that of $180^\circ_{x,y}$ pulses.

-180°_x
The 180°_x pulse inverts the real part of $\exp(i\phi)$, while leaving the imaginary part unchanged. Thus $\exp(i\phi) \rightarrow -\exp(-i\phi)$

-180°_y
The 180°_y pulse inverts the imaginary part of $\exp(i\phi)$, while leaving the real part unchanged. Thus $\exp(i\phi) \rightarrow \exp(-i\phi)$. Note that exactly the same results are achieved if the phases of these (ideal) 180° pulses are reversed: $x \rightarrow -x$,$y \rightarrow -y$.

Next we need to consider the effect of $90^\circ_{x,y}$ pulses on gradient-encoded magnetisation. These move transverse magnetisation out of the plane, to lie along the longitudinal axis for later recall. That component which remains in the transverse plane may be considered to be 'homospoiled'; that is, dephased to a degree that it will no longer contribute to the subsequent NMR signal. This will be achieved either by the residual background field inhomogeneity, or where this is insufficient, by deliberately applying 'homospoil' gradient pulses, pulses that impart no phase shifts to the stored z component, and hence have no impact on the final signal encoding. The use of z-storage requires that we clearly identify the 'coherence pathway' that leads to our ultimate signal. Hence, in what follows we look at combinations of 'storage'–'recall' pulses.

$-90^\circ_x - \tau - 90^\circ_x$
The first 90°_x pulse stores the real part of $\exp(i\phi)$ along the negative z-axis, while the second 90°_x pulse recalls this component to the negative real axis. Thus $\exp(i\phi) \rightarrow -\cos(\phi) = -0.5[\exp(i\phi) + \exp(-i\phi)]$

$-90^\circ_y - \tau - 90^\circ_y$
. The first 90°_y pulse stores the imaginary part of $\exp(i\phi)$ along the negative z-axis, while the second 90°_x pulse recalls this component to the negative imaginary axis. Thus $\exp(i\phi) \rightarrow -i\sin(\phi) = -0.5[\exp(i\phi) - \exp(-i\phi)]$.

$-90^\circ_x - \tau - 90^\circ_{-x}$
The first 90°_{-x} pulse stores the real part of $\exp(i\phi)$ along the positive z-axis, while the second 90°_x pulse recalls this component to the positive real axis. Thus $\exp(i\phi) \rightarrow \cos(\phi) = 0.5[\exp(i\phi) + \exp(-i\phi)]$

$-90^\circ_{-y} - \tau - 90^\circ_y$
. The first 90°_y pulse stores the imaginary part of $\exp(i\phi)$ along the positive z-axis, while the second 90°_{-y} pulse recalls this component to the positive imaginary axis. Thus $\exp(i\phi) \rightarrow i\sin(\phi) = 0.5[\exp(i\phi) - \exp(-i\phi)]$.

Unlike the case of 180° RF pulses, reversal of phase with a single 90° pulse produces an outcome of two transverse plane components with opposite sign phase. This difference turns out to be crucial in PGSE NMR, where we must track the evolution of phase shifts induced by gradient pulses, ensuring the appropriate summation combinations.

The stimulated-echo formation in the absence of homospoil pulses

Care is needed whenever a stimulated echo is formed without the use of homospoil pulses. In each case above, recall to the transverse plane by the final 90° RF pulse in the stimulated-echo train leaves a superposition of $\exp(i\phi)$ and $\exp(-i\phi)$, each with amplitude 1/2. One of these has the phase-cancelling effect needed to produce the echo, again with amplitude 1/2. But without the action of homospoiling pulses, a very different outcome results. Homospoiling destroys remaining transverse magnetisation following z-storage. Without homospoil pulses, and under high background field homogeneity with a sufficiently short z-storage period, this transverse magnetisation will persist. In that case, the outcomes of the above four $90^0 - 90^\circ$ combinations will act in the manner of a concatenated combination, their effect akin to 180° pulses or 0° null pulses. For the four combinations respectively, the effect is 180°_x, $18o^\circ_y$, null and null. The former two result in spin echoes of full amplitude, while the latter two combinations produce no echo.

As the storage time is gradually increased, the action of background field inhomogeneity increasingly destroys the transverse magnetisation, so that echo amplitudes, for the four combinations, fall from from unity to 1/2 in the case of the first two, and rise from zero to 1/2 in the case of the final two. This provides a nice rule for determining whether a homospoil pulse is sufficient for purpose. The stimulated echo, however formed, should be half the amplitude of the spin echo.

5.8.2 The spin echo and stimulated echo

The rules are now in place for handling combinations of RF and gradient pulses for the spin and stimulated echoes, as shown in Fig. 5.33. Note the scheme for labelling the RF pulse phases. The initial 90° RF pulse has phase φ_0, by our convention taken as x, and we will assume that the acquisition phase is set to give a real signal for y-magnetisation. In other words we can regard its phase as coincident with that of the first RF pulse and label it as x.

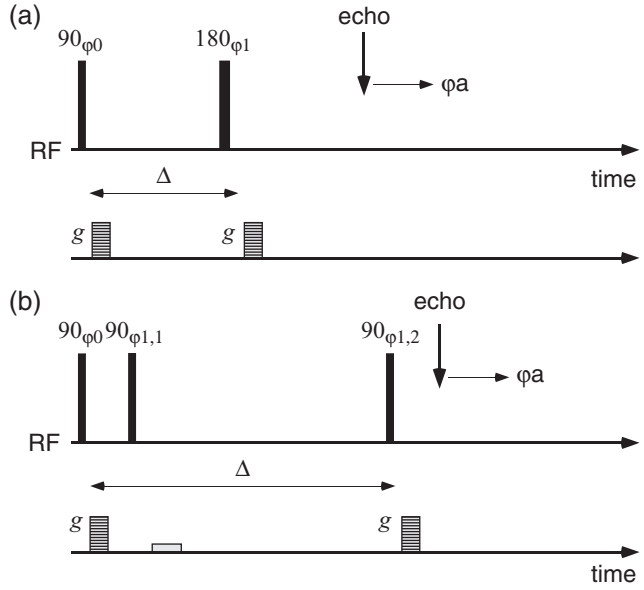

Fig. 5.33 Schematic RF and gradient pulse sequences for (a) spin echo and (b) stimulated-echo PGSE NMR experiments in which the gradient pulse area ($g\delta$) is stepped. A homospoil gradient is included in the case of the stimulated echo.

Suppose we now track what happens in the spin echo where φ_1 is taken as y. After the first RF pulse, the phase factor is 1. After the first gradient pulse it is $\exp(i\phi)$. After the 180°_y RF pulse it is $\exp(-i\phi)$, and after then second gradient pulse it is $\exp(i\Delta\phi) = \exp(i\phi' - i\phi)$.

For the stimulated echo, let us take three examples.

$\varphi_{1,1} = -x$ **and** $\varphi_{1,2} = x$
After the first gradient pulse the phase factor is $\exp(i\phi)$. After the 90°_{-x} RF pulse subsequent homospoil and recall by the 90°_x RF pulse, it is $\cos(\phi)$. After the second gradient pulse it is $0.5[\exp(i\phi' - i\phi) + \exp(i\phi' i + i\phi)]$. The ensemble-averaging process destroys the second exponential term because it represents the cumulative phase shift of both gradient pulses averaging over all macroscopic positions of the spins, rather

than the phase difference, which is sensitive to the microscopic distance the spins have moved. The ensemble average is therefore $0.5\langle\exp(i\phi' - i\phi)]\rangle$.

$\varphi_{1,1} = x$ **and** $\varphi_{1,2} = x$
After the first gradient pulse the phase factor is $\exp(i\phi)$. After the 90°_x RF pulse, subsequent homospoil and recall by the 90°_x RF pulse, it is $-\cos(\phi)$. After the second gradient pulse it is $-0.5[\exp(i\phi' - i\phi) + \exp(i\phi' + i\phi)]$. The ensemble average is $-0.5\langle\exp(i\phi' - i\phi)]\rangle$.

$\varphi_{1,1} = y$ **and** $\varphi_{1,2} = y$
After the first gradient pulse the phase factor is $\exp(i\phi)$. After the 90°_y RF pulse, subsequent homospoil and recall by the 90°_y RF pulse, it is $-i\sin(\phi)$. After the second gradient pulse it is $-0.5[\exp(i\phi' + \phi) - \exp(i\phi' - i\phi)]$. The ensemble average is $0.5\langle\exp(i\phi' - i\phi)\rangle$.

These simple rules will prove particularly useful in considering the cumulative effects of RF and gradient pulses in longer trains.

5.9 Diffusion in the radiofrequency field

Throughout this chapter, we have considered only the case where the spatial dependence of precession arises from gradients in the polarising field, B_0. Of course there is another precession process of central importance to magnetic resonance and that is the nutation around the RF field, B_1. Because these nutations also encode phase information into the spin magnetisation, such gradients in B_1 encode for position and hence may also be used to image spin density, or to measure translational motion. The first suggested use of RF gradients for imaging was by Hoult [62], while the extensive application to diffusion and flow measurements has been made by Canet and co-workers [63, 64].

In this section we show how radiofrequency field gradient precessions relate to phase-encoding ideas covered throughout this chapter, and how such RF gradient experiments may be employed for tracking molecular motion. Finally we ask, what are advantages and disadvantages of this alternative approach?

5.9.1 How RF field gradients work

The mode of action of an RF field gradient, $\mathbf{g}_1 = \nabla B_1$, is no different in principle to that of a B_0 gradient, $\mathbf{g}_0 = \nabla B_0$, as apparent in the rotating-frame description shown in Fig. 5.34. In Fig. 5.34(a) a transverse magnetisation generated by a prior 90°_x RF pulse is subject to precessional dephasing due to a distribution of spin positions, $\mathbf{r}$, in the presence of $\mathbf{g}_0$. In Fig. 5.34(b) a longitudinal magnetisation is subject to nutational dephasing due to a distribution of spin positions, $\mathbf{r}$, in the presence of $\mathbf{g}_1$. In both situations spin phase has been encoded according to a positional coordinate and, in the same way, $\mathbf{k}$-space vectors may be defined. Furthermore, both processes may be reversed by applying the same duration gradient pulse with opposite polarity. Indeed, there is a formal equivalence between the actions of $\mathbf{g}_0$ and $\mathbf{g}_1$ [65] if the RF gradient pulse is bracketed by a pair of perfectly homogeneous 90° RF pulses as shown in Fig. 5.34(c).

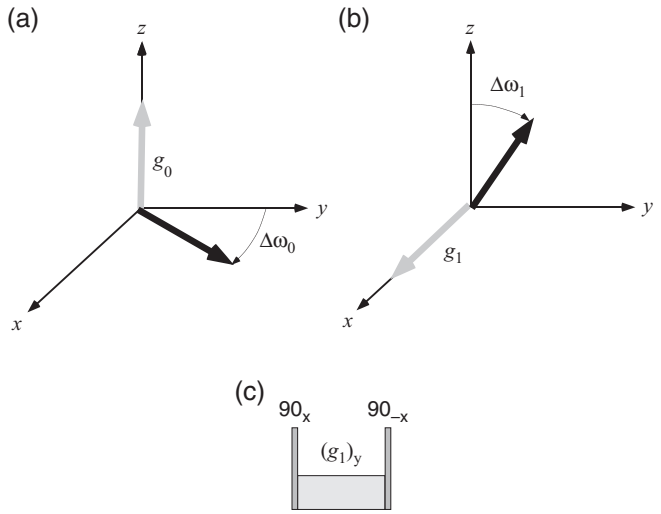

Fig. 5.34 (a) Precession at a rate $\Delta\omega_0 = \gamma \mathbf{g}_0 \cdot \mathbf{r}$ due to a gradient $\mathbf{g}_0$ in the longitudinal static magnetic field (B_0) and (b) nutation under an RF field at a rate $\Delta\omega_1 = \gamma \mathbf{g}_1 \cdot \mathbf{r}$, determined by the position of the spin in a radiofrequency (B_1) gradient, $\mathbf{g}_1$. In both cases the depiction is in the rotating frame. (c) A B_1 gradient pulse directed along the y-axis in the rotating frame, and bracketed by two homogeneous 90° RF pulses. The result is equivalent to a single B_0 gradient pulse of the same magnitude. ((a) to (c) are adapted from Canet [63]).

The bracketed RF gradient pulses could be used in conjunction with a regular Stejskal–Tanner pulse sequence to produce all the motion-encoding effects we have so far seen. However, there is a much simpler way to carry out the RF gradient experiment [63, 66] based on the two RF gradient pulse experiment shown in Fig. 5.35. Each pulse has duration δ, and the pulses are, as in the $\mathbf{g}_0$ case, separated by interval Δ. At the end of the second pulse a homogeneous 90° RF pulse is used to tip any longitudinal magnetisation into the transverse plane. There is, however, an important distinction to be made. In considering $\mathbf{g}_0$ gradients, the phase is embedded in M_+. For $\mathbf{g}_1$ gradients, we need to take account of the behaviour of M_z as well. In a step-by-step analysis of the pulse sequence of Fig. 5.35, it is possible to follow each magnetisation component in turn [63].

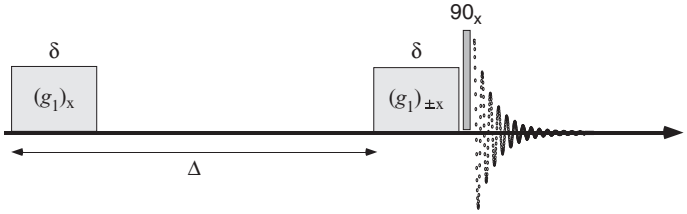

Fig. 5.35 Simple pulse sequence for measuring translational motion of spin-bearing molecules using B_1 gradients.

Let us start at time $t = 0$ and with an isochromat at position $\mathbf{r}$, with uniform magnetisation density, $M_0\hat{\mathbf{k}}$, oriented along $B_0\hat{\mathbf{k}}$, in the direction of the laboratory-frame z-axis. Assuming short RF gradient pulses, we allow that the isochromat of spins starts at $\mathbf{r}$, at the time of the first pulse, but moves to $\mathbf{r}'$ at the time of the second. Unlike the $\mathbf{g}_0$ case, where all precessions are about z, in the RF gradient case both precessions about z and nutations about x play a role. Consequently, care is needed to allow for the condition that spins are 'off-resonance', in other words, that there exists some precession angle ϕ around z in the rotating frame, over the duration between the gradient pulses [63]. The magnetisation density following the first pulse is

$$\begin{aligned} M_x(\mathbf{r},\delta) &= 0 \\ M_y(\mathbf{r},\delta) &= M_0 \sin\theta \\ M_z(\mathbf{r},\delta) &= M_0 \cos\theta \end{aligned} \tag{5.147}$$

where $\theta = \gamma\delta\mathbf{r}\cdot\mathbf{g}_1$. After the duration Δ, and allowing for relaxation of M_x and M_y by $\exp(-\Delta/T_2)$ and M_z to $M_z\exp(-\Delta/T_1) + M_0(1-\exp(-\Delta/T_1)$

$$\begin{aligned} M_x(\mathbf{r},\Delta) &= M_0\exp(-\Delta/T_2)\sin\theta\sin\phi \\ M_y(\mathbf{r},\Delta) &= M_0\exp(-\Delta/T_2)\sin\theta\cos\phi \\ M_z(\mathbf{r},\Delta) &= M_0\cos\theta\exp(-\Delta/T_1) + M_0(1-\exp(-\Delta/T_1) \end{aligned}$$

Choosing the second $\mathbf{g}_{1\pm}$ pulse to be positive or negative, we have, after that pulse,

$$\begin{aligned} M_x(\mathbf{r},\Delta+\delta) &= M_0\exp(-\Delta/T_2)\sin\theta\sin\phi \\ M_y(\mathbf{r},\Delta+\delta) &= M_0\exp(-\Delta/T_2)\sin\theta\cos\phi\cos\theta' \\ &\quad \pm M_0(1-\exp(-\Delta/T_1))\sin\theta' \pm M_0\exp(-\Delta/T_1)\cos\theta\sin\theta' \\ M_z(\mathbf{r},\Delta+\delta) &= \mp M_0\exp(-\Delta/T_2)\sin\theta\cos\phi\sin\theta' \\ &\quad + M_0(1-\exp(-\Delta/T_1))\cos(\theta') + M_0\exp(-\Delta/T_1)\cos\theta\cos\theta' \end{aligned}$$

where $\theta' = \gamma\delta\mathbf{r}'\cdot\mathbf{g}_1$. A phase cycle in which the contributions of positive and negative $\mathbf{g}_1$ second RF gradient pulses are co-added greatly simplifies the result to

$$\begin{aligned} M_x(\mathbf{r},\Delta+\delta) &= M_0\exp(-\Delta/T_2)\sin\theta\sin\phi \\ M_y(\mathbf{r},\Delta+\delta) &= M_0\exp(-\Delta/T_2)\sin\theta\cos\phi\cos\theta' \\ M_z(\mathbf{r},\Delta+\delta) &= M_0(1-\exp(-\Delta/T_1))\cos(\theta') + M_0\exp(-\Delta/T_1)\cos\theta\cos\theta' \end{aligned}$$

5.9.2 Measurement of diffusion and flow

The next step in the analysis is to calculate ensemble averages over all isochromats. Noting the homospoiling effect $\langle\sin\theta\rangle = \langle\cos\theta\rangle = \langle\sin\theta'\rangle = \langle\cos\theta'\rangle = 0$,

$$\begin{aligned} \langle M_x\rangle &= 0 \\ \langle M_y\rangle &= M_0\exp(-\Delta/T_2)\cos\phi\langle\sin\theta\cos\theta'\rangle \\ \langle M_z\rangle &= M_0\exp(-\Delta/T_1)\langle\cos\theta\cos\theta'\rangle \end{aligned}$$

The difference $\theta' - \theta$ tells us about the displacement of spin-bearing molecules over the time Δ. By contrast, the sum $\theta' + \theta$ is a total (homospoiling) positional dephasing

for which $\langle \sin(\theta + \theta') \rangle = \langle \cos(\theta + \theta') \rangle = 0$. Following the case of the narrow gradient pulse depiction of the Stejskal–Tanner experiment, and denoting $\mathbf{R} = \mathbf{r}' - \mathbf{r}$, then $\theta' - \theta = \gamma\delta\mathbf{R} \cdot \mathbf{g}_1$, and

$$\begin{aligned} \langle M_x \rangle &= 0 \\ \langle M_y \rangle &= \tfrac{1}{2} M_0 \exp(-\Delta/T_2) \cos\phi \langle \sin(\gamma\delta\mathbf{R} \cdot \mathbf{g}_1) \rangle \\ \langle M_z \rangle &= \tfrac{1}{2} M_0 \exp(-\Delta/T_1) \langle \cos(\gamma\delta\mathbf{R} \cdot \mathbf{g}_1) \rangle \end{aligned} \tag{5.148}$$

These are the magnetisations before the final recall pulse. If a 90°_x recall pulse is used, the M_y magnetisation is flipped to the z-axis, while M_z is flipped to the transverse plane to contribute our signal. $\langle \cos(\gamma\delta\mathbf{R} \cdot \mathbf{g}_1) \rangle$ is the cosine transform $\int_{-\infty}^{\infty} \overline{P}(Z, \Delta) \cos(qZ) dZ$, where, as before, $q = \gamma\delta g_1$.

In the case of a diffusive propagator, the result is identical to the exponential Fourier transform. Normalised to the result for $g_1 = 0$, the relaxation term disappears and, as before

$$E(q, \Delta) = \exp(-\gamma^2 \delta^2 g_1^2 D\Delta) \tag{5.149}$$

again with Δ replaced by $\Delta - \delta/3$ in the case of finite-duration gradient pulses. For net flow, one no longer obtains a phase-shifted echo signal in the RF gradient experiment, but the cosine oscillation

$$E(q, \Delta) = \cos(\gamma\delta g_1 v\Delta) \tag{5.150}$$

5.9.3 Advantages and disadvantages of RF gradients

The principal motivation for the use of B_1 gradients concerns the ability to switch gradient pulses more easily. B_0 gradient pulses generate eddy-current-related fields during their rise and fall times, typically $\sim 100\,\mu$s. These can significantly perturb the quality of the B_0 field, resulting in resolution loss, or interference with the field-frequency lock system. Unlike B_0 gradient coils, B_1 coils are resonant circuits, allowing rise and fall times on the order of microseconds. B_1 gradients generate no eddy currents. However, they are generally much smaller in magnitude than is possible to achieve with B_0 gradients, and the need to incorporate both homogeneous and gradient B_1 coils in the same RF system presents technical challenges and places limitations on design.

References

[1] E. L. Hahn. Spin echoes. *Phys. Rev.*, 77:746, 1950.
[2] P. Mansfield and P. K. Grannell. NMR diffraction in solids. *J. Phys. C-Solid State Physics*, 6:L422, 1973.
[3] P. C. Lauterbur. Image formtion by local interactions-examples employing nuclear magnetic resonance. *Nature*, 242:190, 1973.
[4] J. Stepisnik. Violation of the gradient approximation in NMR self-diffusion measurements. *Z. Phys. Chem.*, 190:51, 1995.
[5] T. R. Saarinen and C. S. Johnson. Imaging of transient magnetization gratings in NMR-analogies with laser-induced gratings and applications to diffusion and flow. *J. Magn. Reson.*, 78:257, 1988.

[6] P. T. Callaghan. *Principles of Nuclear Magnetic Resonance Microscopy.* Oxford, New York, 1991.
[7] P. Mansfield and P. G. Morris. *NMR Imaging in Biomedicine.* Academic Press, New York, 1982.
[8] P. G. Morris. *NMR Imaging in Biology and Medicine.* Oxford University Press, Oxford, 1986.
[9] E. M. Haacke, R. W. Brown, M. R. Thompson, and R. Venkatesan. *Magnetic Resonance Imaging: Physical Principles and Sequence Design.* Wiley-Liss, New York, 1999.
[10] E. M. Haacke, R. W. Brown, M. R. Thompson, and R. Venkatesan. *NMR Imaaging of Materials.* Oxford University Press, Oxford, 2000.
[11] W. A. Edelstein, J. M. S. Hutchison, G. Johnson, and T. W. Redpath. Spin warp NMR imaging and applications to human whole-body imaging. *Phys. Med. Biol.*, 25:751, 1980.
[12] P. Mansfield and A. A. Maudsley. Planar spin imaging by NMR. *J. Magn. Reson.*, 27:101, 1977.
[13] J. Hennig, A. Nauerth, and H. Friedburg. RARE imaging: A fast imaging method for clinical MR. *Magn. Reson. Med.*, 3:823, 1986.
[14] D. R. Bailes and D. J. Bryant. NMR imaging. *Contemp. Phys.*, 25:441, 1984.
[15] P. R. Locher. Computer simulation of selective excitation in NMR imaging. *Phil. Trans. Royal Society B*, 289:537, 1980.
[16] J. Frahm and W. Hanicke. Comparitive study of pulse sequences for selective excitation in NMR imaging. *J. Magn. Reson.*, 60:320, 1984.
[17] H. Y. Carr and E. M. Purcell. Effects of diffusion on free prcession in nuclear magnetic resonance experiments. *Phys. Rev.*, 94:630, 1954.
[18] M. Abramowitz and I. A Stegun. *Handbook of Mathematical Functions with Formulas, Graphs, and Mathematical Tables.* Dover, New York, 1972.
[19] K. R. Harris, R. Mills, P. J. Back, and D. S. Webster. Improved spin echo apparatus for measurement of self-diffusion coefficients-diffusion of water in aqueous electrolyte solutions. *J. Magn. Reson.*, 29:473, 1978.
[20] P. P. Zanker, J. Schmidt, J. Schmiedeskamp, R. H. Acosta, and H. W. Spiess. Spin echo formation in the presence of stochastic dynamics. *Phys. Rev. Lett.*, 99:263001, 2007.
[21] H. C. Torrey. Bloch equation with diffusion terms. *Phys. Rev.*, 104:563, 1956.
[22] A. Abragam. *Principles of Nuclear Magnetism.* Clarendon Press, Oxford, 1961.
[23] D. W. McCall, D. C. Douglass, and E. W. Anderson. Self-diffusion studies by means of nuclear magnetic resonance spin echo techniques. *Ber. Bunsenges. Physik. Chem.*, 67:336, 1963.
[24] E. O. Stejskal and J. E. Tanner. Spin diffusion measurements: Spin echoes in the presence of a time-dependent field gradient. *J. Chem. Phys.*, 42:288, 1965.
[25] P. Stilbs and M. E. Moseley. Nuclear spin-echo experiments on standard Fourier transform NMR spectrometers. Application to multicomponent self-diffusion studies. *Chem Scripta*, 13:26, 1979.
[26] P. Stilbs and M. E. Moseley. Multicomponent self-diffusion measurement by the pulsed-gradient spin-echo method on standard Fourier transform NMR spectrometers. *Chem Scripta*, 15:176, 1980.

[27] E. O. Stejskal. Use of spin choes in a pulsed magnetoic field gradient to study anisotropic, restricted diffusion and flow. *J. Chem. Phys.*, 43:3597, 1965.
[28] P. T. Callaghan. Pulsed field gradient nuclear magnetic resonance as a probe of liquid state molecular organisation. *Australian Journal of Physics*, 37:359, 1984.
[29] P. Stilbs. Fourier transform pulsed-gradient spin-echo studies of molecular diffusion. *Progress in Nuclear Magnetic Resonance Spectroscopy*, 19:1, 1987.
[30] W. S. Price. Pulsed-field gradient nuclear magnetic resonance as a tool for studying translational diffusion: Part 1. Basic theory. *Concepts in Magnetic Resonance*, A9:299, 1997.
[31] W. S. Price. Pulsed-field gradient nuclear magnetic resonance as a tool for studying translational diffusion: Part 2. Experimental aspects. *Concepts in Magnetic Resonance*, A10:197, 1998.
[32] W. S. Price. *NMR Studies of Translational Motion*. Cambridge, 2009.
[33] P. T. Callaghan, C. M. Trotter, and K. W. Jolley. A pulsed field gradient system for a Fourier transform nmr spectrometer. *J. Magn. Reson.*, 37:247, 1980.
[34] C. M. Trotter. *PhD thesis.* Massey University, Palmerston North, New Zealand, 1981.
[35] W. S. Price and P. W. Kuchel. Effect of nonrectangular field gradient pulses in the Stejskal and Tanner (diffusion) pulse sequence. *J. Magn. Reson.*, 94:133, 1991.
[36] J. E. Tanner. Use of the stimulated echo in NMR diffusion studies. *J. Chem. Phys.*, 52:2523, 1970.
[37] W. D. Williams, E. F. W. Seymour, and R. M. Cotts. A pulsed-gradient multiple-spin-echo NMR technique for measuring diffusion in the presence of background magnetic field gradients. *J. Magn. Reson.*, 31:271, 1978.
[38] A. Germanus, H. Pfeifer, W. Heink, and J. Kärger. On the application of the spin-locking technique for NMR self-diffusion measrements by pulsed field gradients. *Annalen der Physik*, 495:161, 1983.
[39] R. F. Karlicek and I. J. Lowe. A modified pulsed gradient technique for measuring diffusion in the presence of large background gradients. *J. Magn. Reson.*, 37:75, 1980.
[40] R. M. Cotts, M. J. R. Hoch, T. Sun, and J. T. Markert. Pulsed field gradient stimulated echo methods for improved NMR diffusion measurements in heterogeneous systems. *J. Magn. Reson.*, 83:252, 1989.
[41] P. Z. Sun, J. G. Seland, and D. Cory. Background gradient suppression in pulsed gradient stimulated echo measurements. *J. Magn. Reson.*, 161:168, 2003.
[42] J. G. Seland, G. H. Sorland, K. Zick, and B. Hafskjold. Diffusion measurement at long observation times in the presence of spatially variable internal magnetic field gradients. *J. Magn. Reson.*, 146:14, 2000.
[43] P. Galvosas, F. Stallmach, and J. Kärger. Background gradient suppression in stimulated echo NMR diffusion studies using magic pulsed field gradient ratios. *J. Magn. Reson.*, 166:164, 2004.
[44] C. Buckley, K. G. Hollingsworth, A. J. Sederman, D. J. Holland, M. L. Johns, and L. F. Gladden. Applications of fast diffusion measurement using Difftrain. *J. Magn. Reson.*, 161:168, 2003.

[45] A. Haase, J. Frahm, D. Matthei, and K. D. Merbold. FLASH imaging: rapid NMR imaging using low flip angle pulses,. *J. Magn. Reson.*, 67:258, 1986.
[46] Y-Q Song. Categories of coherence pathways in the CPMG sequence. *J. Magn. Reson.*, 157:82, 2002.
[47] E. E. Sigmund, H. Cho, and Y-Q Song. Multiple-modulation-multiple-echo magnetic resonance. *Concepts in Magnetic Resonance*, 30A:358, 2007.
[48] M. D. Hürlimann. Diffusion and relaxation effects in general stray field NMR experiments. *J. Magn. Reson.*, 148:367, 2001.
[49] J. Hennig. Echoes—how to generate, recognize, use or avoid them in MR-imaging sequences. *Concepts in Magnetic Resonance*, 3:179, 1991.
[50] G. A. Morris and R. Freeman. Selective excitation in Fourier-transform nuclear magnetic-resonance. *J. Magn. Reson.*, 29:433, 1978.
[51] K. Szutkowski and I. Furó. Effective and accurate single-shot nmr diffusion experiments based on magnetization grating. *J. Magn. Reson.*, 195:123, 2008.
[52] L. Zha and I. J. Lowe. Optimized ultra-fast imaging sequence (OUFIS). *Magn. Reson. Med.*, 33:377, 1995.
[53] P. J. Basser, J. Mattiello, and D. LeBihan. MR diffusion tensor spectroscopy and imaging. *Biophysical Journal*, 66:259, 1994.
[54] P. T. Callaghan, C. D. Eccles, and Y. Xia. NMR microscopy of dynamic displacements: k-space and q-space imaging. *Journal of Physics E*, 21:820, 1988.
[55] J. Kärger and W. Heink. The propagator representation of molecular-transport in microporous crystallites. *J. Magn. Reson.*, 51:1, 1983.
[56] A. Caprihan, L. Z Wang, and E. Fukushima. A multiple-narrow-pulse approximation for restricted diffusion in a time-varying field gradient. *J. Magn. Reson.*, 118:94, 1996.
[57] P. T. Callaghan. A simple matrix formalism for the spin echo analysis of restricted diffusion under generalised gradient waveforms. *J. Magn. Reson.*, 129:74, 1997.
[58] J. Stepisnik. Analysis of NMR self-diffusion measurements by a density matrix calculation. *Physica*, 104B:350, 1981.
[59] J. Stepišnik. Measuring and imaging of flow by NMR. *Progr. NMR Spectrosc.*, 17:187, 1985.
[60] N. Bloembergen, E. M. Purcell, and R. V. Pound. Relaxation effects in nuclear magnetic resonance absorption. *Phys. Rev.*, 73:679, 1948.
[61] P. T. Callaghan and J. Stepišnik. Frequency domain analysis of spin motion using modulated gradient NMR. *J. Magn. Reson.*, A117:118, 1995.
[62] D. I. Hoult. Rotating frame zeugmatography. *J. Magn. Reson.*, 33:183, 1979.
[63] D. Canet. Radiofrequency field gradient experiments. *Progr. NMR Spectrosc.*, 30:101, 1997.
[64] F. Humbert, M. Valtier, A. Retournard, and D. Canet. Diffusion measurements using radiofrequency field gradient: Artifacts, remedies, practical hints. *J. Magn. Reson.*, 134:245, 1998.
[65] C. Counsell, M. H. Levitt, and R. R. Ernst. Analytic theory of composite pulses. *J. Magn. Reson.*, 63:133, 1985.
[66] D. Bourgeois and M. Decorps. A B1 gradient method for the detection of slow coherent motion. *J. Magn. Reson.*, 91:128, 1991.